(2)

A STUDY ON THE STABILITY OF AQUEOUS OXIDE SUSPENSIONS

1994

HIROKI YOTSUMOTO

Contents

Acknowledgement

I am greatly indebted to Dr. Takahide Wakamatsu, professor of Department of Mineral Science and Technology, Faculty of Engineering, Kyoto University, for his scholastic guidance in completing this thesis. I am also grateful to Dr. Ko Higashitani, professor of Department of Chemical Engineering, Faculty of Engineering, Kyoto University, and to Dr. Natsuo Hatta, professor of Department of Mineral Science and Technology, Faculty of Engineering, Kyoto University, for their invaluable advisory.

I express my appreciation to Dr. Yoshitaka Nakahiro, associate professor of the Department of Mineral Science and Technology, Faculty of Engineering, Kyoto University, for his helpful comments and suggestions.

A part of this research was carried out at Virginia Center for Coal and Minerals Processing, Virginia Polytechnic Institute and State University, under the financial support from Science and Technology Agency of Japan. I would like to extend my deepest thanks to Dr. Roe-Hoan Yoon, director of the Virginia Center for Coal and Minerals Processing, for his advisory and support in conducting research.

I am extremely thankful to Dr. Hiroshi Sakamoto, Director of Materials Processing Department, National Institute for Resources and Environment, and Mr. Shinichi Ito, Chief of Mineral Processing Division, Materials Processing Department, for their continuous support and kind help. I also wish to thank all my colleagues of Materials Processing Department, for their constructive comments and suggestions on this research.

Chapter 1 Introduction

In many industrial products, fine particles are often used being dispersed in various liquid media. Ink and paint are well known examples. Magnetic fluids are the suspensions of magnetic solid particles in non-aqueous media such as kerosene. Most friction modifiers consist of solid lubricant particles designed to be dispersed in motor oil. Since the stability of dispersion in such suspensions is the main factor affecting the products' quality, various methods have been employed to prevent the coagulation of constituent fine particles. The stability of dispersion is also a major interest in many industrial processes. In dense media separation, for example, the suspension of magnetite particles are used as dense media to separate light materials form heavy ones. The decrease of the stability of magnetite dispersion deteriorates the separation efficiency of the process[1]. When the removal of fine particles, on the contrary, is the objective of processes, such as water and wastewater treatment, the coagulation of particles is necessary to increase process efficiency[2]. The mutual separation of particles, such as selective coagulation[3], is based on a technique to coagulate particles of interest, keeping the other particles being dispersed. In this case, the control of coagulation is the key of the process.

It is, therefore, important to understand the behavior of fine particles in liquid media, and it has been one of the major interests in colloid science to predict the stability of such suspensions. The first theoretical approach was made by two different research groups independently. Russian scientists, Derjaguin and Landau introduced the concept of disjoining pressure of liquid films between two solid surfaces in order to explain the coagulation of particles[4]. Disjoining pressure (Π) is given by the algebraic sum of two pressure components from different origins:

$$\Pi = \Pi_e + \Pi_d \,, \qquad [1.\ 1]$$

where Π_e is an electrostatic pressure component caused by the superposition of electric double layers extending from solid surface to liquid bulk phase, and Π_d is a London–van der Waals component originated in molecular interaction among the constituent molecules of the solid and the liquid medium. Each component is a function of surface separation. For symmetrical system Π_e is generally repulsive decaying exponentially with separation distance, while attractive Π_d decays following a power law. At small and large distances, the power law of attraction dominates the exponential decay of repulsion, creating the primary and secondary minima, where Π is negative. At intermediate distances, the repulsion usually exceeds the attraction, which gives rise to a pressure barrier. The schematic diagram of disjoining pressure vs. surface separation (H) is shown in Fig. 1. 1(a). When external pressure overcome the barrier, the film became unstable and finally ruptures to allow direct contact of solid surfaces, causing the coagulation of particles.

At the same time, Dutch scientists Verwey and Overbeek published a similar concept of predicting the stability of colloidal dispersion[5]. Instead of using pressure, they introduced a total interaction energy (V_t) between two particles, and assumed that the V_t is expressed by the sum of two energy components, an electrostatic energy component (V_e) and a London–van der Waals energy component (V_d). The origin of each energy component is the same as Π_e and Π_d, respectively. Then the equation becomes:

$$V_t = V_e + V_d \,. \qquad [1.\ 2]$$

Although the functional forms of V_e and V_d as to the separation distance of surfaces are different from those of Π_e and Π_d, the V_e still decays exponentially with distances and V_d

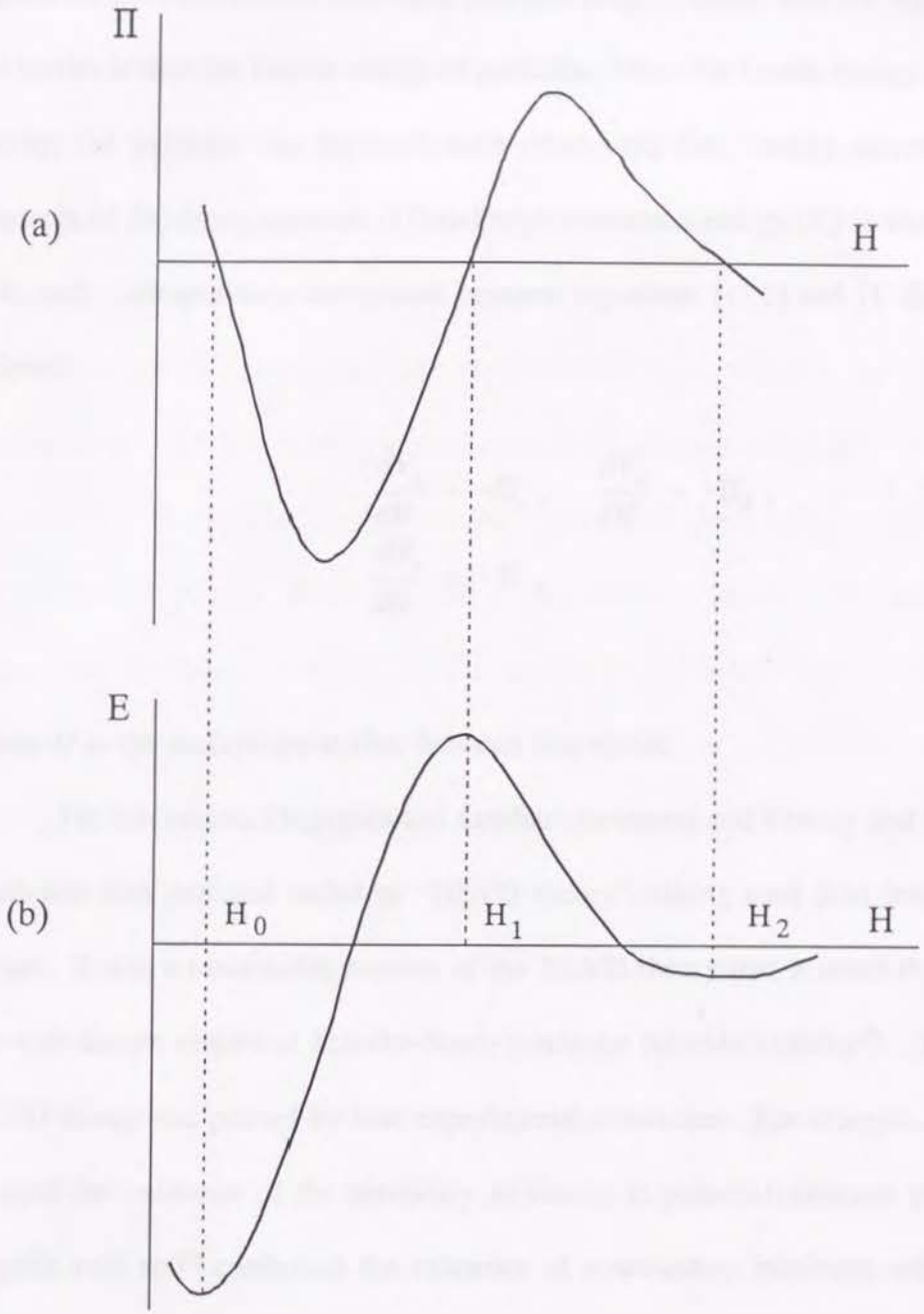

Fig. 1. 1 Schematic diagrams of (a): disjoining pressure (Π) vs. distance (H) and (b): interaction energy (E_1) vs. distance.

decays with a power law. Therefore, there is usually an energy barrier at intermediate surface separation as in the case of disjoining pressure (Fig. 1. 1(b)). The driving force to overcome the barrier is then the kinetic energy of particles. When the kinetic energy exceeds the energy barrier, the particles can approach each other until they contact directly. Therefore the concepts of disjoining pressure (Π) and total interaction energy (V_t) is virtually the same. In fact, each corresponding component between equations [1. 1] and [1. 2] can be related as follows:

$$\frac{dV_e}{dH} = -\Pi_e , \quad \frac{dV_d}{dH} = -\Pi_d , \quad \frac{dV_t}{dH} = -\Pi , \qquad [1.\ 3]$$

where H is the surface separation between two solids.

For this reason, Derjaguin and Landau's treatment and Verwey and Overbeek's one are combined into one and called as "DLVO theory", taking each first letter from scientists' names. It was a remarkable success of the DLVO theory that it could theoretically explain the well known empirical Schultz–Hardy's rule on colloid's stability[5]. The validity of the DLVO theory was proved by later experimental researches. For example, the DLVO theory predicts the existence of the secondary minimum in potential–distance curve. A study on tungstic acid sol[6] confirmed the existence of a secondary minimum where the reversible coagulation of tungstic acid particles was observed. Not only colloidal particles, the theory was also applied to macroscopic bodies. Researches on the equilibrium thickness of soap films in the air[7] found that the thickness was close to that of predicted by the DLVO theory. It was also reported that the coalition of mercury droplets in aqueous electrolyte solution was able to be explained by the DLVO theory[8].

Despite its time-honored success, the application of the DLVO theory has its limitations. The stability of lyophilic colloids cannot be described by the DLVO theory. It is believed that lyophilic colloids are stabilized by the solvation of their surfaces[9]. A polymer often forms a lyophilic colloid being dissolved in a suitable solvent. It also adsorbs onto lyophobic colloidal particles and changes their surfaces into lyophilic. In both cases the colloidal particles are stabilized by a steric repulsion originated in the superposition of polymer segments. The quantitative evaluation of steric repulsion and the incorporation of it with the DLVO theory have been conducted by many researchers[10-14].

In addition to the polymer colloids, the DLVO theory still has difficulties to describe some colloidal systems. When water is the dielectric medium in which colloidal particles are suspended, the theory generally fails to predict the stabilities of very hydrophilic and very hydrophobic particle suspensions. Colloidal suspensions of hydrophilic particles such as silica show an anomalous stability, and will not coagulate even when the surface potential of silica is very small[15]. On the contrary, hydrophobic particles such as methylated silica coagulate in spite of high surface potentials[16-17]. The flotation of mineral particles is another example. The process is based on the hetero-coagulation[18] between hydrophobized particles and hydrophobic air bubbles. This hetero-coagulation often occurs when both V_e and V_d between a bubble and a particle is repulsive[19], and, therefore, V_t becomes infinitely repulsive as the bubble and particle approach each other. In this case, a bubble-particle attachment is impossible according to the DLVO theory.

Since the development of surface force apparatus[20], it has been reported that interaction energies other than V_e and V_d exist for very hydrophobic surfaces and very hydrophilic surfaces. For the case of hydrophobic surfaces, Israelachvili and Pashley[21] were the first to directly measure the extraneous force on surfactant(CTAB)-coated mica surfaces.

They and other investigators[22-26] showed that the non-DLVO force was attractive and could be 10-100 times larger than the London-van der Waals force. This non-DLVO force is now referred to as *hydrophobic force* or *hydrophobic attraction*. Israelachvili and Pashley showed that hydrophobic force (F) varied exponentially in the 0-10 nm range:

$$F/R = C\exp(-H/D_o) , \qquad [1.4]$$

in which R is the curvature of the mica surface, D_o, a parameter referred to as decay length, and C is the pre-exponential parameter. For very hydrophobic surfaces, whose advancing water contact angles (θ_a) are greater than 90°, however, the hydrophobic force can be best described by double exponential terms. At separation distances below approximately 10 nm, D_o is usually in the range of 1-2 nm[27], while at longer distances it is as long as 10-16 nm[23-24, 28].

For hydrophilic surfaces, the existence of non-DLVO forces was recognized much earlier. Derjaguin and Zorin[29] and Pashley and Kitchener[30] measured the disjoining pressure at the quartz-water-air interface to be much larger than those due to the electrostatic and dispersion forces, both of which are repulsive. More recently, many investigators conducted surface force measurements with mica[31-34] and glass[35-37] and confirmed the existence of the repulsive non-DLVO force. It is a much shorter range force than the attractive hydrophobic force, D_o being in the range of 0.6-1.1 nm for 1:1 electrolytes. This non-DLVO force is now referred to as *hydration force* or *hydration repulsion*. The hydration force is strongly dependent on the type and concentration of electrolytes present in solution. For the case of mica, the hydration force becomes stronger with the increasing electrolyte concentration. The hydration force also becomes stronger with the increasing hydration energy of the cations involved[29],[34], however, the concentration at which the hydration force becomes significant

increases with the increasing hydration energies of the cations[32-33]. Pashley[33] showed that the hydration force for mica immersed in various 1:1 electrolyte solutions is best described by a double exponential function, the first (D_1) and the second (D_2) decay lengths being in the range of 0.17–0.3 nm and 0.60–1.10 nm, respectively. The values of D_2 are 2.0 and 3.0 nm, respectively, for electrolytes of divalent and trivalent cations, which are more strongly hydrated than monovalent cations[38].

One reason that the DLVO theory fails with very hydrophobic and hydrophilic particle suspensions is that the medium (water) separating the surfaces has been treated as a structureless continuum. This approach may be applicable at large separation distances. At short distances from the surface, however, the medium may have a discrete structure that may be significantly different from that of the bulk. Evidence for this is given by the oscillation of the repulsive hydration forces measured on mica surfaces[27,39]. As has been noted by Derjaguin and Churaev[40], the classical DLVO theory may be applicable only for those lyophobic colloids, for which the bulk property of the medium extends up to the surface of the particle. The non–DLVO forces can be generally referred to as the structural forces. For the colloids which exhibit the structural forces, one can write an extended form of the classical DLVO theory as follows:

$$V_t = V_e + V_d + V_s , \qquad [1.5]$$

in which V_s is the structural energy. For the lyophobic (partially wetting) colloids V_s may be considered to be zero.

At present, there is no theoretical basis of determining V_s, and it should be determined experimentally. Direct force measurement using the surface force apparatus[20] is the most exact method to evaluate the V_s. However, it requires that the sample should be molecularly

smooth, very thin (a few μm), transparent and having the same thickness for 1 cm x 1 cm square dimensions. This condition limits the possibility of materials for experimental samples. Therefore, most direct force measurements have been conducted using mica with only few exceptions, glass and fused silica. As to various oxide, sulfide and metal particles used in many industrial processes and products, it has not been found a method to apply the direct force measurement. It is, therefore, the objective of this study to present a method of estimating V_s for oxides in aqueous media with their coagulation experiment. As will be shown, oxides may be categorized into two groups, silica type which develops a primary hydration repulsion, and mica type which develops a secondary hydration repulsion.

The second chapter of this article will deal with the primary hydration force observed with silica suspensions[41-42] and a concept of estimating the magnitude of hydration repulsion will be presented. The secondary hydration force with rutile suspensions[43-44] will be discussed in the third chapter. In the forth chapter, the secondary hydration force with stannic oxide suspensions[45] will be discussed with the mechanism of primary and secondary hydration forces. The effect of alcohols and an alkyl amine salt on hydration force will be investigated in the fifth chapter, where a hydrophobic attraction caused by the adsorption of alkyl amine on oxide surfaces will also be discussed[46]. In the sixth chapter, the hydration forces with the hetero-coagulation between silica and stannic oxide will be discussed, and the effect of polymer to promote the selective coagulation will be reported[47].

1. 1 References

1. Klein, B., Laskowski, J.S., and Mular, A.L., Proceedings of 11th International Coal Preparation Congress, **1**, 51, Tokyo, Japan (1990)
2. Culp, R.L., and Culp, G.L., "Advanced wastewater treatment," 17, Van Nostrand Reinhold, New York (1971)
3. Somasundaran, P., "Fine particles processing," ed. Somasundaran, P., **2**, 947, Amer. Inst. Min. Metallur. Petrol. Eng., New York (1980)
4. Derjaguin, B.V., and Landau, L.D., *USSR Acta Phisicochim.*, **14**, 633 (1941)
5. Verwey, E.J., and Overbeek, J.Th.G., "Theory of the stability of lyophobic colloids," 66, Elsevier, New York (1948)
6. Hachisu, S., and Furusawa, K., *Science of Light*, **12**, 157 (1963)
7. Lyklema, J., and Mysels, K.J., *J. Amer. Chem. Soc.*, **87**, 2539 (1965)
8. Watanabe, A., and Gotoh, R., *Kolloid Z.*, **191**, 36 (1963)
9. Overbeek, J.Th.G., and Bungenberg de Jong, H.G., "Colloid Science," ed. Kruyt, H.R., **2**, 197, Elsevier, New York (1949)
10. Mackor, E.L., *J. Colloid Sci.*, **6**, 492 (1951)
11. Fischer, E.W., *Kolloid Z.*, **160**, 120 (1958)
12. Clayfield, E.J., and Lumb, E.C., *J. Colloid Interface Sci.*, **22**, 285 (1966)
13. Meier, D.J., *J. Phys. Chem.*, **71**, 1861 (1967)
14. Napper, D.H., *J. Colloid Interface Sci.*, **32**, 106 (1970)
15. Allen, L.H., and Matijević, E., *J. Colloid Interface Sci.*, **31**, 287 (1969)
16. Xu, Z., and Yoon R.H., *J. Colloid Interface Sci.*, **132**, 532 (1989)
17. Xu, Z., and Yoon R.H., *J. Colloid Interface Sci.*, **134**, 427 (1990)
18. Hogg, T., Healy, T.W., and Fuerstenau, D.W., *Trans. Faraday Soc.*, **62**, 1638 (1966)

19. Laskowski, J., and Kitchener, J.A., *J. Colloid Interface Sci.*, **29**, 670 (1969)

20. Israelachvili, J.N., and McGuiggan P.M., *J. Mater. Res.*, **5**, 2223 (1990)

21. Israelachvili, J.N., and Pashley, R.M., *J. Colloid Interface Sci.*, **98**, 500 (1984)

22. Pashley, R.M., McGuiggan, P.M., Ninham, B.W., and Evans, D.F., *Science*, **229**, 1088 (1985)

23. Claesson, P.M., and Christenson, H.K., *J. Phys. Chem.*, **92**, 1650 (1988)

24. Rabinovich, Ya.I., and Derjaguin, B.V., *Colloids and Surfaces*, **30**, 243 (1988)

25. Parker, J.L., Cho, D.L., and Claesson, P.M., *J. Phys. Chem.*, **93**, 6121 (1989)

26. Tsao, Y., Yang,.S.X., Evans, D.F., and Wennerstrom, H., *Langmuir*, **7**, 3154 (1991)

27. Israelachvili, J.N., *Surface Science Reports*, **14**, 111 (1992)

28. Christenson, H., and Claesson, P.M., *Science*, **239**, 390 (1988)

29. Derjaguin, B.V., and Zorin, Z.M., Proceedings of the 2nd International Congress of surface Activity, **2**, 14, Butterworths, London (1957)

30. Pashley, R.M., and Kitchener, J.A., *J. Colloid Interface Sci.*, **71**, 491 (1979)

31. Israelachvili, J.N., and Adams G.E., *J. Chem. Soc. Faraday Trans. I*, **74**, 975 (1978)

32. Pashley, R.M., *J. Colloid Interface Sci.*, **83**, 531 (1981)

33. Pashley, R.M., *Adv. Colloid Interface Sci.*, **16**, 57 (1982)

34. Pashley, R.M., *Chem. Scr.*, **25**, 22 (1985)

35. Rabinovich, Ya.I., Derjaguin, B.V., and Churaev, N.V., *Adv. Colloid Interface Sci.*, **16**, 63 (1982)

36. Rabinovich, Ya.I., and Derjaguin, B.V., *Langmuir*, **3**, 625 (1987)

37. Horn, R.G., Smith, D.T., and Haller, W., *Chem. Phys. Lett.*, **162**, 404 (1989)

38. Pashley, R.M., and Quirk, J.P., *Colloids and Surfaces*, **9**, 1 (1984)

39. Pashley, R.M., and Quirk, J.P., *Soil Sci. Am. J.*, **53**, 1660 (1989)

40. Derjaguin, B.V., and Churaev, N.V., *Colloids and Surfaces*, **41**, 223 (1989)

41. Yotsumoto, H., and Yoon, R.H., *J. Colloid Interface Sci.*, **157**, 434 (1993)

42. Yotsumoto, H., Yoon, R.H., Wakamatsu, T., Ito, S., and Sakamoto, H, *Shigen To Sozai*, **109**, 909 (1993)

43. Yotsumoto, H., and Yoon, R.H., *J. Colloid Interface Sci.*, **157**, 426 (1993)

44. Yotsumoto, H., Yoon, R.H., Wakamatsu, T., Ito, S., and Sakamoto, H, *Shigen To Sozai*, **109**, 613 (1993)

45. Yotsumoto, H., Yoon, R.H., Wakamatsu, T., Ito, S., and Sakamoto, H, *Resources Processing, in press*

46. Yotsumoto, H., Yoon, R.H., Wakamatsu, T., Ito, S., and Sakamoto, H, *Shigen To Sozai, in press*

47. Yotsumoto, H., and Wakamatsu, T, *Resources Processing*, **35**, 131 (1988)

Chapter 2 Primary hydration force with silica

2. 1 Objective of research

It is well known that silica exhibits exceptional stability. Allen and Matijević[1]showed that Ludox HS precipitated silica does not coagulate in acidic pH where the electrophoretic mobility is minimum. Even at alkaline pH where coagulation does occur, the electrolyte concentration required is significantly higher than predicted by the DLVO theory[2-3]. The resistance to coagulation is not limited to the precipitated silica, which has high concentrations of silanol groups. Harding[4] showed that anomalous stability is also exhibited by a pyrogenic silica with small particle diameters but not with large particles. Watillon and Gérard[5] attributed the exceptional stability of silica suspensions to the presence of an immobilized surface water layer, perhaps one molecule deep.

These findings point to the likelihood that silica is subjected to a repulsive hydration force not considered in the DLVO theory. The first direct evidence for the hydration force was given by Derjaguin and Zorin[6] in 1955, who measured the disjoining pressure at the glass–water–air interface as a function of the film thickness. The measured pressure was larger than the sum of the London–van der Waals and electrostatic components, both of which are repulsive at the asymmetric interface. The excess pressure is now considered due to the hydration force[7]. More recently, Pashley and Kitchener[8] showed that the disjoining pressure measured at the quartz–water–air interface is significantly larger than that calculated using Langmuir's equation of electrostatic interaction[9-10] and the non retarded Hamaker constant. They also showed that even the heat–dehydroxylated quartz exhibits considerable hydration force, which is in agreement with the surface force measurements conducted by Horn et al.[11] with fused silica. Further evidence for the existence of the repulsive hydration force was

given by Rabinovich et al.[12], who measured significant hydration force with glass fibers. Interestingly, their investigations showed evidence that the hydration force decreases with increasing KCl concentration, which is contrary to the cases with mica[13-15].

In this chapter, turbidity measurement was conducted with aqueous suspensions of precipitated silica in order to confirm the existence of the hydration force, and the magnitude of it was evaluated, which has not been achieved even by the surface force measurements. The results will be discussed using the extended DLVO theory.

2. 2 Model development

2. 2. 1 Extended DLVO theory

According to the constant potential model, the electrostatic energy (V_e) between two identical spheres is given by:

$$V_e = \frac{\varepsilon a \psi_\delta^2}{2} \ln\{1 + \exp(-\kappa H)\}, \qquad [2.\ 1]$$

where ε is the dielectric constant of water, a the particle radius, ψ_δ the Stern potential which is often substituted by ζ-potential as an approximation, κ the Debye parameter, and H is the closest approach distance between the spheres.

The London-van der Waals energy (V_d) is expressed as:

$$V_d = -\frac{aA_{131}}{12H} f, \qquad [2.\ 2]$$

where A_{131} is the Hamaker constant of particles 1 interacting in a medium 3 (water). f is the correction factor for the retardation effect[16] and is given by:

$$f = \frac{1}{1+1.77p} , \qquad [2.\ 3]$$

where $p=2\pi H/\lambda$. λ is the wavelength of the intrinsic electronic oscillations, and is usually assumed to be 100 nm. Eq.[2. 3] is valid for $p \leq 0.5$. When $p>0.5$, the following relationship can be used:

$$f = \frac{2.45}{5p} - \frac{2.17}{15p^2} + \frac{0.59}{35p^3} . \qquad [2.\ 4]$$

As suggested by Pashley[14], the structural (hydration) energy (V_s) may be described by a double-exponential function:

$$V_s = \frac{a}{2}\{C_1 D_1 \exp(-H/D_1) + C_2 D_2 \exp(-H/D_2)\} , \qquad [2.\ 5]$$

where C_1, C_2 are the pre-exponential parameters and D_1, D_2 are the decay lengths.

The total interaction energy (V_t) can be given by the summation of Eqs. [2. 1],[2. 2] and [2. 5]:

$$V_t = V_e + V_d + V_s . \qquad [2.\ 6]$$

Fig. 2. 1 represents a typical plot of Eq.[2. 6] versus H. V_t will go through the energy barrier E_1 at H_1 and a secondary energy minimum E_2 at H_2. If the kinetic energies of particles are smaller than E_2, coagulation will occur with an equilibrium interparticle distance of H_2. If the kinetic energies are larger than E_2 and E_1, but smaller than the sum of the primary energy minimum (not shown in Fig. 2. 1) and E_1, coagulation will occur at a distance smaller than H_1.

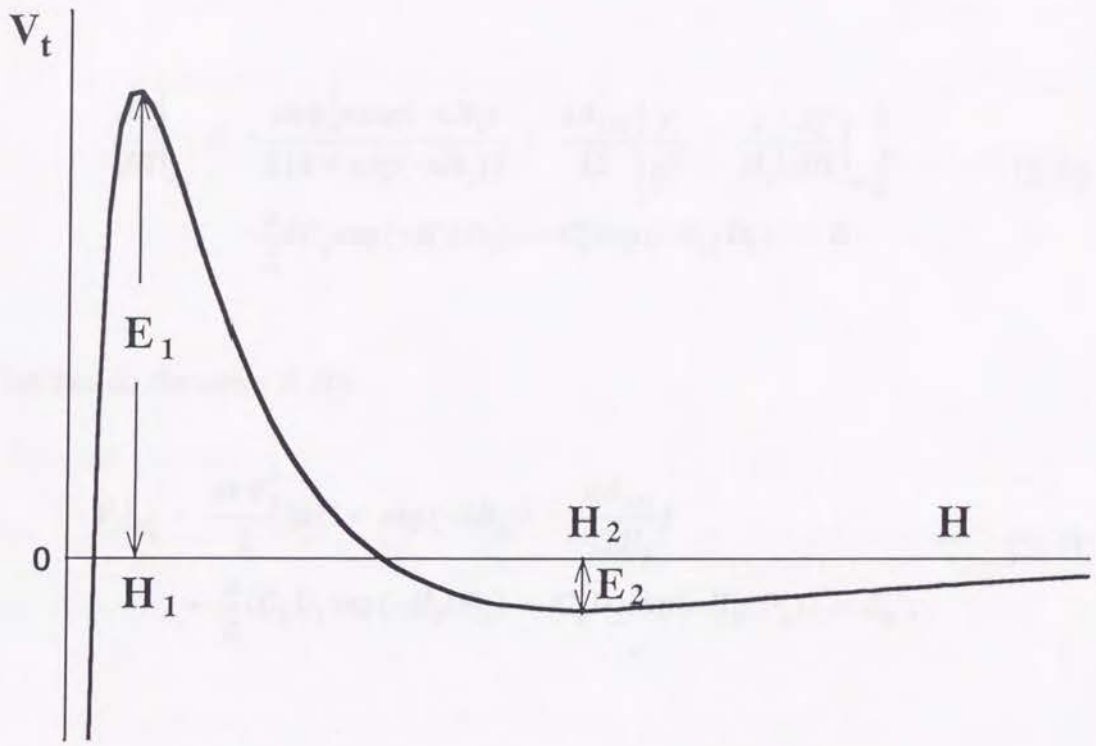

Fig. 2. 1 Potential energy (V_t) vs. distance (H) diagram. E_1 represents the energy barrier and E_2 the secondary energy minimum.

With reference to the V_t vs. H diagram shown in Figure 2. 1, one can write the following boundary conditions at H_1:

$$V_t|_{H_1} = \frac{a\varepsilon\psi_\delta^2}{2}\ln\{1+\exp(-\kappa H_1)\} - \frac{aA_{131}}{12H_1}f + \frac{a}{2}\{C_1D_1\exp(-H_1/D_1) + C_2D_2\exp(-H_1/D_2)\} = E_1 , \quad [2.\ 7]$$

and

$$\left.\frac{dV_t}{dH}\right|_{H_1} = -\frac{a\varepsilon\psi_\delta^2\kappa\exp(-\kappa H_1)}{2[1+\exp(-\kappa H_1)]} + \frac{aA_{131}}{12}\left\{\frac{f}{H_1^2} - \frac{1}{H_1}\left(\frac{df}{dH}\right)_{H_1}\right\} - \frac{a}{2}\{C_1\exp(-H_1/D_1) + C_2\exp(-H_1/D_2)\} = 0 . \quad [2.\ 8]$$

One can do the same at H_2:

$$V_t|_{H_2} = \frac{a\varepsilon\psi_\delta^2}{2}\ln\{1+\exp(-\kappa H_2)\} - \frac{aA_{131}}{12H_2}f + \frac{a}{2}\{C_1D_1\exp(-H_2/D_1) + C_2D_2\exp(-H_2/D_2)\} = E_2 , \quad [2.\ 9]$$

and

$$\left.\frac{dV_t}{dH}\right|_{H_2} = -\frac{a\varepsilon\psi_\delta^2\kappa\exp(-\kappa H_2)}{2[1+\exp(-\kappa H_2)]} + \frac{aA_{131}}{12}\left\{\frac{f}{H_2^2} - \frac{1}{H_2}\left(\frac{df}{dH}\right)_{H_2}\right\} - \frac{a}{2}\{C_1\exp(-H_2/D_1) + C_2\exp(-H_2/D_2)\} = 0 . \quad [2.\ 10]$$

Eqs. [2. 7]–[2. 10] have eight unknown parameters, i.e., C_1, C_2, D_1, D_2, E_1, E_2, H_1, and H_2. If four of these parameters are known, the equations can be solved simultaneously to determine the rest of parameters. In the present work, E_1 is determined from turbidity

measurements as will be described later, while E_2 is assumed to be −3 kT. The choice of such a small E_2 value implicitly suggests that coagulation of silica is induced by the primary rather than the secondary minimum.

Eqs. [2. 7]–[2. 10] are then solved using different values of D_1 and D_2 at a given pH and electrolyte concentration. There are many combinations of D_1 and D_2 that give solutions. With each solution, one can calculate the values of V_s using Eq. [2. 5]. Assuming that V_s changes with electrolyte concentration but not pH, one can calculate the values of E_1 for the data points obtained at other pH values using Eq. [2. 7]. The turbidity data obtained at various pH's are then plotted against the E_1 values obtained as such. Of the various sets of D_1 and D_2 values that give solutions, the one that gives the best correlation between turbidity and E_1 is chosen.

2. 2. 2 Hamaker constant

The Hamaker constant (A_{11}) of a solid in vacuum can be obtained from the dispersion component of surface tension of the solid (γ_s^d) using the following relationship[17]:

$$A_{11} = 6\pi r_{11}^2 \gamma_s^d , \qquad [2. 11]$$

in which r_{11} is the inter-atomic distance and $6\pi r_{11}^2$ is often assumed to be 1.44×10^{-18} m^2 for water and systems with volume elements such as oxide ions, metal atoms, CH_2 or CH groups which have nearly the same size. The Hamaker constant of solid in water A_{131} is given by:

$$A_{131} \fallingdotseq (\sqrt{A_{11}} - \sqrt{A_{33}})^2 , \qquad [2. 12]$$

where A_{33} is the Hamaker constant of water. Substituting Eq. [2. 11] for A_{11} and A_{33} into Eq. [2. 12], one can obtain:

$$A_{131} = 1.44x10^{-18}(\sqrt{\gamma_s^d} - \sqrt{\gamma_w^d})^2 , \qquad [2.\ 13]$$

where γ_w^d (=21.8x10^{-3} N/m)[17] is the dispersion component of the surface tension of water.

In the present work, γ_s^d has been determined using the following relationship:

$$\sqrt{\gamma_s^d} = \frac{\gamma_2 - \gamma_1 + \gamma_{13}\cos\theta_1 - \gamma_{23}\cos\theta_2}{2(\sqrt{\gamma_2^d} - \sqrt{\gamma_1^d})} , \qquad [2.\ 14]$$

where θ_1 is the contact angle of liquid 3 (water) on a solid immersed in liquid 1, θ_2 is the same in liquid 2, γ_1 and γ_2 are the surface tensions of liquid 1 and 2, γ_1^d and γ_2^d are their dispersion components, and γ_{13} and γ_{23} are the interfacial tensions.

2. 3 Experimental

2. 3. 1 Sample preparation

A reagent grade precipitated silica was obtained from Wako Chemicals. The sample was ground in a steel ball mill, boiled first in a 6 N HCl solution for 2 hours and then in a conc. HNO_3 solution for 5 hours to remove iron and organic impurities. This cleaning procedure was similar to the method employed by Pashley and Kitchener[8]. After the acid leaching, the silica was washed repeatedly by double distilled water until the pH of the supernatant water reached 5.8. The sample was then filtered and dried in a vacuum desiccator at ambient temperature. The median size of the silica powder was 1.07 μm as measured by a Microtrack particle size analyzer. The dried powder was re-dispersed in conductivity water at 1 wt% solids and used as feed stock for preparing particle suspensions for ζ-potential and turbidity measurement.

2. 3. 2 Contact angle measurement

The fused silica plate used for contact angle measurement was of optical grade, and was cleaned by boiling in conc. HNO_3 for 5 hours followed by washing with conductivity water and drying under nitrogen. This procedure was the same as employed for cleaning the Wako precipitated silica. Cyclohexane, octane and decane are chosen as liquid 1 and 2 of Eq. [2. 14]. The contact angles of water droplets were measured through the hydrocarbon phase using a Ramé-hart goniometer.

2. 3. 3 ζ-potential measurement

The zeta potentials of silica sample were measured at 20 °C using a Pen Kem Laser Zee 3000 particle electrophoresis apparatus. An aliquot of the 1 % stock suspension was diluted to 120-240 ppm in a NaCl solution of known concentration, and the pH was adjusted by adding NaOH or HCl solutions. The suspension was agitated by means of a magnetic stirrer for 10 minutes before taking the measurement. The ζ-potentials were calculated from the mobility measurement using the Smoluchowski's equation[18].

2. 3. 4 Turbidity measurement

The turbidity of silica suspensions was measured at ambient temperature using a Brice-Phoenix DM2000 light scattering apparatus. Applying blue light the wave length of which was 436 nm, the intensity of transmitted light (I_0) and that of 90° scattered light (I_{90}) were measured for each suspension. The ratio of I_{90}/I_0 was regarded as the turbidity of the suspension. The 1 % stock solution was diluted to 300 ppm in an NaCl solution of known concentration and pH. The dilute suspension was agitated at approximately 200 rpm for 10 minutes in a 50 ml beaker by means of a Teflon-coated magnetic bar before transferring to

the light scattering apparatus. The turbidity was measured after 10 minutes of settling time in the apparatus, and the pH was recorded after the turbidity measurement. It was found that the turbidities did not change significantly when the agitation speed was varied in the range of 200–400 rpm.

2. 4 Analysis on the stability of silica suspensions

2. 4. 1 Analysis using the classical DLVO theory

Table 2. 1 shows the contact angle data, which were used for calculating γ_s^d of the fused silica plate using Eq. [2.14]. The surface and interfacial tension data used for the calculation were taken from Ref. 17. The γ_s^d values were then used for the calculations of A_{131} using Eq. [2. 13]. An average of 1.2×10^{-20} J was obtained as the value of A_{131}, which is in agreement with the theoretical ($0.83–1.4\times10^{-20}$ J)[19-22] and experimental (1.35×10^{-20} J)[12] results reported by others.

Table 2. 1 Contact angles of water droplet on fused silica soaked in various hydrocarbons

	Cyclohexane –Octane	Octane –Decane	Decane –Cyclohexane	Average
θ_1 (°)	22	17	22	–
θ_2 (°)	17	22	22	–
γ_s^d (mN/m)	57	53	62	57
A_{131} (10^{-20} J)	1.2	1.0	1.5	1.2

The ζ–potential measurements conducted in different concentrations of NaCl solutions are shown in Fig. 2. 2. Although the ζ–potentials of silica becomes less negative with decreasing pH, its i.e.p. cannot be clearly defined. One can see that the ζ–potentials become less negative with increasing electrolyte concentrations due to double layer compression.

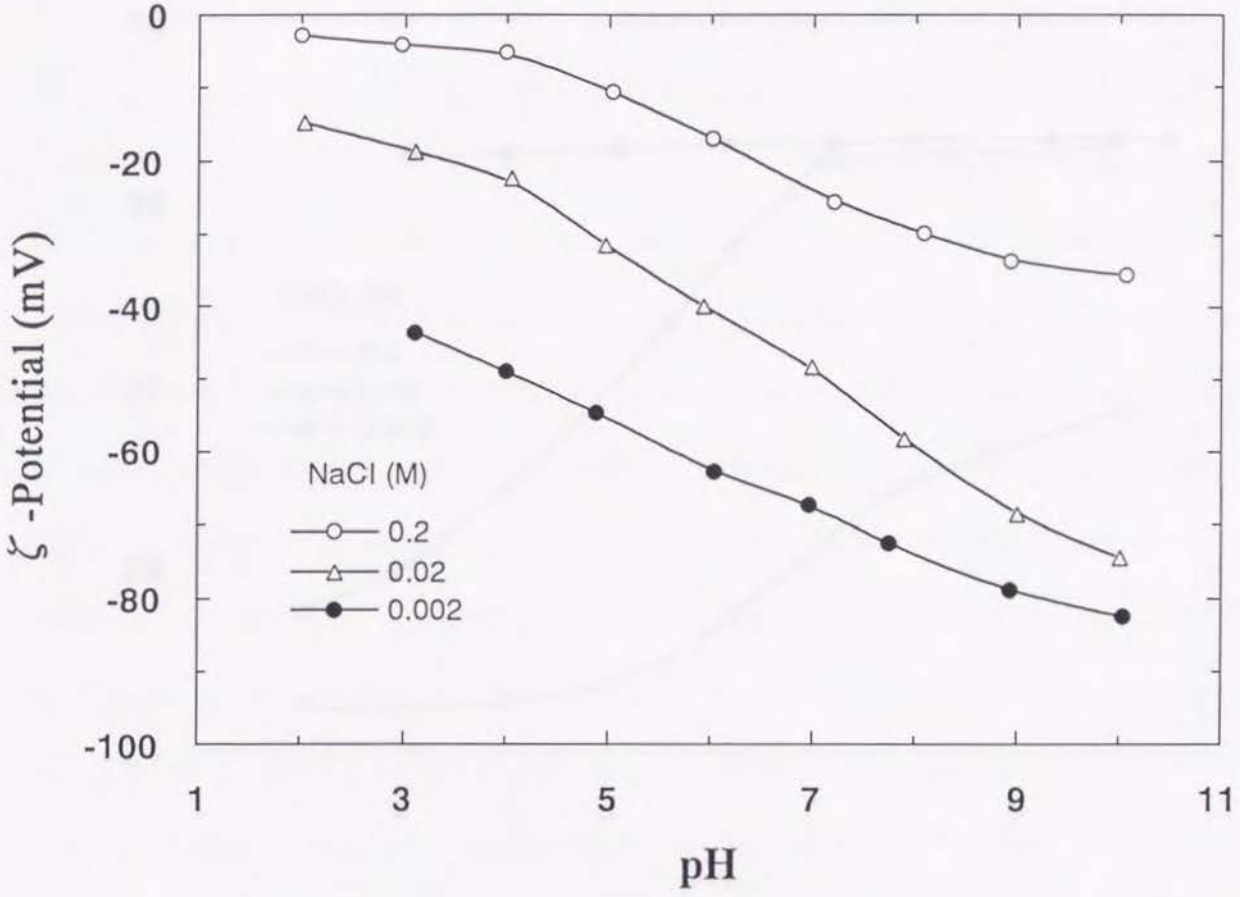

Fig. 2. 2 ζ–potential measurements conducted with precipitated silica as a function of pH at different NaCl concentrations.

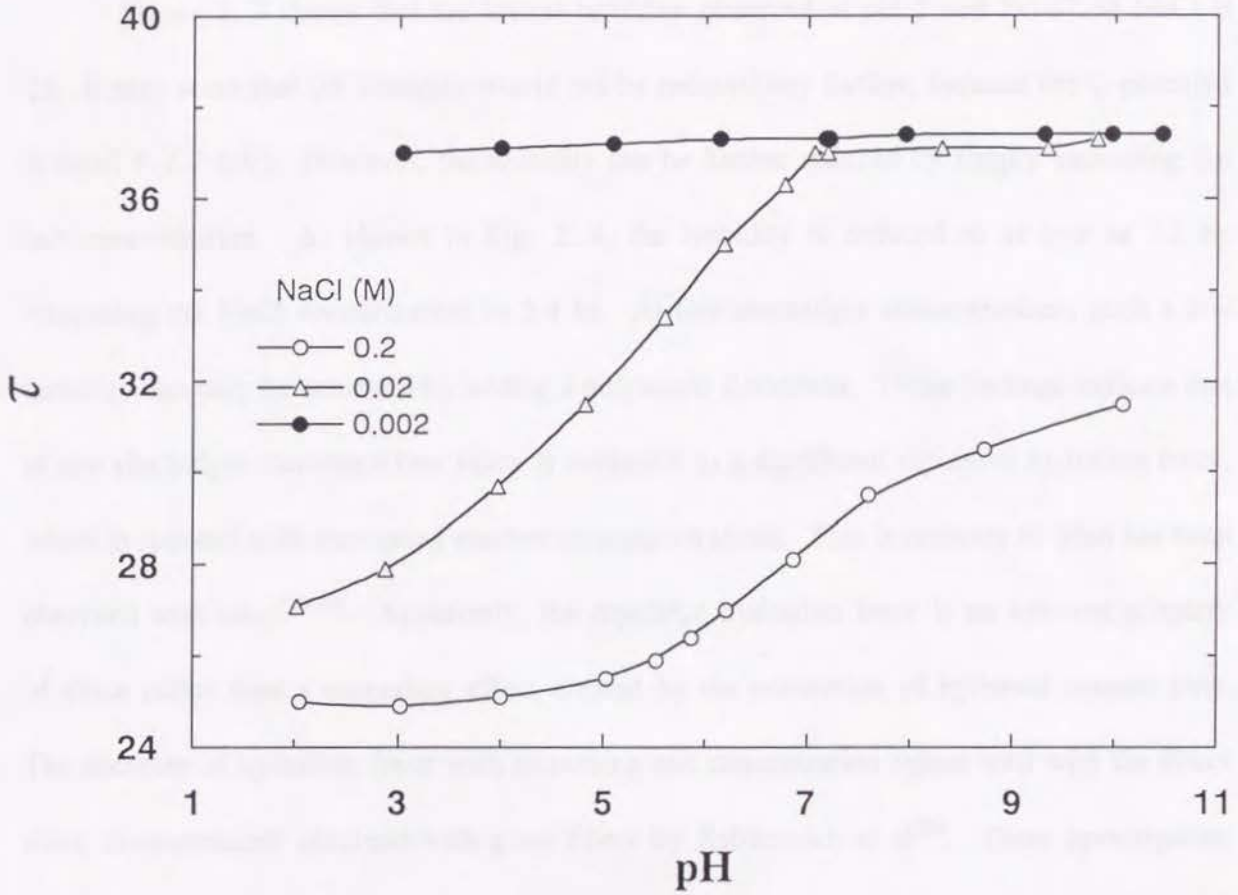

Fig. 2. 3 Turbidity (τ) measurements conducted with precipitated silica as a function of pH at different NaCl concentrations.

The turbidities (τ) of silica suspensions measured in different NaCl concentrations are shown in Fig. 2. 3. At $2x10^{-3}$ M NaCl, the silica suspension is stable throughout the entire pH range studied. The silica suspension is also stable at $2x10^{-2}$ M NaCl at alkaline pH where the ζ–potentials are high, but the stability begins to decrease sharply below pH 7 where ζ= –48.3mV. At $2x10^{-1}$ M, the turbidity is as low as 31.5 at pH 10, where the ζ–potential is –35.5 mV due to the double layer compression, and then further reduced with decreasing pH.

Figure 2. 3 shows that the lowest turbidity observed at pH 2 and $2x10^{-1}$ M NaCl is 25. It may seem that the turbidity would not be reduced any further, because the ζ–potential is small (–2.7 mV). However, the turbidity can be further reduced by simply increasing the salt concentration. As shown in Fig. 2. 4, the turbidity is reduced to as low as 7.1 by increasing the NaCl concentration to 5.4 M. At low electrolyte concentrations, such a low turbidity can only be achieved by adding a polymeric flocculant. These findings indicate that at low electrolyte concentrations silica is subjected to a significant repulsive hydration force, which is reduced with increasing electrolyte concentrations. This is contrary to what has been observed with mica[13–15]. Apparently, the repulsive hydration force is an inherent property of silica rather than a secondary effect created by the adsorption of hydrated counter ions. The decrease of hydration force with increasing salt concentration agrees well with the direct force measurements obtained with glass fibers by Rabinovich et al[23]. These investigators showed that the hydration force decreases when KCl concentration is increased from $1.1x10^{-4}$ to $1x10^{-2}$ M; however, the concentration dependency of the hydration force is discernable only at separation distances larger than approximately 2.5 nm. It is also shown in Fig. 2. 4 that the decrease of turbidity is larger at alkaline pH when NaCl concentration is between 1 and 4 M, suggesting that the repulsive hydration force decreases with increasing pH at these NaCl concentrations, because the contributions from V_e to V_t is actually zero due to the double layer

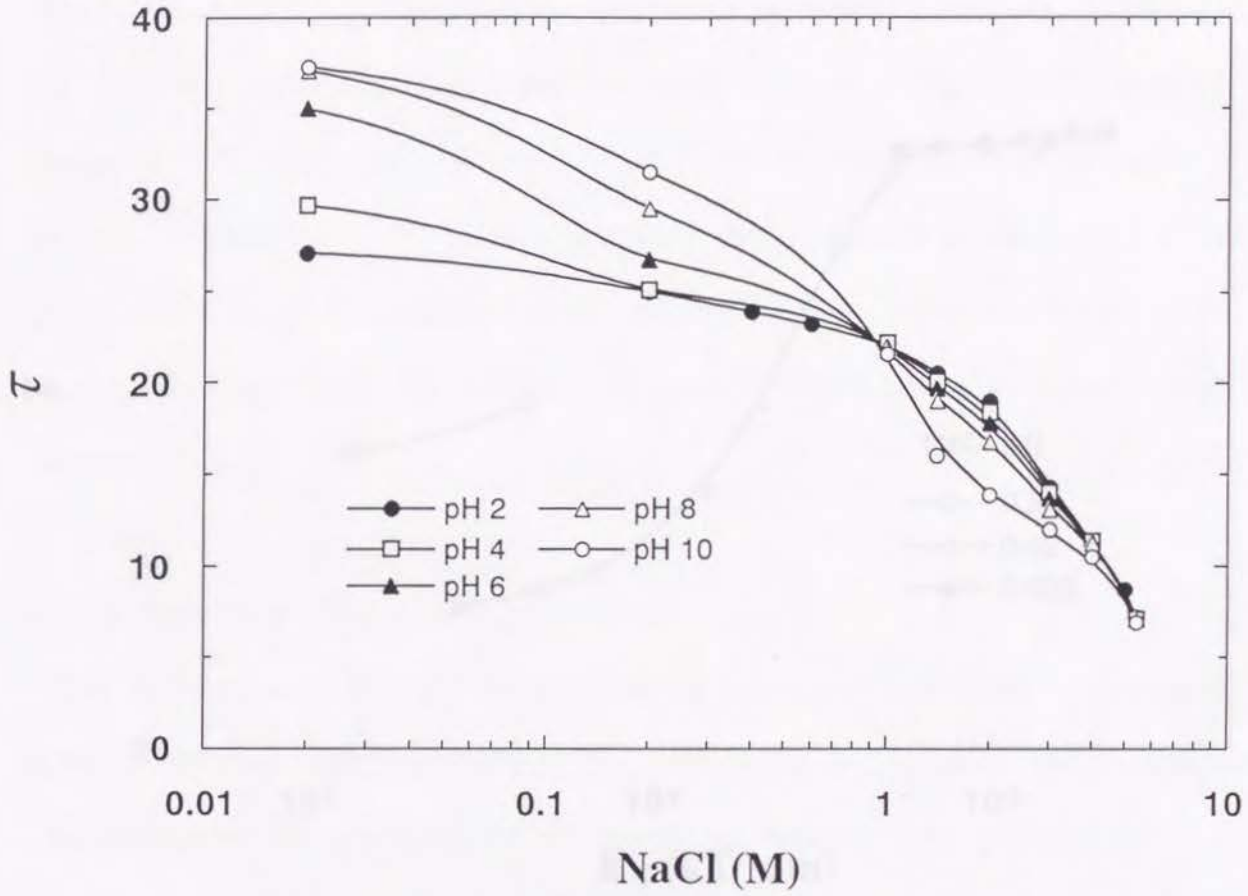

Fig. 2. 4 Turbidities (τ) of silica suspensions at various pH shown as a function of NaCl concentration.

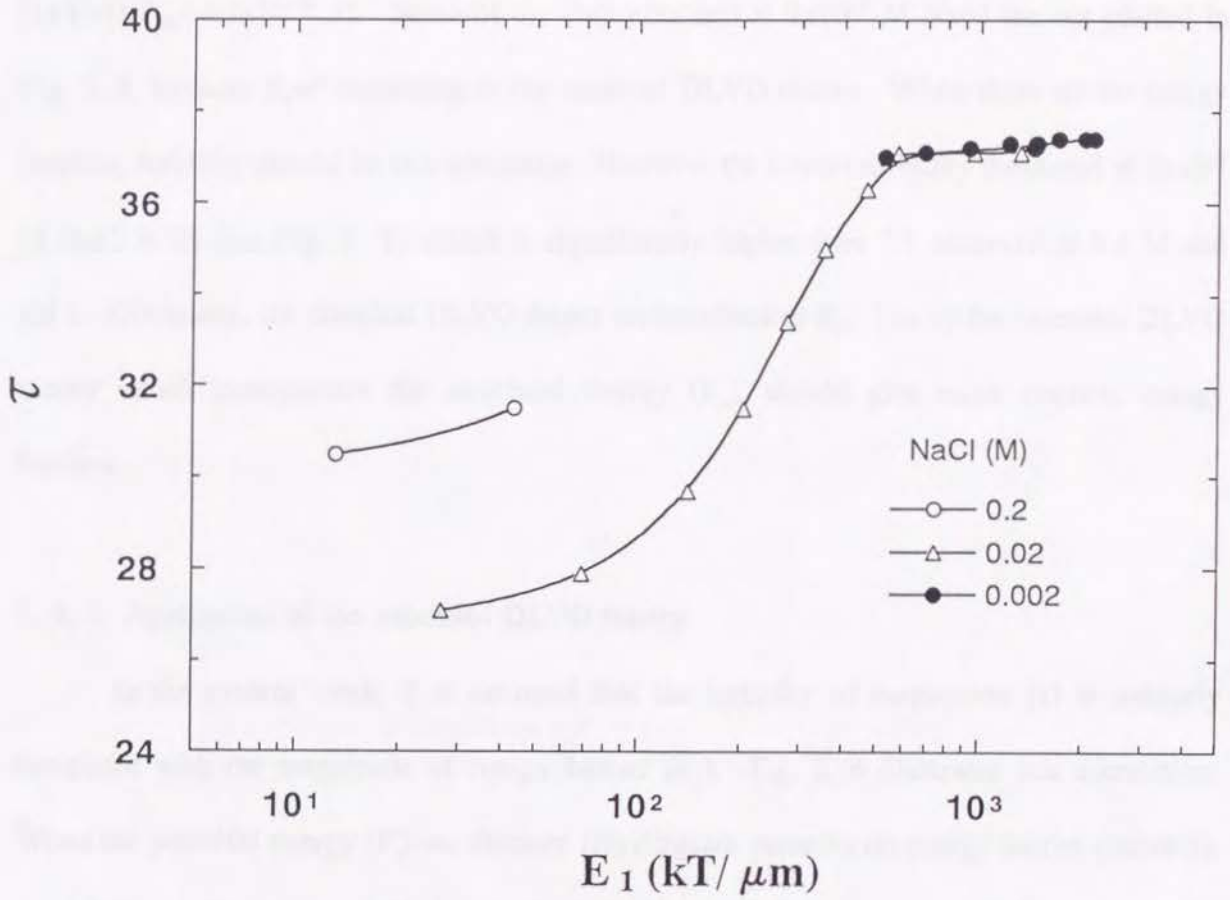

Fig. 2. 5 Turbidities (τ) of silica suspensions plotted vs. energy barriers (E_1) calculated using the classical DLVO theory. Some of the data points obtained at $2x10^{-1}$ M are not shown because of the negative total interaction energy (V_t).

compression at these salt concentrations.

Fig. 2. 5 shows the turbidity (τ) vs. energy barrier (E_1) plots obtained for the data in Fig. 2. 3. The energy barriers were calculated using the classical DLVO theory on the basis of the ζ–potentials (Fig. 2. 2) and the Hamaker constant (A_{131}=1.2x10^{-20} J) obtained in the present work. All the calculations of E_1 in this chapter and following chapters were conducted for a particle of 1 μm diameter and the obtained E_1 was expressed with unit kT (1kT=1kT$_{298}$=4.1x10^{-21} J). Some of the data obtained at 2x10^{-1} M NaCl are not plotted in Fig. 2. 5, because $E_1 \leq 0$ according to the classical DLVO theory. When there are no energy barriers, turbidity should be at a minimum. However the lowest turbidity measured at 2x10^{-1} M NaCl is 25 (see Fig. 2. 3), which is significantly higher than 7.1 observed at 5.4 M and pH 2. Obviously, the classical DLVO theory underestimates E_1. Use of the extended DLVO theory which incorporates the structural energy (V_s), should give more realistic energy barriers.

2. 4. 2 Application of the extended DLVO theory

In the present work, it is assumed that the turbidity of suspension (τ) is uniquely correlated with the magnitude of energy barrier (E_1). Fig. 2. 6 illustrates this correlation. When the potential energy (V_t) vs. distance (H) diagram presents no energy barrier (curve 1), coagulation will occur spontaneously and the turbidity will reach a minimum. As the electrostatic interaction energy (V_e) increases, e.g., by increasing pH or decreasing NaCl concentration, the energy barrier increases (curves 2–3), stabilizing the suspension and, hence, increasing the turbidity (τ). Thus, τ is uniquely defined by E_1. The discrepancy between this concept and Fig. 2. 5 is attributed to the fact that the classical DLVO theory does not include structural energy (V_s). As will be shown later, V_s is so determined as to give only one

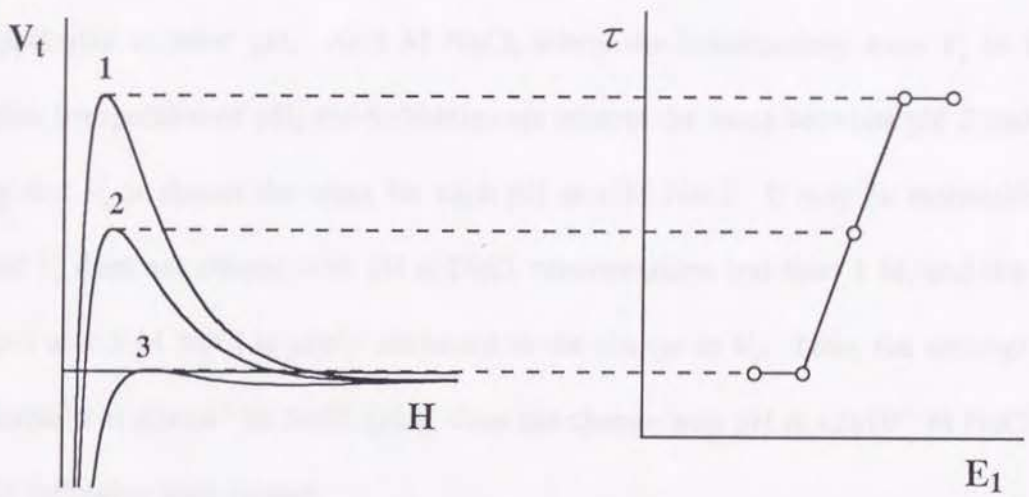

Fig. 2. 6 Relationship between energy barrier (E_1) and turbidity (τ). The height of each V_t vs. H curve represents E_1.

correlation curve between τ and E_1 for all the NaCl concentrations.

Fig. 2. 4 shows that the turbidity decreases with increasing electrolyte concentration. The changes are gradual at low concentrations, but the slope becomes steeper above 1.4 M NaCl. At very high concentrations, V_s may become insignificantly small, resulting in a small E_1 and, hence, a more complete coagulation. Between $2x10^{-1}$ M and 5.4 M NaCl at pH 2, the changes in V_e are minimal because ζ-potentials are already very small (−2.7 mV) at $2x10^{-1}$ M; therefore, the changes in τ may be attributed solely to the changes in V_s. On the other hand, as the NaCl concentration is reduced further from $2x10^{-1}$ to $2x10^{-2}$ M, the ζ-potentials become significantly more negative, i.e., from −2.7 to −14.8 mV. In this region, the small changes in τ may be attributed largely to the changes in V_e. Therefore, it may be reasonable to assume that V_s remains constant at $\leq 2x10^{-1}$ M NaCl. The same discussion may be also applicable to other pH. At 1 M NaCl, where the contributions from V_e to V_t is actually zero irrespective of pH, the turbidities are almost the same between pH 2 and 10, suggesting that V_s is almost the same for each pH at 1 M NaCl. It may be reasonable to assume that V_s does not change with pH at NaCl concentrations less than 1 M, and that the changes in τ at < 1 M NaCl is solely attributed to the change in V_e. Thus, the assumption: (a) V_s is constant at $\leq 2x10^{-1}$ M NaCl, (b) V_s does not change with pH at $\leq 2x10^{-1}$ M NaCl are used in the following calculations.

In order to determine the contributions from V_s to V_t and, hence, to E_1, it is necessary to determine the four parameters (C_1, C_2, D_1 and D_2) of Eq. [2. 5]. As has already been discussed, these parameters can be obtained by solving Eqs. [2. 7]–[2. 10] to find the solutions that can best correlate all the τ values with E_1. In the present work, the solutions of four equations have been obtained by treating E_1, E_2, D_1 and D_2 as known parameters. While E_1 can be determined from turbidity measurements and E_2 is assumed to be small, D_1

and D_2 are actually unknowns. Therefore, Eqs. [2. 7]–[2. 10] can only be solved iteratively.

At $2x10^{-1}$ M NaCl, pH 2, τ is 25 as shown in Fig. 2. 4. Considering that this value is much greater than 7.1 at 5.4 M, there should be an energy barrier E_1 which is greater than zero. The value of this E_1 is arbitrarily assumed to be 100 kT and this particular E_1 may be designated as E_1^{25} to distinguish it from others. As for the value of E_2, an assumption is made that the coagulation of silica is induced by the primary energy minimum, which requires that the secondary minimum be shallow. In the present work, it is arbitrary assumed that E_2=–3 kT.

Using the values of E_1 and E_2 obtained as described above, Eqs. [2. 7]–[2. 10] have been solved using different values of D_1 and D_2. The results show, however, that when D_1<1 nm, only D_2 in the neighborhood of 3 nm can satisfy the assumption of shallow secondary minimum as will be shown later. Although the value of D_1 is assumed arbitrarily, the most probable one can be determined by the following procedures. For each set of D_1 and D_2=3.0 nm, C_1 and C_2 are obtained by solving the equations, and V_s can be calculated by Eq. [2. 5]. Assuming that V_s does not change with pH, the values of E_1 are then calculated using the extended DLVO theory (Eq. [2. 6]) for all the turbidity measurements obtained in $2x10^{-3}$ to $2x10^{-1}$ M NaCl solutions of various pH's. By plotting τ vs. E_1, one can determine how all the turbidity data can be correlated with E_1. Fig. 2. 7 schematically shows the change of this correlation depending on what value is assumed for D_1. If large D_1 is taken, the τ–E_1 curve of 0.2 M is placed above that of 0.02 M and the unique relationship between τ and E_1 cannot be obtained (Fig. 2. 7(a)). If small D_1 is assumed, the curve of 0.2 M is placed beneath that of 0.02 M (c). When an appropriate D_1 is assumed, the both curves is combined into one τ–E_1 correlation curve, and this D_1 is regarded as the most probable one (b).

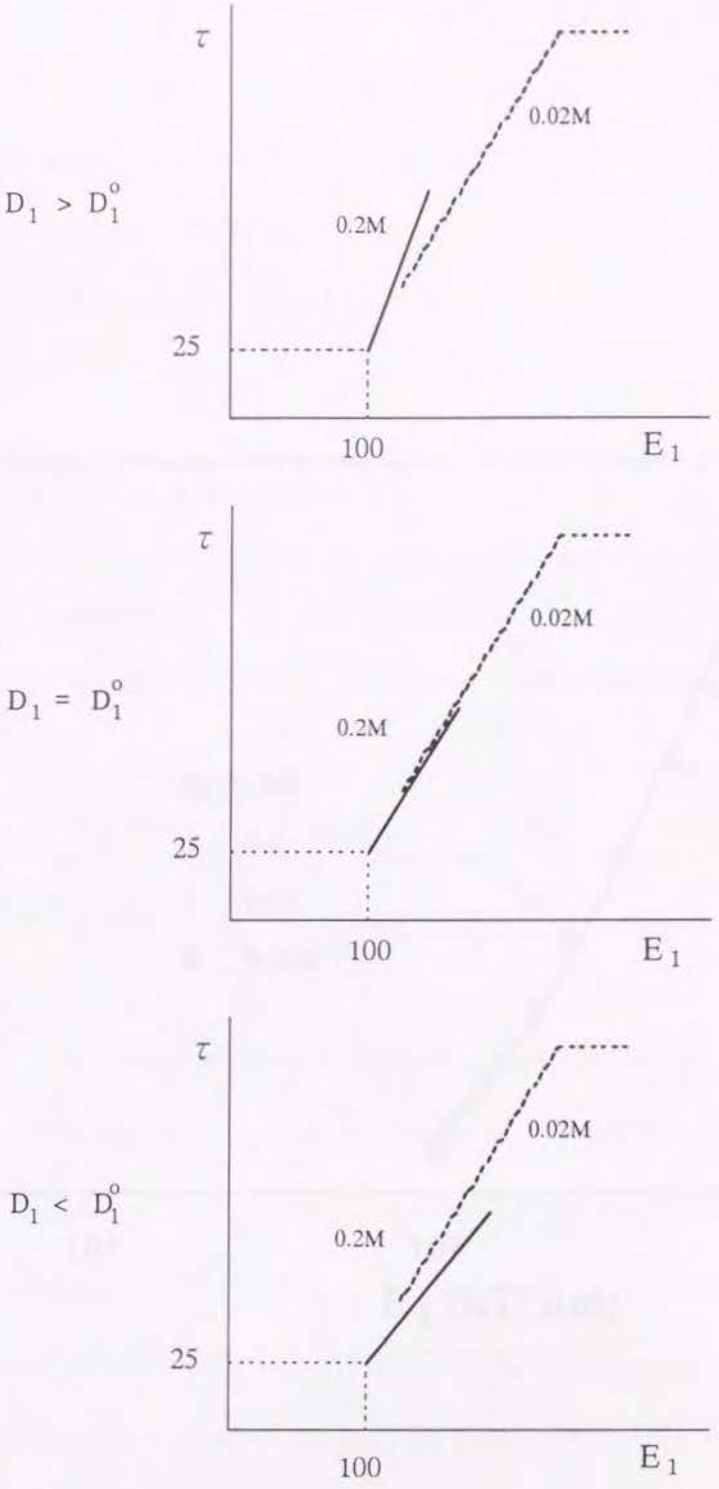

Fig. 2. 7 The change in turbidities (τ) vs. energy barrier (E_1) diagram by adding the structural energy (V_s) having different decay lengths (D_1). When D_1 equals to a certain value (D_1^o), a unique correlation is obtained.

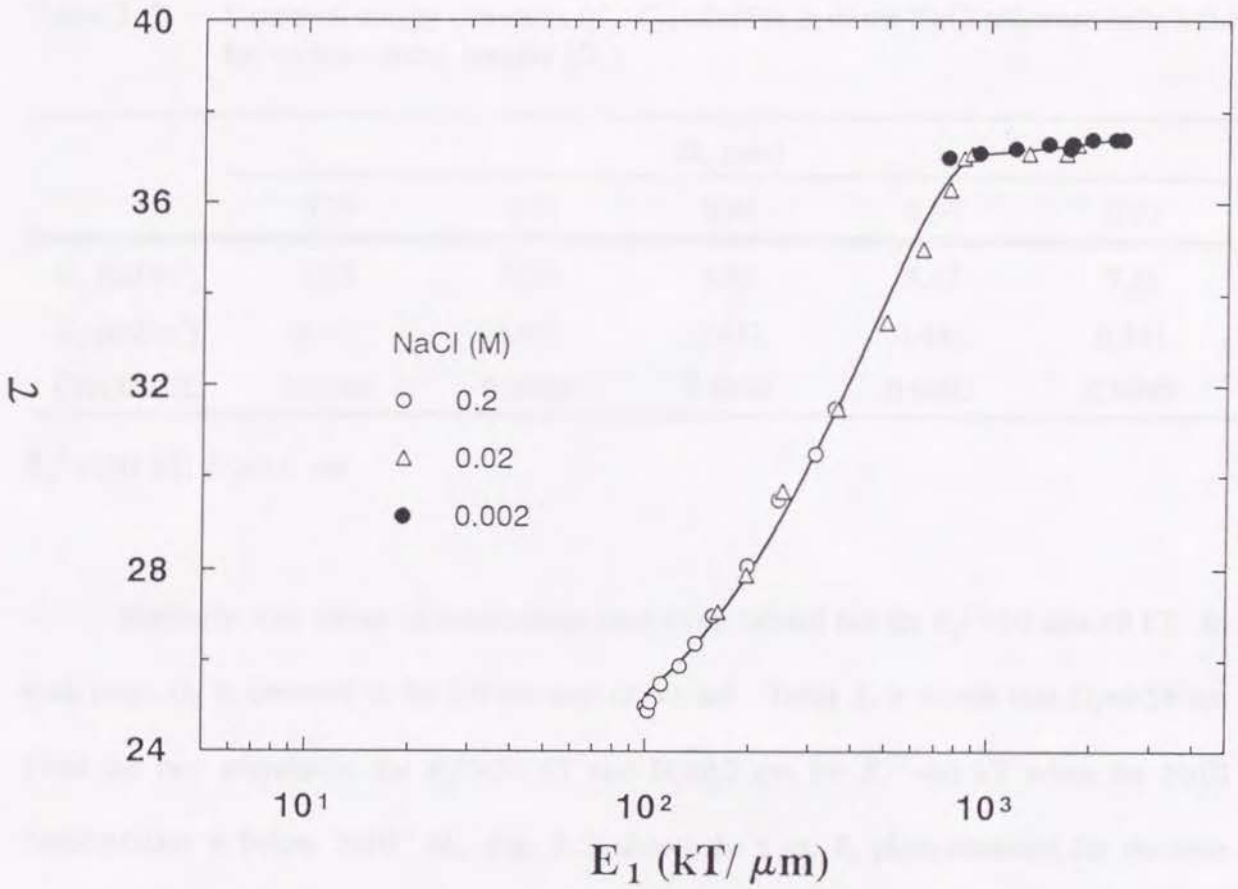

Fig. 2. 8 Turbidities (τ) vs. energy barriers (E_1) calculated using the extended DLVO theory. The contributions from structural energy (V_s) were calculated assuming that E_1=100 kT at $2x10^{-1}$ M and pH 2.0. This energy barrier corresponds to τ=25.

Table 2. 2 shows that of the various D_1 values used in the present work, D_1=0.84–0.86 nm gives the best correlation. Fig. 2. 8 shows the τ vs. E_1 plots obtained using 0.84 nm D_1 for the turbidity measurements conducted at $\leq 2\times10^{-1}$ M NaCl. The fact that all the data obtained in NaCl solutions of different concentrations and pH's are fitted by a single curve demonstrates the utility of the extended DLVO theory.

Table 2. 2 Structural energy constants (C_1, C_2) of silica in dilute NaCl solutions calculated for various decay lengths (D_1).

	D_1 (nm)				
	0.70	0.82	0.84	0.86	0.92
C_1 (mJ/m^2)	12.3	9.23	8.84	8.47	7.51
C_2 (mJ/m^2)	0.441	0.441	0.441	0.441	0.441
Corr.Coeff.	0.9981	0.9989	0.9990	0.9990	0.9989

E_1^{25}=100 kT, D_2=3.0 nm

Similarly, two series of calculations have been carried out for E_1^{25}=30 and 60 kT. In each case, D_2 is assumed to be 3.0 nm and D_1 varied. Table 2. 3 shows that D_1=0.58 nm gives the best correlation for E_1^{25}=30 kT and D_1=0.7 nm for E_1^{25}=60 kT when the NaCl concentration is below 2×10^{-1} M. Fig. 2. 9 shows the τ vs. E_1 plots obtained for the case considered. Also shown are the τ vs. E_1 plots for the data obtained at $>2\times10^{-1}$ M NaCl (filled symbols). The E_1 values at $>2\times10^{-1}$ M NaCl have been obtained by extrapolating the results obtained below 2×10^{-1} M NaCl (for which τ >25). Among the E_1 values at $>2\times10^{-1}$ M NaCl, those at pH 2 are given in Table 2. 4. Also shown in this table are the C_1 values for the case of E_1^{25}=100 kT using the same D_1 (=0.84 nm) as for $\leq 2\times10^{-1}$ M NaCl.

Table 2. 3 Structural energy constants (C_1, C_2) obtained assuming various E_1^{25} and D_1.

	D_1 (nm)				
	0.40	0.56	0.58	0.60	0.70
C_1 (mJ/m^2)	27.4	12.9	12.0	11.1	7.84
C_2 (mJ/m^2)	0.441	0.441	0.441	0.441	0.441
Corr. Coeff.	0.9940	0.9977	0.9978	0.9977	0.9968

E_1^{25}=30 kT, D_2=3.0 nm

	D_1 (nm)				
	0.50	0.68	0.70	0.72	0.80
C_1 (mJ/m^2)	19.7	10.6	9.98	9.43	7.65
C_2 (mJ/m^2)	0.441	0.441	0.441	0.441	0.441
Corr. Coeff.	0.9956	0.9977	0.9978	0.9977	0.9975

E_1^{25}=60 kT, D_2=3.0 nm

Table 2. 4 Energy barriers (E_1) at pH 2.0 in different NaCl solutions and structural energy constants (C_1) calculated for the case of E_1^{25}=100 kT. The E_1 values are calculated by extrapolating the E_1–τ relationship obtained for data at < 2x10^{-1} M NaCl.

		NaCl (M)						
		0.4	1.0	2.0	3.0	4.0	5.0	5.4
E_1(kT)	E_1^{25}=30 kT	17.9	5.4	0.4	0	0	0	0
	E_1^{25}=60 kT	41.9	21.5	5.2	0.3	0	0	0
	E_1^{25}=100 kT	80.1	54.1	25	6.7	2.8	1.2	0.7
	C_1 (mJ/m^2)*	7.99	6.69	4.91	3.13	2.24	1.30	0.77

*: D_1=0.84 nm, C_2=0.441 mJ/m^2, D_2=3.0 nm

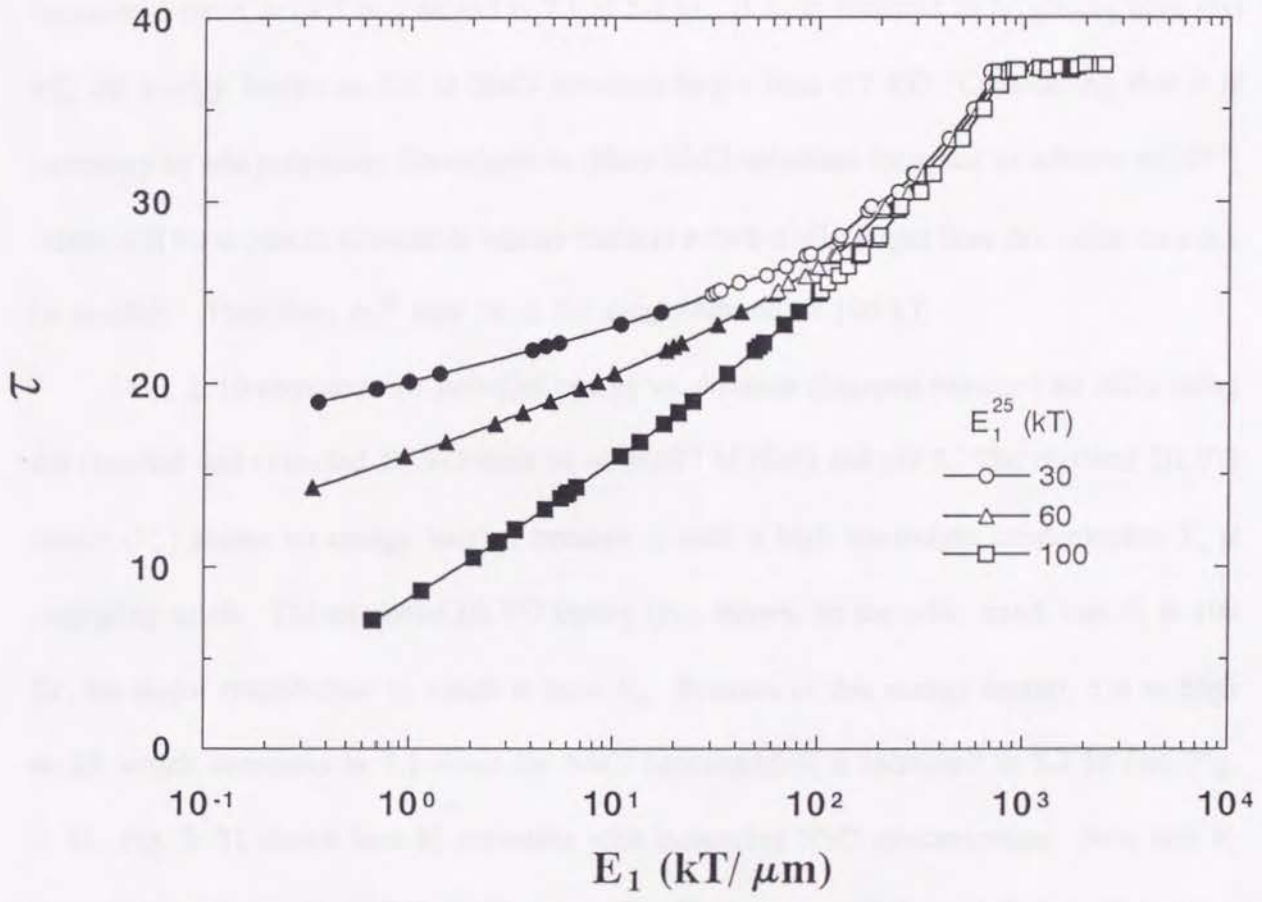

Fig. 2. 9 Turbidities (τ) of silica suspensions plotted vs. energy barriers (E_1) calculated using the extended DLVO theory. Three different cases, in which E_1^{25} is assumed to be 30, 60 and 100 kT, were considered. E_1^{25} is the energy barrier at $2x10^{-1}$ M NaCl and pH 2.0, where τ=25.

Table 2. 4 shows that when E_1^{25}=30 kT, there is no energy barrier at ≥3 M NaCl. This is difficult to accept because the turbidity continues to decrease as the NaCl concentration is increased from 3 M to 5.4 M. The turbidity should be at a minimum and stay the same as long as E_1=0. The same is true for the case of E_1^{25}=60 kT and NaCl concentrations above 4 M. On the other hand, when E_1^{25}=100 kT, E_1 decreases from 6.7 kT at 3 M to 0.7 kT at 5.4 M. These energy barriers provide a reasonable correlation with the turbidity measurements: τ is 14.3 at 3 M and is 7.1 at 5.4 M. If E_1 is assumed to be greater than 100 kT, the energy barrier at 5.4 M NaCl becomes larger than 0.7 kT. Considering that it is necessary to add polymeric flocculants in dilute NaCl solutions for silica to achieve $\tau<10^{(2-4)}$, which will be shown in Chapter 6, energy barriers substantially larger than this value may not be realistic. Therefore, E_1^{25} may be in the neighborhood of 100 kT.

Fig. 2. 10 compares the potential energy vs. distance diagrams obtained for silica using the classical and extended DLVO theories at 2×10^{-1} M NaCl and pH 2. The classical DLVO theory (V_{t1}) shows no energy barrier, because at such a high electrolyte concentration V_e is negligibly small. The extended DLVO theory (V_{t2}) shows, on the other hand, that E_1 is 100 kT, the major contribution to which is from V_s. Because of this energy barrier, τ is as high as 25, which decreases to 7.1 when the NaCl concentration is increased to 5.4 M (see Fig. 2. 4). Fig. 2. 11 shows how V_s decreases with increasing NaCl concentration. Note that V_s reaches a maximum at ≤0.2 M NaCl (curve 1). The parameters C_1, and C_2 for pH 3–10 at >1 M NaCl have been calculated in the same manner. Fig. 2. 12 shows the changes in C_1 with pH, where D_1=0.84 nm, C_2=0.441 mJ/m^2 and D_2=3.0 nm are the same throughout all the pH's and NaCl concentrations. At 1.4 and 2.0 M NaCl, the decrease of C_1 with increasing pH is remarkable as has already been expected from Fig. 2. 4.

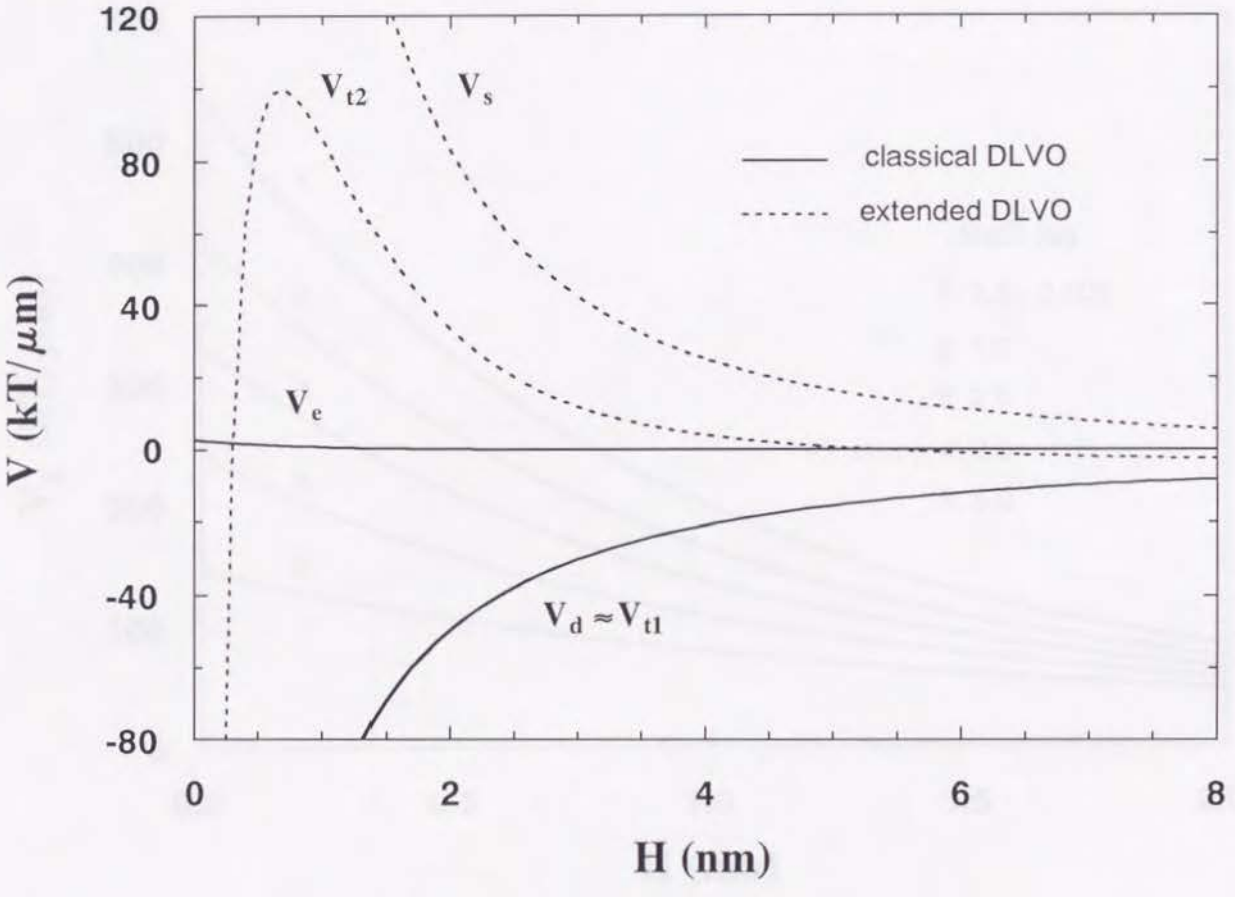

Fig. 2. 10 Potential energies (V) vs. separation distance (H) diagram for silica at $2x10^{-1}$ M NaCl and pH 2.0. The classical DLVO theory gives no energy barrier (E_1), while the extended DLVO theory assumes E_1=100 kT. Because of this energy barrier, the silica suspension gives anomalous stability.

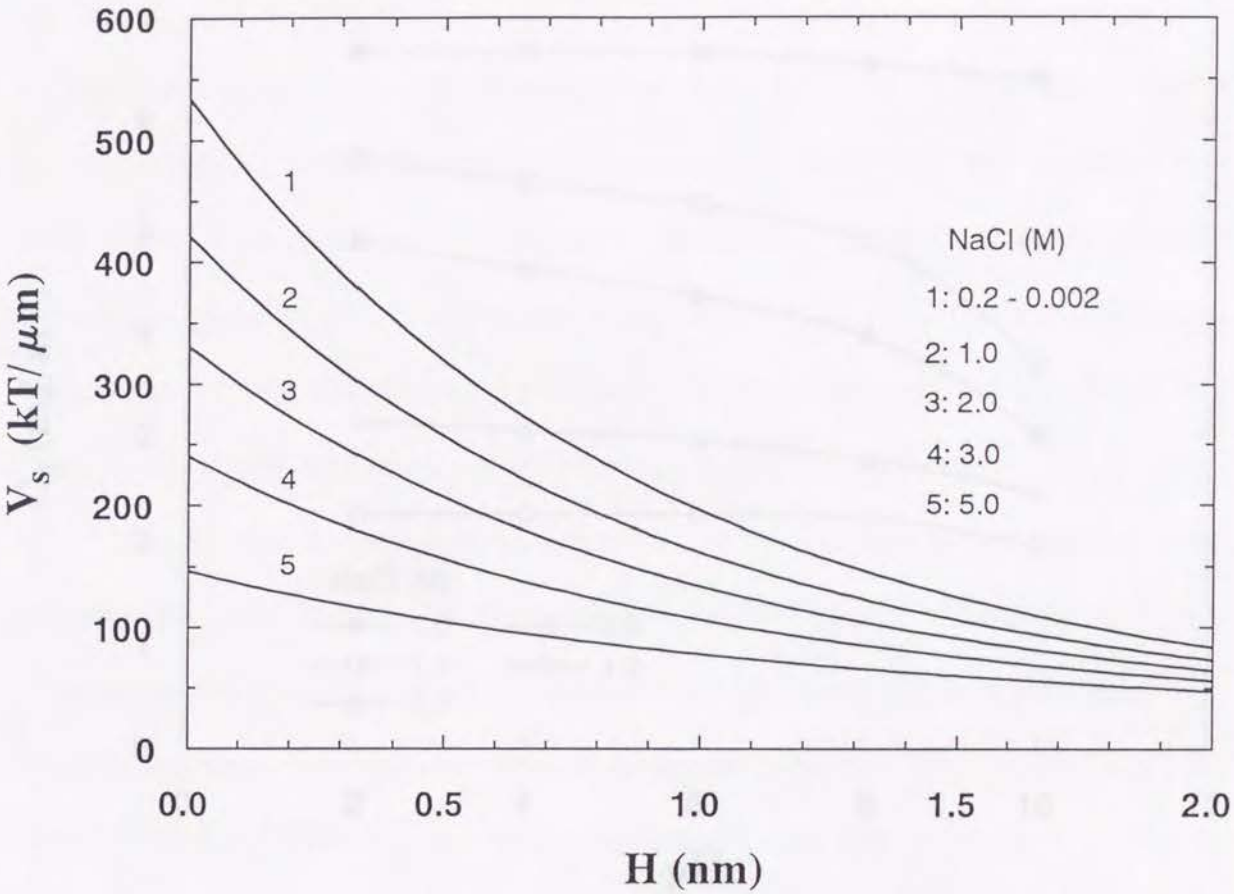

Fig. 2. 11 Structural energy (V_s) vs. separation distance (H) diagrams at various NaCl concentrations at pH 2.0. V_s is shown to decrease with increasing electrolyte concentration.

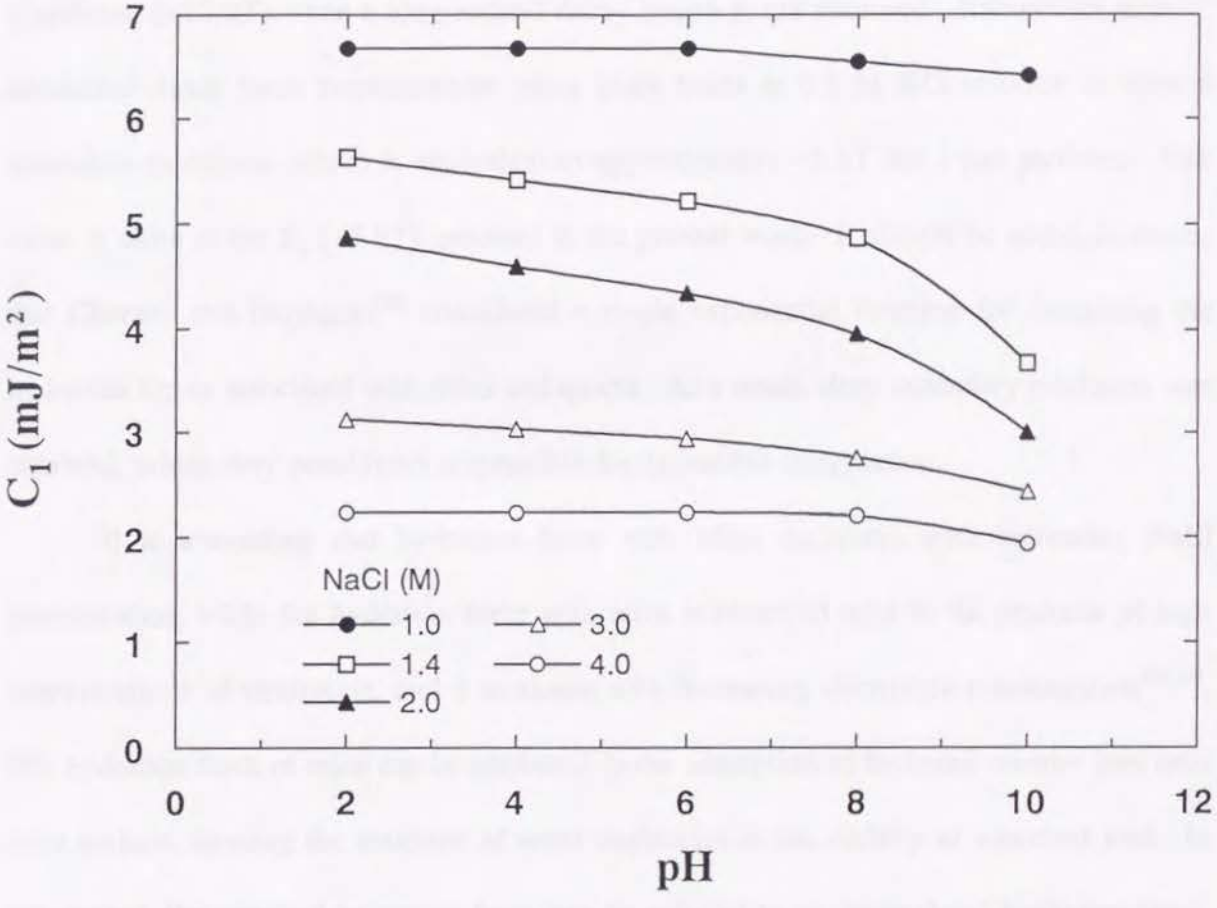

Fig. 2. 12 Structural force constants (C_1) as a function of pH at different NaCl concentrations.

In the present work, the secondary energy minimum (E_2) is assumed to be small, which implies that the coagulation of silica is driven by the primary rather than the secondary energy minimum. This assumption requires a relatively long second decay length (D_2=3.0 nm). As to the validity of the long decay length will be discussed in detail in Chapter 2. Fig. 2. 13 shows V_t vs. H curves at $2x10^{-1}$ M NaCl and pH 2 obtained when D_2=3.0 nm (curve 1) and C_2=0 (single exponential V_s, curve 2). The secondary minimum becomes significant (−15 kT) when a long second decay length is not assumed. Rabinovich et al.[12] conducted direct force measurements using glass fibers in 0.1 M KCl solution to show a secondary minimum, which is equivalent to approximately −5 kT for 1 μm particles. This value is close to the E_2 (−3 kT) assumed in the present work. It should be noted, however, that Churaev and Derjaguin[25] considered a single exponential function for describing the hydration forces associated with silica and quartz. As a result, deep secondary minimum was obtained, which they considered responsible for reversible coagulation.

It is interesting that hydration force with silica decreases with increasing NaCl concentration, while the hydration force with mica is observed only in the presence of high concentrations of electrolyte, and it increases with increasing electrolyte concentration[13-15]. The hydration force of mica can be attributed to the adsorption of hydrated counter ions onto mica surface, forming the structure of water molecules in the vicinity of adsorbed ions. In this regard, the acquired hydration force can be referred to as "secondary" hydration force. On the other hand, the hydration force of silica can be attributed to the strong hydration of silanol groups on its surface, which is inherent property of silica. Thus, the hydration force of silica can be referred to as "primary" hydration force. The difference between "primary" and "secondary" may be attributed to the surface composition of each oxide.

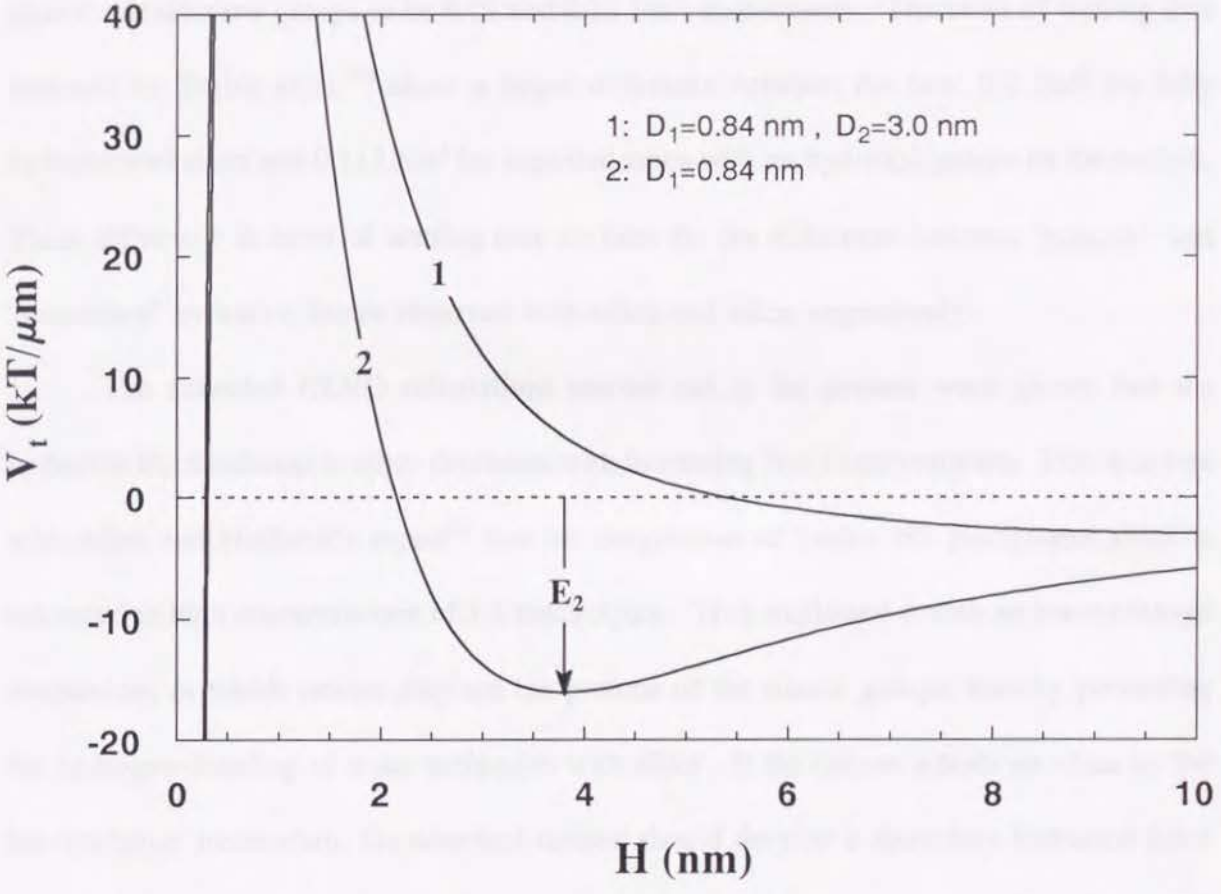

Fig. 2. 13 Total interaction energy (V_t) vs. separation distance (H) diagrams in the cases of double (curve 1) and single (curve 2) exponential functions for the structural energy (V_s).

Although water molecules are also hydrogen bonded to mica surfaces[26-27], it is not likely that the hydrogen bonding is as strong as that on silica because mica surfaces are composed of siloxane groups. When silica is heat-treated, some of the silanol groups transform to siloxane groups as indicated by the decrease in the concentration of hydroxyl groups on the surface[28]. Based on the heats of wetting data obtained with various silica powders of different degrees of surface hydration, Iler[28] estimated the heats of wetting of silanol and siloxane groups to be 0.19 and 0.13 J/m^2, respectively. The heats of wetting data obtained by Taylor et al.[29] show a larger difference between the two: 0.2 J/m^2 for fully hydroxylated silica and 0.117 J/m^2 for annealed silica with no hydroxyl groups on the surface. These difference in heats of wetting may account for the difference between "primary" and "secondary" hydration forces observed with silica and mica, respectively.

The extended DLVO calculations carried out in the present work shows that the hydration force inherent to silica decreases with increasing NaCl concentration. This is in line with Allen and Matijević's report[1] that the coagulation of Ludox HS precipitated silica is enhanced in high concentrations of 1:1 electrolytes. They explained it with an ion-exchange mechanism, in which cations displace the protons of the silanol groups, thereby preventing the hydrogen-bonding of water molecules with silica. If the cations adsorb on silica by the ion-exchange mechanism, the adsorbed cations should develop a secondary hydration force as has been the case with mica. This is contrary to what has been observed in the present work, although it is possible that the amount of hydrated cations adsorbed on silica by the ion-exchange mechanism may not be significant enough to create the secondary hydration force.

Iler[30] proposed a somewhat different hypothesis that hydrated cations act as a bridging agent. He suggested that the sodium ion can bridge two silica particles by having at least two

of its water of hydration displaced by the hydroxyls of the surface silanol groups. The detail of this concept will be discussed in Chapter 4 together with the mechanisms of "primary" and "secondary" hydration forces.

2. 5 Conclusion

As predicted by the classical DLVO theory, the stability of precipitated silica decreases with increasing NaCl concentration. However, the silica suspension is not fully destabilized even when the ζ–potentials are reduced to a minimum. This finding suggests that there is a hydration force not considered in the DLVO theory preventing the coagulation. Therefore, an extended DLVO theory has been developed by incorporating a term representing the hydration force. Based on the turbidity data obtained in the present work, the hydration force parameters have been estimated and used for calculating the structural energy. It has been found that the structural energy is at a maximum in dilute electrolyte solutions and decreases significantly as the NaCl concentration is increased beyond $2x10^{-1}$ M. The extended DLVO theory is useful for predicting the stability of the silica suspensions over a wide range of pH and electrolyte concentrations.

2. 6 References

1. Allen, L.H., and Matijević, E., *J. Colloid Interface Sci.*, **31**, 287 (1969)
2. Derjaguin, B.V., and Landau, L.D., *Acta Physicochim.*, **14**, 633 (1941)
3. Verwey, E.J., and Overbeek, J.Th.G., "Theory of the Stability of Lyophobic Colloids," 66, Elsevier, New York (1948)
4. Harding, R.D., *J. Colloid Interface Sci.*, **35**, 172 (1971)
5. Watillon, A., and Gérard, P., Proceedings of International Congress on Surface Activity, **4**, 1261 (1964)
6. Derjaguin, B.V., and Zorin, Z.M., *Zh. Fiz. Khim.*, **29**, 1755 (1955); Proceedings of the 2nd International Congress on Surface Activity, **2**, 14 (1957)
7. Derjaguin, B.V., Churaev, N.V., and Muller, V.M., "Surface Forces," 231, Consultants Bureau, New York, (1987)
8. Pashley, R.M., and Kitchener, J.A., *J. Colloid Interface Sci.*, **71**, 491 (1979)
9. Derjaguin, B.V., and Churaev, N.V., *J. Colloid Interface Sci.*, **49**, 249 (1974)
10. Langmuir, I., *Science*, **88**, 430 (1938)
11. Horn, R.G., Smith, D.T., and Haller, W., *Chem. Phys. Lett.*, **162**, 404 (1989)
12. Rabinovich, Ya.I., Derjaguin, B.V. and Churaev, N.V., *Adv. Colloid Interface Sci.*, **16**, 63 (1982)
13. Pashley, R.M., *J. Colloid Interface Sci.*, **83**, 531 (1981)
14. Pashley, R.M., *Adv. Colloid Interface Sci.*, **16**, 57 (1982)
15. Pashley, R.M. and Quirk, J.P., *Colloids and Surfaces*, **9**, 1 (1984)
16. Schenkel, J.H., and Kitchener, J.A., *Trans. Faraday Soc.*, **561**, 161 (1960)
17. Fowkes, F.M., *Ind. Chem. Eng.*, **56**, 40 (1964)

18. Overbeek, J.Th.G., and Bungenberg de Jong, H.G., "Colloid Science," ed. Kruyt, H.R., **2**, 194, Elsevier, New York (1949)

19. Gregory, J., *Adv. Colloid Interface Sci.*, **2**, 396 (1970)

20. Visser, J., *Adv. Colloid Interface Sci.*, **3**, 331 (1972)

21. Israelachvili, J.N., "Intermolecular and Surface Forces," 190, Academic Press, London (1985)

22. Rabinovich, Ya.I., and Churaev, N.V., *Colloid J. USSR*, **52**, 256 (1990)

23. Rabinovich, Ya.I., and Derjaguin, B.V., *Langmuir*, **3**, 625 (1987)

24. Yotsumoto, H., and Wakamatsu, T., *Resources Processing*, **35**, 131 (1988)

25. Churaev, N.V., and Derjaguin, B.V., *J. Colloid Interface Sci.*, **103**, 2 (1985)

26. Mathieson, A.M., and Walker, G.F., *Am. Miner.*, **39**, 231 (1954)

27. Slade, P.G., Stone, P.A., and Radosholvich, E.W., *Clays Clay Miner.*, **33**, 51 (1985)

28. Iler, R.K., "The Chemistry of Silica," 622, John Wiley and Sons, New York, (1979)

29. Taylor, J.A.G., Hockey, J.A., and Pethica, B.A., Proceedings of British Ceramic Society, **5**, 133 (1965)

30. Iler, R.K., "The Chemistry of Silica," 375, John Wiley and Sons, New York, (1979)

Chapter 3 Secondary hydration force with rutile

3. 1 Objective of research

Since the development of surface force apparatus[1], it has been reported that a strong repulsive force between two mica samples soaked in aqueous solutions with high electrolyte concentration[2-6]. The force decays exponentially with increasing surface separation, the decay length of which is much shorter than that of an electrostatic repulsion. The force is not considered in the DLVO theory[7-8] and may be attributed to the adsorption of hydrated counter ions on the mica surfaces[9] and successive structure forming of water molecules by hydrogen-bonding.

In the previous chapter, it has been shown that the similar hydration force is observed with aqueous suspensions of silica, where the force is at a maximum in a solution of low electrolyte concentrations and decreases with increasing electrolyte concentration. This is contrary to what has been observed with mica. The force may be attributed to the hydration of surface silanol groups and, is, therefore, inherent to silica, different from the acquired hydration force with mica.

The hydration of surface itself is common to most oxides, while the degree of hydration may be different from each other depending on the surface compositions. Therefore, the hydration force may not be peculiar to mica and silica, and may be observed in other oxides if an appropriate measurement is employed. The coagulation experiment and successive calculations described in the previous chapter is applicable to any oxides particles. It is a distinctive advantage of this method against the surface force measurement, whose requirements for sample preparation is difficult to satisfy for most oxide.

It is, therefore, the objective of this chapter to analyze the coagulation of rutile and

to evaluate the hydration force if it exists with rutile. The results will be processed using the extended DLVO theory described in the previous chapter.

3. 2 Experimental

3. 2. 1 Sample preparation

A commercial grade synthetic rutile was obtained from Tioxide Chemicals, Ltd. Its median size was 1.9 μm as measured by using a Microtrack particle size analyzer. The rutile contained 6 % chlorine, which was removed by repeated washing with double-distilled water. The conductivity of the supernatant water from the final washing step was 3.8×10^{-4} Ʊ/m. The sample was then dried in a vacuum desiccator at ambient temperature. To facilitate the wetting process, the dried powder was re-dispersed in conductivity water at 1 % solids by weight. This suspension was used as a feed stock for preparing particle suspensions for ζ-potential and turbidity measurements.

3. 2. 2 ζ-potential measurement

The ζ-potential of the rutile sample was measured at ambient temperature using a Pen Kem Laser Zee 500 particle electrophoresis apparatus. An aliquot of the 1 % stock suspension was diluted to 20-80 ppm in a NaCl solution of known concentration, and the pH was adjusted by adding NaOH or HCl. The suspension was agitated by means of a magnetic stirrer for 10 minutes before taking the measurement. The ζ-potentials were automatically converted from mobilities using Smoluchowski's equation and were normalized to the values at 20 °C inside the Laser Zee 500.

3. 2. 3 Turbidity measurement

The turbidity of rutile suspensions at ambient temperature was determined from the extinction of white light measured by a nephelometer (Monitek Model 21). The 1 % stock suspension was diluted to 200 ppm in an NaCl solutions of known concentration and pH. The dilute suspension was agitated at approximately 200 rpm for 10 minutes in a 50 ml beaker by means of a Teflon coated magnetic bar before transferring to the nephelometer. The turbidity was measured after 5 minutes of settling time in the nephelometer, and pH was recorded after the turbidity measurement.

3. 3 Analysis on the stability of rutile suspensions

3. 3. 1 Analysis using the classical DLVO theory

The ζ-potentials of rutile are shown in Fig. 3. 1. Its isoelectric point (i.e.p.) is observed at pH 6.2, which is close to the values reported in literature (pH 6.0-6.7)[10-11]. The ζ-potentials are reduced with increasing electrolyte concentration due to double layer compression. The ζ-potentials measured in $2x10^{-3}$ and $2x10^{-4}$ M NaCl solutions are almost the same below pH 8.5. Above this pH range, however, the ζ-potentials at $2x10^{-3}$ M are slightly more negative than at $2x10^{-4}$ M.

The results of turbidity measurements are shown in Fig. 3. 2. The turbidity is at a minimum (or coagulation is at a maximum) near the i.e.p. of rutile, which can be explained by the reduced electrostatic repulsive energy (V_e), as suggested by the classical DLVO theory. The turbidity decreases with increasing NaCl concentration over the entire pH range studied, which can also be explained by the decrease of V_e.

Fig. 3. 3 shows the turbidity (τ) of rutile suspensions measured at various pH with changing NaCl concentration. It is interesting to see that rutile is re-dispersed at

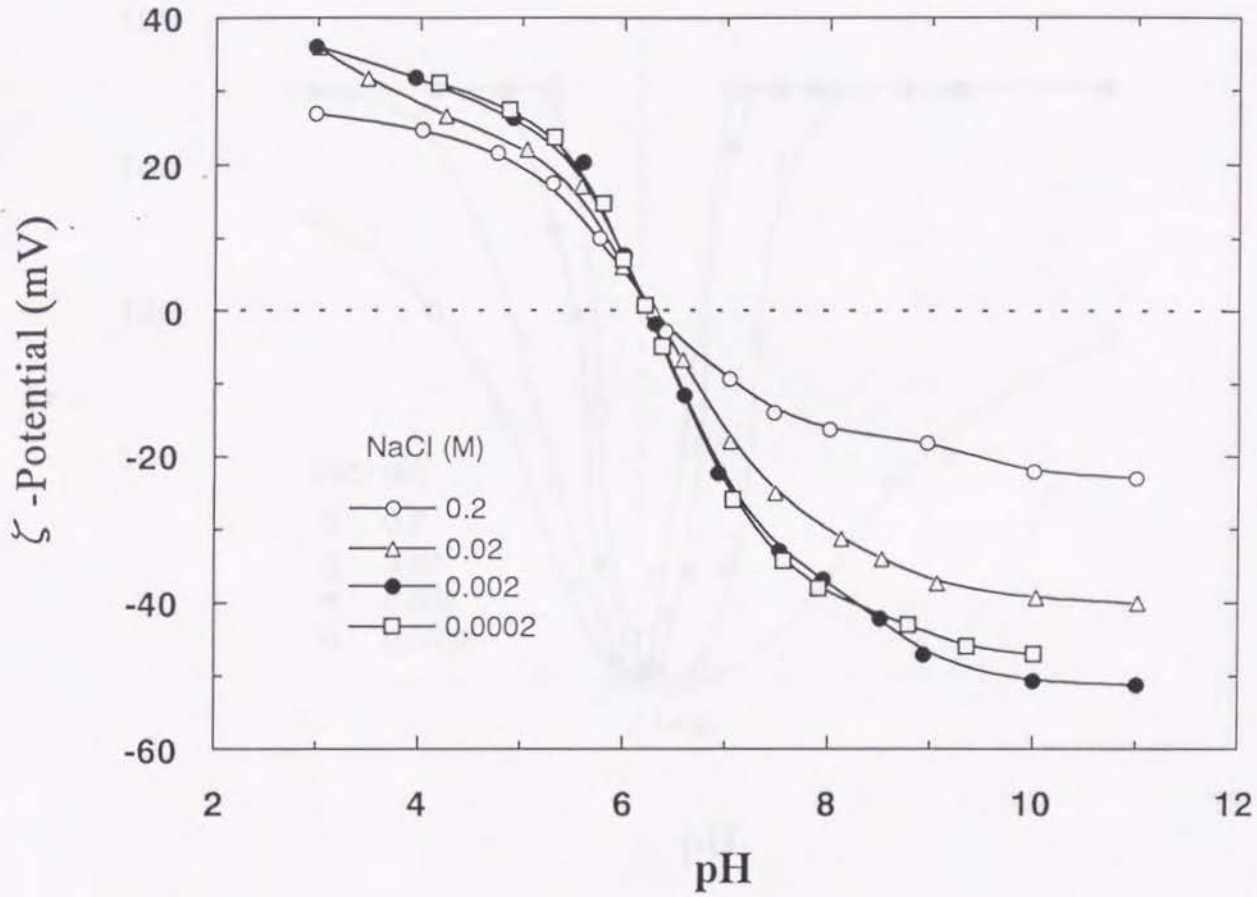

Fig. 3. 1 ζ–potentials of synthetic rutile as a function of pH at different NaCl concentrations. The i.e.p. occurs at pH 6.2.

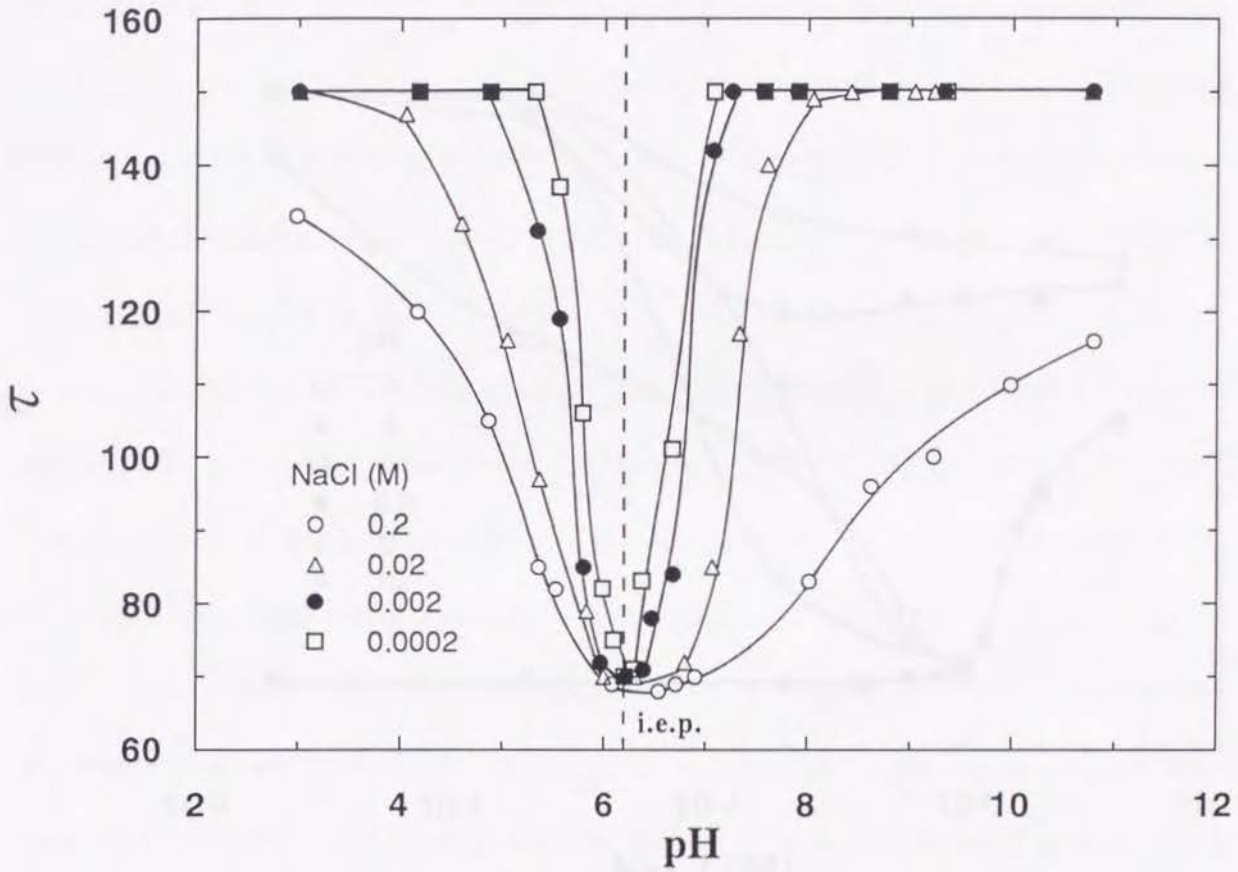

Fig. 3. 2 Results of turbidity (τ) measurements conducted with rutile as a function of pH at different NaCl concentrations.

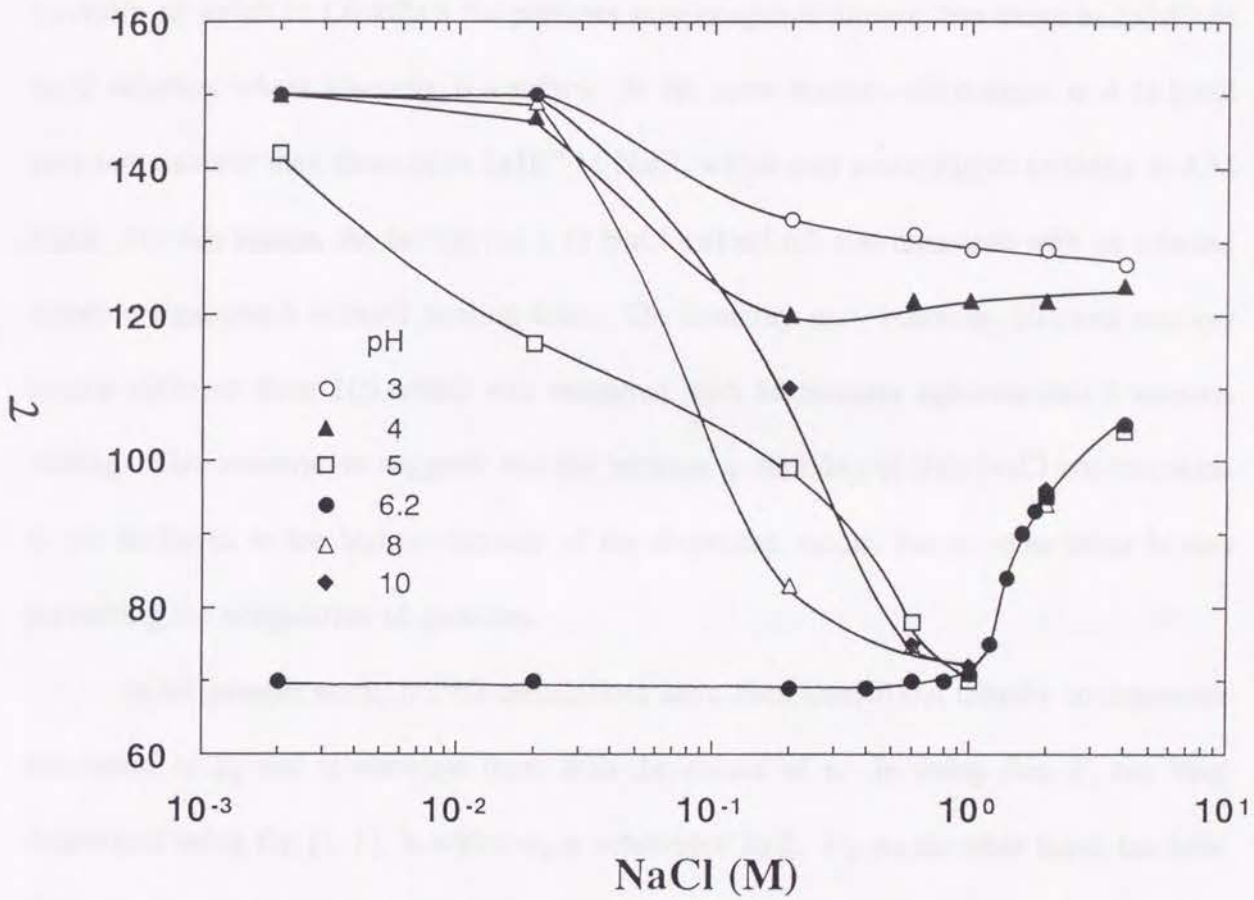

Fig. 3. 3 Turbidities (τ) of rutile suspensions at different pH shown as a function of NaCl concentrations.

concentrations above 1 M NaCl in spite of the zero ζ–potential at i.e.p. (pH 6.2). This observation cannot be explained by the classical DLVO theory. As will be shown later, the DLVO theory begins to fail at concentrations as low as $2x10^{-2}$ M. At above 1 M NaCl, the turbidities at pH 5–10 are almost the same, while at pH 4 and 3 the turbidities are much higher than those at pH 5–10. Since the coagulation of particles is a dynamic process, it is affected by the viscosity of the dispersing medium. For instance, in 4 M NaCl solutions the viscosity of which is 1.6 mPa·s the particles may coagulate slower than those in $2x10^{-4}$ M NaCl solution, whose viscosity is 1 mPa·s. In the same manner, the coagula in 4 M NaCl may settle slower than those of in $2x10^{-4}$ M NaCl, which may cause higher turbidity in 4 M NaCl. For this reason, the turbidity at 4 M NaCl and pH 6.2 was measured with 16 minutes agitation time and 8 minutes settling time. The turbidity was, however, 104 and was not largely different from 105 which was measured with 10 minutes agitation and 5 minutes settling. This observation suggests that the increase in turbidity at high NaCl concentration is not attributed to the higher viscosity of the dispersing media, but to some other factors preventing the coagulation of particles.

In the present work, DLVO calculations have been carried out initially to determine the values of E_1 and to correlate them with the values of τ. In doing this, V_e has been determined using Eq. [2. 1], in which ψ_δ is substituted by ζ. V_d, on the other hand, has been determined using Eq. [2. 2], for which the value of A_{131} needs to be known. The Hamaker constant has been estimated on the basis of the ζ–potential and turbidity measurements (Figs. 3. 1 and 3. 2). To do this, an assumption is made that $E_1 \leq 0$ when τ is at a minimum. In a $2x10^{-3}$ M NaCl solution, τ is at a minimum (≈70) at pH 6.0–6.4, where the ζ–potential varies in the range of +6.7 to −4.7 mV. At these low ζ–potentials, $V_e \leq -V_d$ according to the classical DLVO theory (Eq. [1. 2]) and the assumption made in the present work. From the value of

V_e that can be calculated using Eq. [2. 1] for ζ=+6.7 mV (at pH 6.0), one can then estimate that $A_{131} \geq 1.0 \times 10^{-20}$ J using Eq. [2. 2]. Note that at pH 6.5 the ζ-potential becomes more negative (−7.8 mV), and the τ increases to 78. To account for this increase in τ, it may be reasonable to assume that $E_1 \geq 0$. It follows then that $A_{131} < 1.4 \times 10^{-20}$ J. Based on the data obtained at 2×10^{-3} M NaCl, the value of A_{131} should be in the range of $1.0-1.4 \times 10^{-20}$ J.

Likewise, the data obtained at 2×10^{-4} M NaCl may be used to estimate that A_{131} should be in the range of $1.1-2.8 \times 10^{-20}$ J. Considering both case, the value of $1.1-1.4 \times 10^{-20}$ J may be used as the Hamaker constant of rutile in water. As shown later, the larger the Hamaker constant, the larger the estimated structural energy (V_s) which overcomes the van der Waals energy (V_d) and makes an energy barrier (E_1) corresponding to turbidity (τ). In order to prevent overestimation of V_s, the lower limit 1.1×10^{-20} J was taken for the following calculations. It should be noted, however, that the Hamaker constant of this value is considerably lower than those ($3.8-10 \times 10^{-20}$ J) reported in literature[12-13].

In Fig. 3. 4, τ is plotted against the values of E_1 obtained using the classical DLVO theory. As shown, the data obtained at 2×10^{-4} M and 2×10^{-3} M are fitted by a single curve, suggesting that the classical DLVO theory is useful for predicting E_1. However, the data obtained at 2×10^{-2} M NaCl and higher deviate from those at lower concentrations. The results obtained at 2×10^{-1} M are not even shown in Fig. 3. 4 because the E_1's are negative. Obviously, the DLVO theory underestimates V_t at high salt concentrations. As suggested by Eq. [2. 6], one must include the repulsive structural (or hydration) energy (V_s) to predict the energy barriers correctly.

3. 3. 2 Application of the extended DLVO theory

The method of estimating V_s for rutile is essentially the same as described for silica

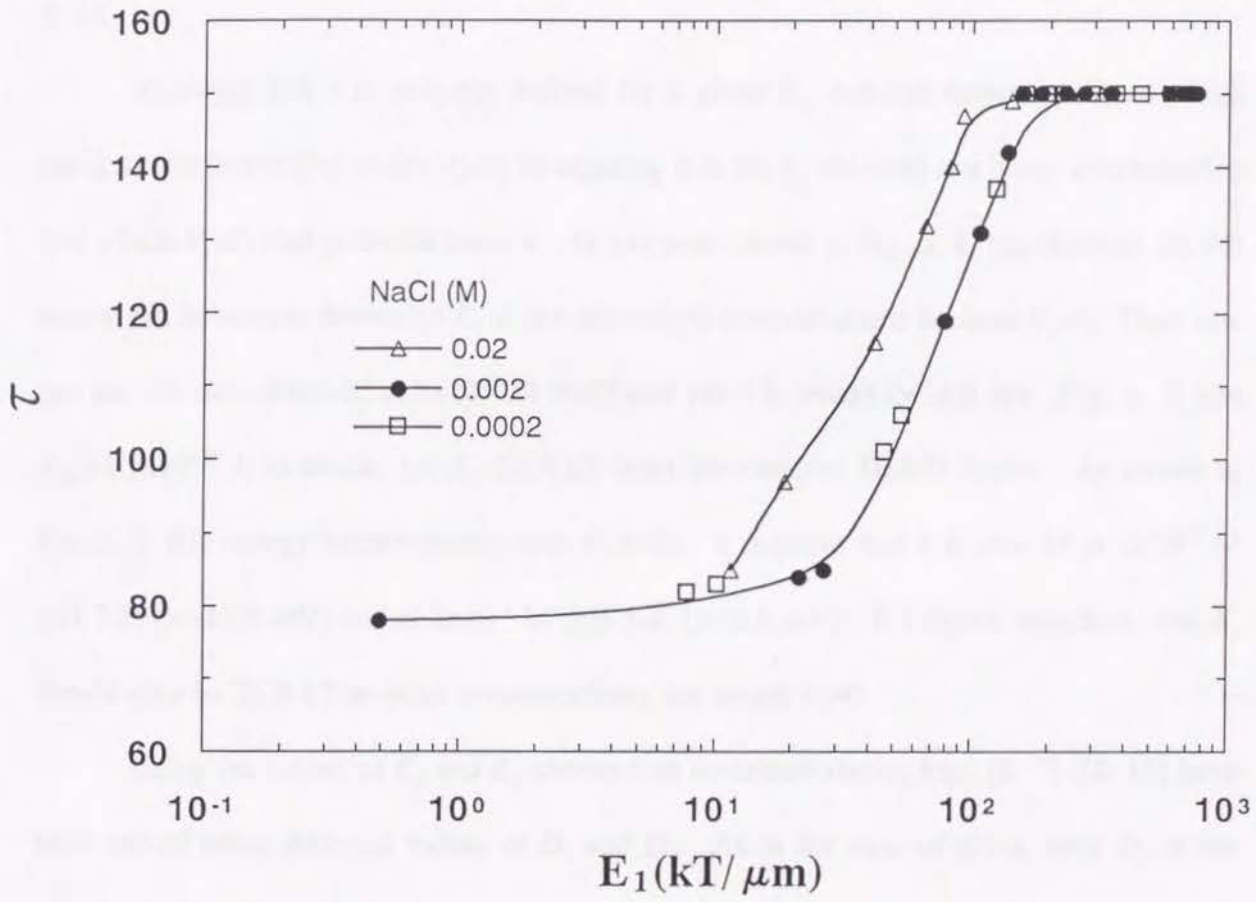

Fig. 3. 4 Turbidity (τ) of rutile suspensions plotted vs. energy barriers (E_1) calculated using the classical DLVO theory. The turbidity data obtained at $2x10^{-1}$ M NaCl are not shown because V_t is negative.

in the previous chapter. The values of E_1, E_2, D_1 and D_2 are used as the input to the model (Eqs. [2. 7]–[2. 10]), and the values of C_1, C_2, H_1 and H_2 are obtained as the output. The values of C_1, C_2, D_1 and D_2 are then used to calculate V_s using Eq. [2. 5]. As with silica, the secondary minimum is assumed to be shallow (E_2=−3 kT) to suggest that coagulation of rutile is induced by the primary energy minimum rather than E_2. This assumption may be justified by the excellent correlation between E_1 and τ observed at low NaCl concentrations (see Fig. 3. 4).

Knowing that τ is uniquely defined for a given E_1, one can determine E_1 at a high NaCl concentration (for which V_s≠0) by equating it to the E_1 obtained at a lower concentration (for which V_s=0) that gives the same τ. As has been shown in Fig. 3. 4, the classical DLVO theory can be used to determine E_1 at low electrolyte concentrations because V_s=0. Thus, one can use the data obtained at 2×10^{-3} M NaCl and pH 5.8, where ζ=14.0 mV (Fig. 3. 1) and $A_{131}=1.1\times10^{-20}$ J, to obtain that E_1=26.8 kT from the classical DLVO theory. As shown in Fig. 3. 2, this energy barrier corresponds to τ=85. It happens that τ is also 85 at 2×10^{-2} M (pH 7.1; ζ=−17.9 mV) and at 2×10^{-1} M (pH 5.4; ζ=16.6 mV). It follows, therefore, that E_1 should also be 26.8 kT at these concentrations, for which V_s≠0.

Using the values of E_1 and E_2 obtained as described above, Eqs. [2. 7]–[2. 10] have been solved using different values of D_1 and D_2. As in the case of silica, only D_2 in the neighborhood of 3 nm can satisfy the assumption of shallow secondary minimum when D_1<1 nm. Fig. 3. 5 compares different E_2's obtained by different D_2 values. When D_1=0.48 nm and D_2=3 nm, E_2 is as shallow as −3 kT (curve 1). When D_1=0.44 nm and D_2=1 nm, a deep secondary minimum is observed at a short separation distance (curve 2). A relatively long single decay length (D_1=0.7 nm) also gives a deep secondary minimum (curve 3).

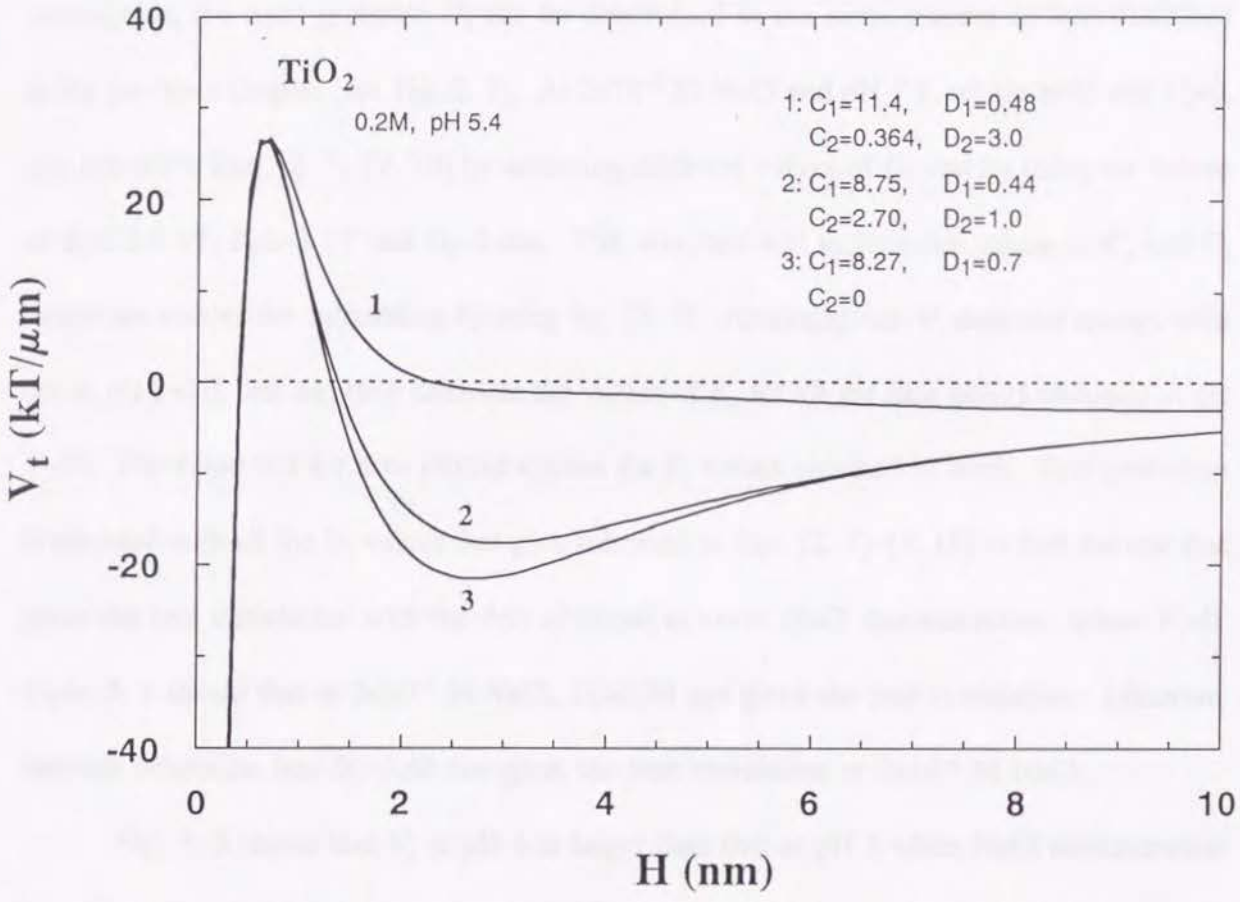

Fig. 3. 5 Total interaction energy (V_t) vs. distance (H) diagram obtained using the extended DLVO theory. When D_1<1 nm, only D_2≈3 nm gives the shallow secondary energy minimum.

As shown in Fig. 3. 3, the turbidities at above 1 M NaCl do not depend on pH at pH 5–10. It suggest that V_s does not depends on pH in this region, because the contributions from V_e to V_t and, hence, E_1 at these high salt concentrations are almost zero due to the double layer compression, and the change of E_1 is solely attributed to the change of V_s. From this insensitivity of V_s to pH at high NaCl concentrations, it may be derived the assumption that V_s does not change at pH 5–10 when NaCl concentrations $\leq 2\times10^{-1}$, too. By using this assumption, the most probable D_1 can be determined in the same manner as was described in the previous chapter (see Fig. 2. 7). At 2×10^{-2} M NaCl and pH 7.1, where τ=85 and $V_s \neq 0$, one can solve Eqs. [2. 7]–[2. 10] by assuming different values of D_1 and by using the values of E_1=26.8 kT, E_2=−3 kT and D_2=3 nm. The solutions will include the values of C_1 and C_2 which are needed for calculating V_s using Eq. [2. 5]. Assuming that V_s does not change with pH at pH 5–10, one can then calculate the values of E_1 for all the data points obtained at pH 5–10. The value of τ are now plotted against the E_1 values obtained as such. This procedure is repeated with all the D_1 values that give solutions to Eqs. [2. 7]–[2. 10] to find the one that gives the best correlation with the data obtained at lower NaCl concentrations, where V_s=0. Table 3. 1 shows that at 2×10^{-2} M NaCl, D_1=0.38 nm gives the best correlation. Likewise, one can determine that D_1=0.48 nm gives the best correlation at 2×10^{-1} M NaCl.

Fig. 3. 3 shows that V_s at pH 4 is larger than that at pH 5 when NaCl concentration is above 1 M. If this also holds at $\leq 2\times10^{-1}$ M NaCl, E_1 value at pH 4 calculated using V_s derived for ≥pH 5 is smaller than that corresponds to the turbidity. At 2×10^{-2} M and pH 4, τ is 147, the E_1 of which is 151 kT according to the τ–E_1 curve of $\leq 2\times10^{-3}$ M. On the other hand, the calculated E_1 using V_s obtained for ≥pH 5 (D_1=0.38 nm) gives 148 kT. However, the difference of 3 kT is smaller than the 5 kT which is the maximum scattering of data regressed with the correlation coefficient of 0.998. The difference of 3 kT can be, therefore,

Table 3. 1 Structural energy constants (C_1, C_2) with rutile obtained for various D_1.

$2x10^{-2}$ M NaCl

	D_1 (nm)				
	0.20	0.36	0.38	0.40	0.50
C_1 (mJ/m^2)	34.3	19.8	15.9	12.6	4.61
C_2 (mJ/m^2)	0.132	0.132	0.132	0.132	0.132
Corr. Coeff.	0.9952	0.9978	0.9980	0.9973	0.9938

D_2=3.0 nm

$2x10^{-1}$ M NaCl

	D_1 (nm)				
	0.40	0.46	0.48	0.50	0.60
C_1 (mJ/m^2)	17.7	12.6	11.4	10.3	6.72
C_2 (mJ/m^2)	0.364	0.364	0.364	0.364	0.364
Corr. Coeff.	0.9977	0.9980	0.9981	0.9980	0.9973

D_2=3.0 nm

regarded as an allowable error. At $2x10^{-1}$ M, the E_1 is estimated as 113.3 kT for pH 3 and 82.2 kT for pH 4 from the τ–E_1 curve at $\leq 2x10^{-3}$ M, while the calculation using the V_s for ≥pH 5 (D_1=0.48 nm) gives 112.5 kT and 83.4 kT, respectively. The differences of 0.8 kT and 1.2 kT is also smaller than the maximum scattering of 4 kT in the regression with correlation coefficient of 0.9981. It may be concluded from this observation that at pH 3–10, V_s is not affected by pH when NaCl concentration is $\leq 2x10^{-1}$ M. Fig. 3. 6 shows the τ vs. E_1 plots made using the parameters of V_s that give the best fit for each NaCl concentration. The fact that all the data points obtained at various NaCl concentrations can be fitted by a single curve demonstrates that the extended DLVO theory can be used for predicting E_1 over a wide range

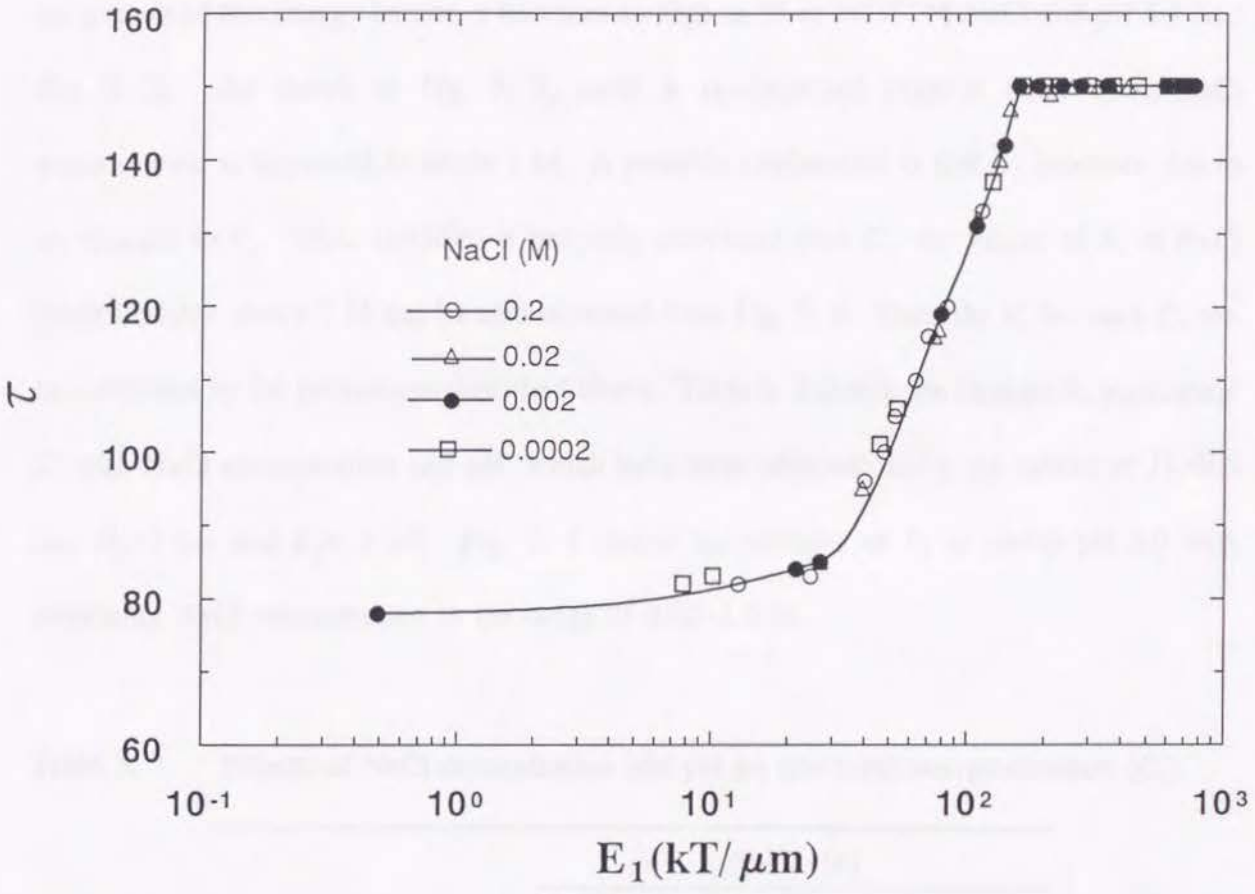

Fig. 3. 6 Turbidities (τ) of rutile suspensions plotted vs. energy barriers (E_1) calculated using the extended DLVO theory. The turbidity data obtained at all NaCl concentrations are correlated with E_1 by a single curve.

of electrolyte concentrations.

Fig. 3. 7 compares the potential energy vs. distance diagrams obtained using the classical and extended DLVO theories for rutile at $2x10^{-1}$ M NaCl and pH 5.4. At such a high NaCl concentration, the classical DLVO theory (V_{t1}) gives no energy barrier because V_e is negligibly small. On the other hand, the extended DLVO theory (V_{t2}) shows that V_s presents the major repulsive energy and give rise to a significant energy barrier (E_1=26.8 kT). As a result of this energy barrier, τ becomes as high as 85 at $2x10^{-1}$ M NaCl and pH 5.4 (see Fig. 3. 2). As shown in Fig. 3. 3, rutile is re-dispersed even at i.e.p. when NaCl concentration is increased to above 1 M. A possible explanation is that E_1 increases due to an increase in V_s. Since turbidity is uniquely correlated with E_1, the values of E_1 at NaCl concentrations above 1 M can be also obtained from Fig. 3. 6. Then the V_s for each E_1 can be calculated by the procedures described above. Table 3. 2 shows the changes in parameters C_1 with NaCl concentration and pH, which have been obtained using the values of D_1=0.6 nm, D_2=3 nm and E_2=−3 kT. Fig. 3. 8 shows the changes of V_s at above pH 5.0 with increasing NaCl concentration in the range of 0.02–4.0 M.

Table 3. 2 Effects of NaCl concentration and pH on structural energy constant (C_1).

		NaCl (M)		
		1.4	2.0	4.0
C_1 (mJ/m^2)	pH 3	16.3	16.3	16.0
	pH 4	15.2	15.2	15.5
	> pH 5	10.2	11.7	12.9

D_1=0.6 nm, C_2=0.363 mJ/m^2, D_2=3.0 nm

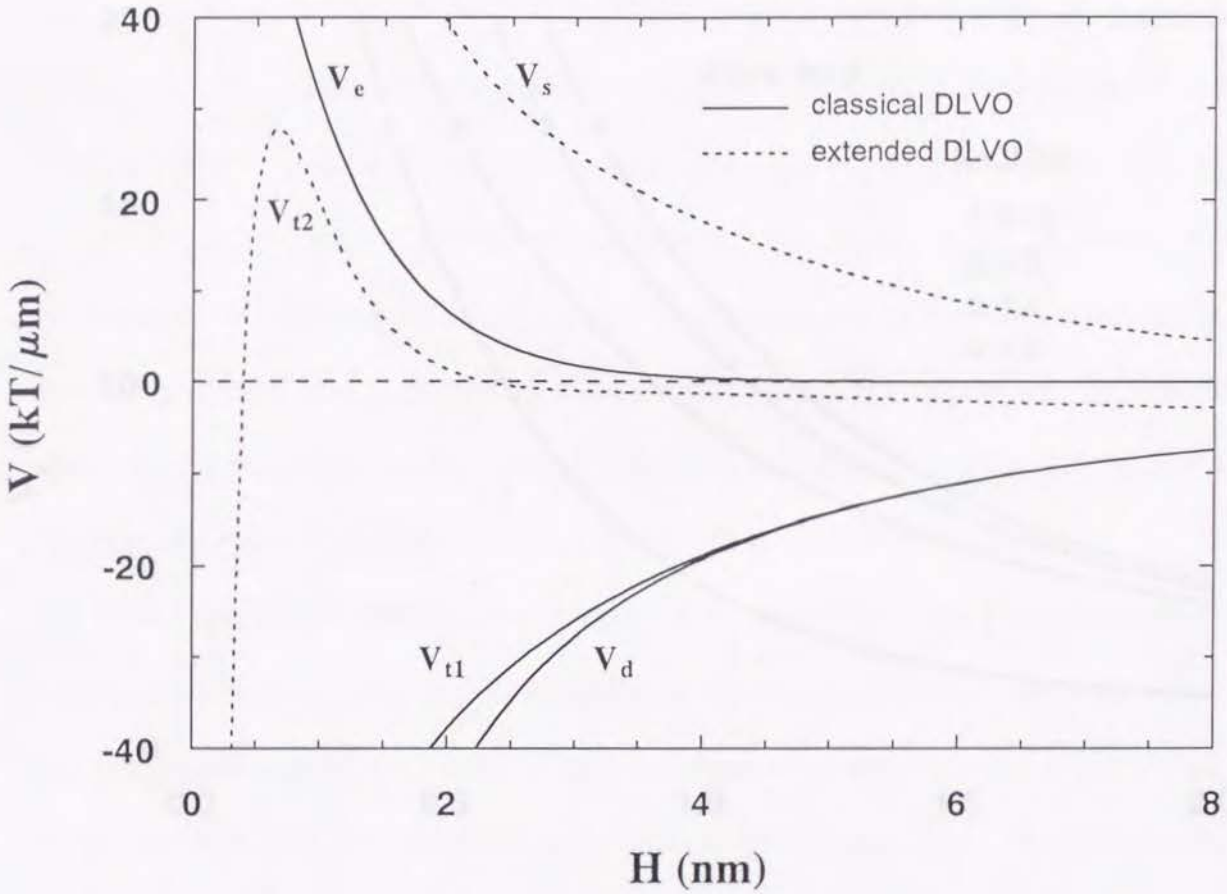

Fig. 3. 7 Comparison of the classical and extended DLVO plots for the rutile suspension in $2x10^{-1}$ M NaCl solution at pH 5.4. The classical DLVO theory gives no energy barrier (E_1), while the extended DLVO theory gives E_1=26.8 kT for 1μm particle. Because of this energy barrier, the rutile suspension is not completely destabilized.

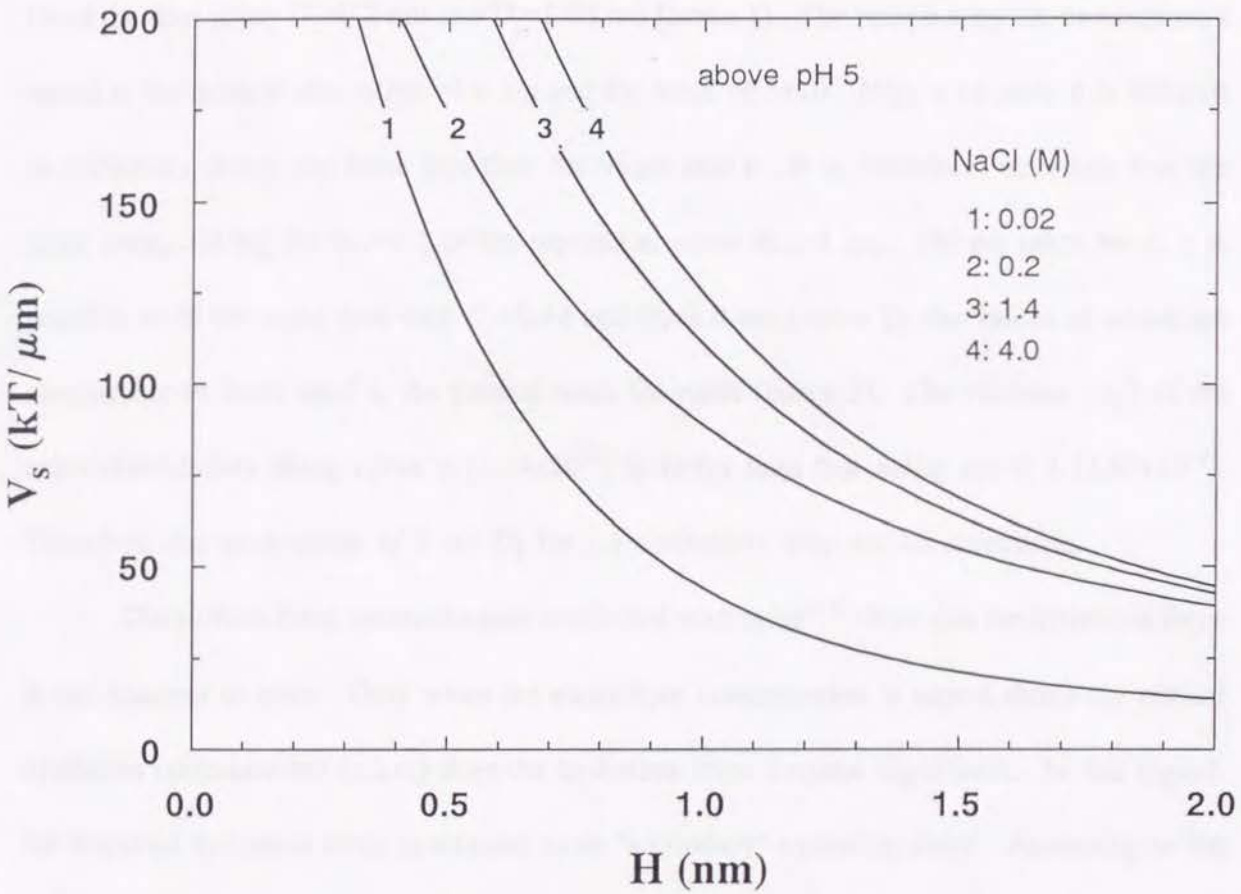

Fig. 3. 8 Effect of NaCl concentration on the structural energy (V_s) at above pH 5 vs. separation distance (H) plots. V_s is shown to increase with increasing NaCl concentration.

The D_1 values obtained in the present work are a little longer than those (0.17–0.30 nm)[4] obtained from surface force measurements conducted with mica in 1:1 electrolyte solutions. On the other hand, the value of D_2 (=3.0 nm) used in the present work is significantly larger than those (0.6–1.10 nm) for mica in 1:1 electrolyte solutions. Only in the presence of hydrolyzable cations such as La^{3+} does D_2 become 3.0 nm[14]. Fig. 3. 9 shows the surface forces measured with mica in 2 M NaCl solutions by Pashley and Quirk[14]. They fitted the data using D_1=0.3 nm and D_2=1.05 nm (curve 1). The reason why the measurement ended at the surface separation of 4 nm and the force of $5x10^{-4}$ N/m is because it is difficult to accurately detect the force less than the value above. It is, therefore, uncertain that the force decays along the curve 1 at the separation more than 4 nm. On the other hand, it is possible to fit the same data with D_1=0.44 and D_2=3.0 nm (curve 2), the values of which are comparable to those used in the present work for rutile (curve 3). The variance (σ_y^2) of the experimental data along curve 2 ($3.34x10^{-5}$) is better than that along curve 1 ($3.60x10^{-5}$). Therefore, the assumption of 3 nm D_2 for 1:1 electrolyte may not be unrealistic.

The surface force measurements conducted with mica[2-6] show that the hydration force is not inherent to mica. Only when the electrolyte concentration is raised above the critical hydration concentration (c.h.c.) does the hydration force become significant. In this regard, the acquired hydration force is referred to as "secondary" hydration force. According to the site–bonding model developed by Pashley[9], the pK values for the adsorption of the hydrated cations are in the range of 3–4. Because the pK values are so small, c.h.c.'s are high (usually in the range of 10^{-4}–10^{-1} M). In general, c.h.c. increases with increasing hydration energy of the cations involved, indicating that the more strongly a cation is hydrated, the less likely the hydrated cations will remain adsorbed on the surface when two curved mica cylinders approach each other during the surface force measurements. Also, the magnitude of the

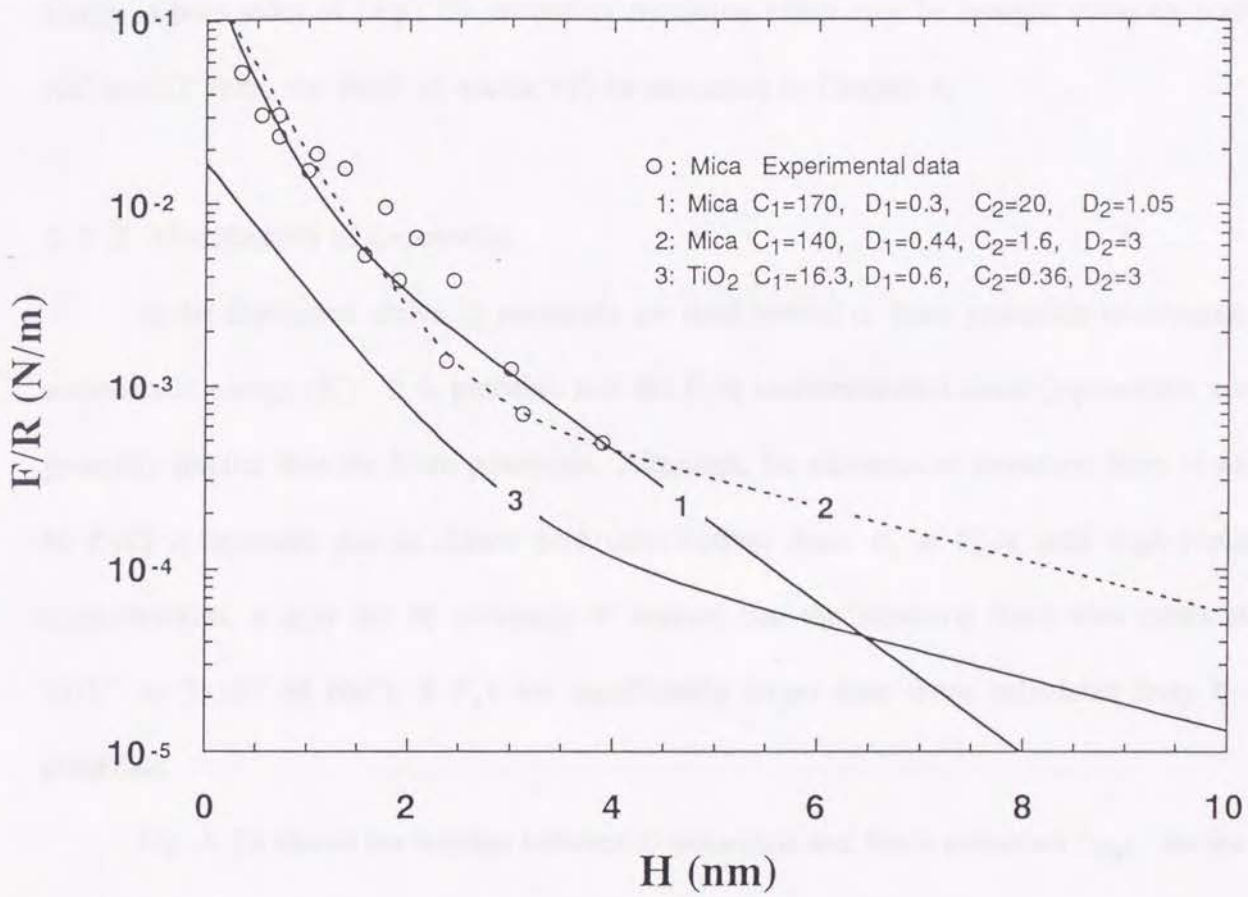

Fig. 3. 9 Surface forces measured by Pashley and Quirk[14] with curved mica surfaces in 2 M NaCl solutions. A longer D_2 (=3.0 nm) value assumed for rutile may also be useful for the data obtained with mica.

hydration force increases with increasing hydration energy, because it would require more energy to remove the water of hydration from more strongly hydrated cations.

Similar results were obtained with the synthetic rutile used in the present work. The hydration force becomes discernable at approximately $2x10^{-2}$ M and increases with increasing NaCl concentration, suggesting that it is a secondary hydration force created by the adsorbed ions on the rutile surfaces. Since the turbidities cannot be predicted by the classical DLVO theory at both sides of i.e.p., the secondary hydration effect may be brought about by both Na^+ and Cl^- ions, the detail of which will be discussed in Chapter 4.

3. 3 .3 Modification of ζ–potential

In the discussion above, ζ–potentials are used instead of Stern potentials to calculate electrostatic energy (V_e). It is probable that the V_e is underestimated since ζ–potentials are generally smaller than the Stern potentials. Although, the existence of structural force at ≥1 M NaCl is apparent due to almost zero contributions form V_e to V_t at such high NaCl concentrations, it may not be necessary to assume that the structural force also exists at $2x10^{-1}$ to $2x10^{-2}$ M NaCl, if V_e's are significantly larger than those calculated from ζ–potentials.

Fig. 3. 10 shows the relation between ζ–potentials and Stern potentials (ψ_δ). As the potential decays exponentially outside the Stern layer, ψ_δ can be expressed as:

$$\psi_\delta = \zeta \exp(\kappa X) , \qquad [3.\ 1]$$

where κ is Debye parameter and X is the separation distance between Stern plane and shear plane. While Lyklema[15] and others[16–19] suppose that $X \approx 0$, Webb et al.[20] estimate the X of synthesized anatase in NaCl solution as 12 Å at $1x10^{-2}$ M NaCl, 20 Å at $2x10^{-3}$ M and 25

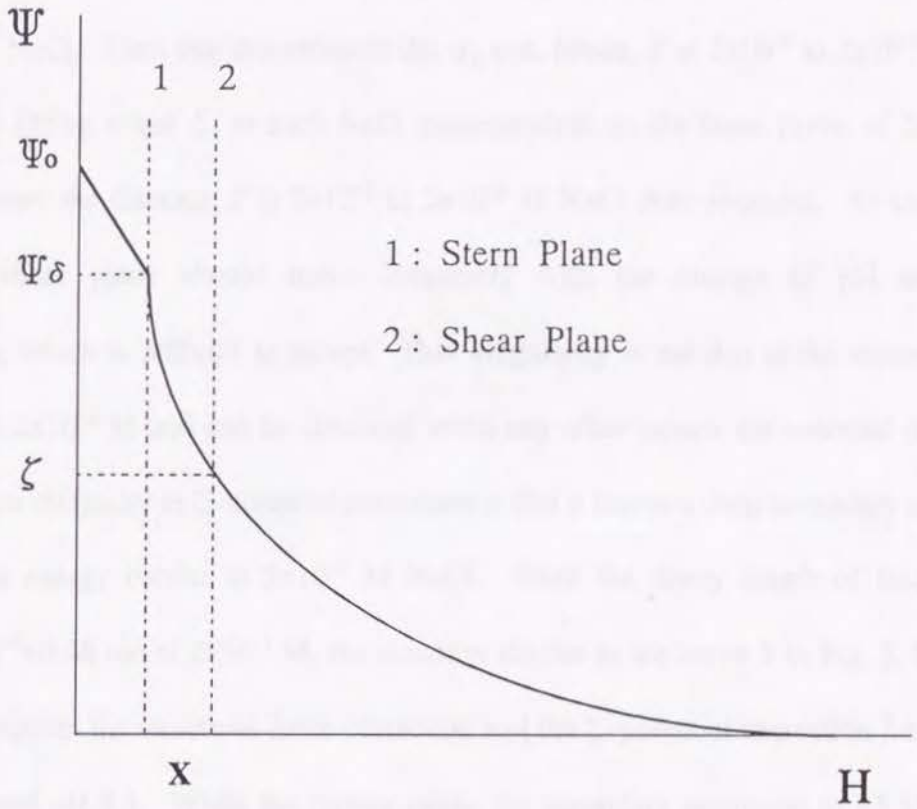

Fig. 3. 10 Potential distribution in an electric double layer. Ψ_o, Ψ_δ and ζ represent the surface, Stern and zeta potentials respectively.

Å at $4x10^{-4}$ M. It will be investigated in the following the effect of ζ–potential correction from the standpoint of Webb et al.

Since the length of X at $2x10^{-4}$ M is not available, it is arbitrarily assumed to be 30 Å. Then it is calculated that $\psi_\delta=1.15\zeta$ from Eq.[3. 1]. Using this ψ_δ, the Hamaker constant can be estimated to be $2.1x10^{-20}$ J$\leq A_{131}<3.7x10^{-20}$ J with the same process described earlier. Then it is arbitrarily assumed that $A_{131}=2.1x10^{-20}$ J. Now one can calculate E_1 for each turbidity measurement at $2x10^{-4}$ M NaCl using these ψ_δ and A_{131} and can plot new τ–E_1 curve for $2x10^{-4}$ M NaCl. Then one can estimate the ψ_δ and, hence, X at $2x10^{-3}$ to $2x10^{-1}$ M NaCl necessary for fitting τ and E_1 at each NaCl concentration on the same curve of $2x10^{-4}$ M. Fig. 3. 11 shows the distance X at $2x10^{-3}$ to $2x10^{-1}$ M NaCl thus obtained. As shown, the position of shear plane should move irregularly with the change of pH and NaCl concentration, which is difficult to accept. This irregularity is not due to the assumption of 30 Å for X at $2x10^{-4}$ M and can be observed when any other values are assumed for the X.

Another difficulty in ζ–potential correction is that it leaves a deep secondary minimum E_2 behind the energy barrier at $2x10^{-1}$ M NaCl. Since the decay length of electrostatic repulsion is $\kappa^{-1}=0.68$ nm at $2x10^{-1}$ M, the situation similar to the curve 3 in Fig. 3. 5 occurs. Fig. 3. 12 compares the structural force correction and the ζ–potential correction for the data at $2x10^{-1}$ M and pH 5.4. While the former raises the secondary minimum to −3 kT by the contributions from $D_2=3$ nm, the latter leaves the −40 kT minimum. It is difficult to assume that this deep secondary minimum does not affect the coagulation of rutile.

Considering the both problems in ζ–potential correction, it seems reasonable to conclude that the structural force also exists at NaCl concentration $2x10^{-2}$ to $2x10^{-1}$ M in rutile suspensions.

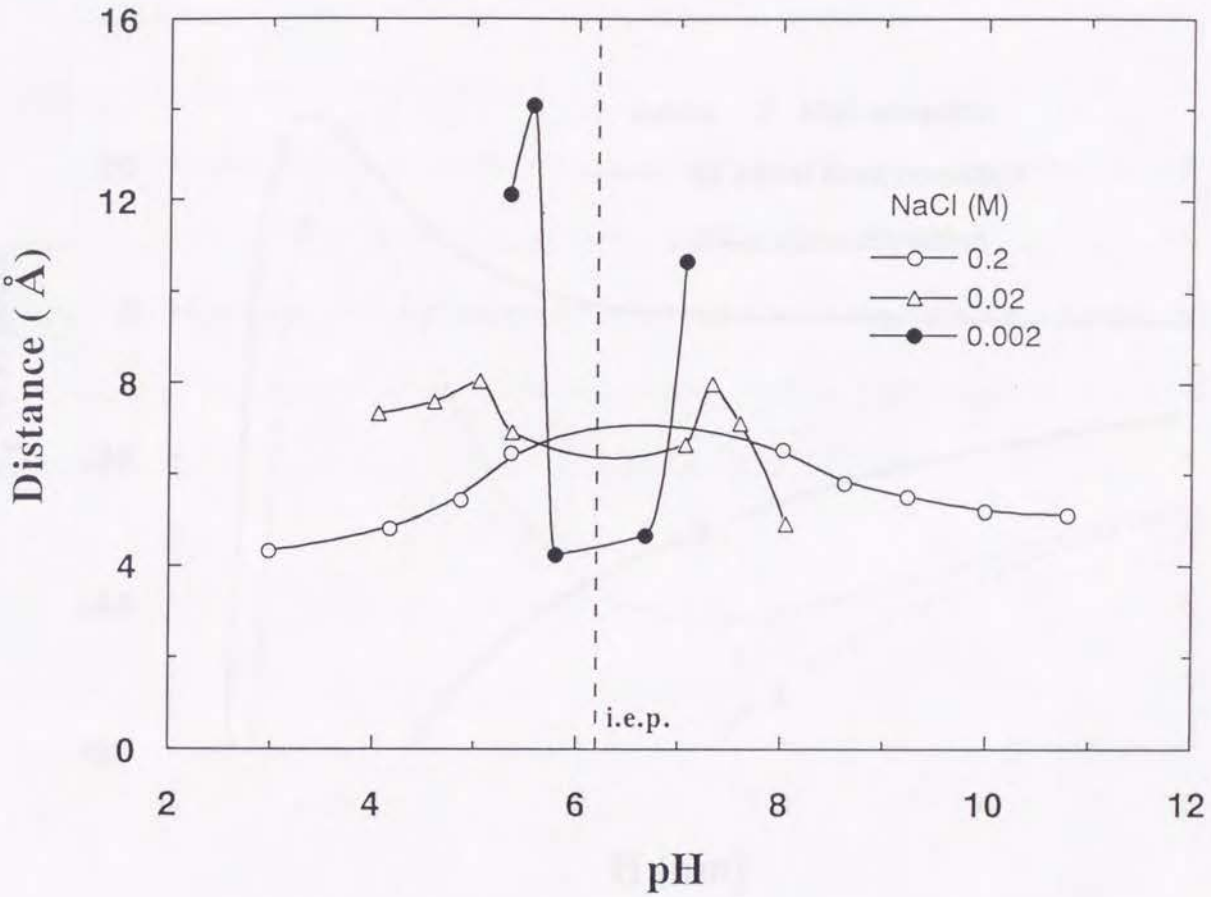

Fig. 3. 11 Distance between Stern and shear planes for the zeta potential correction. The shear plane should move irregularly with the change of pH in order to obtain an unique τ–E_1 correlation similar to the structural force correction (Fig. 3. 6).

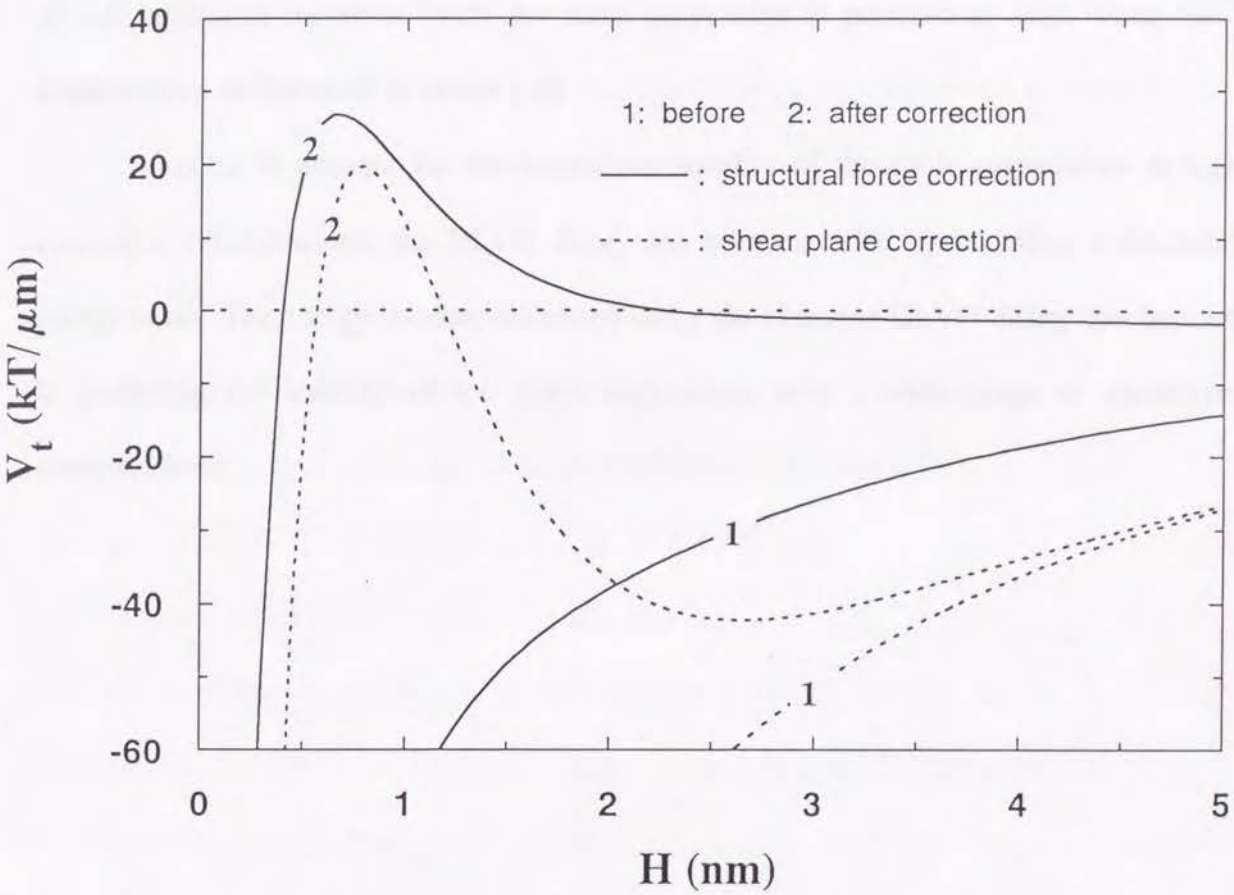

Fig. 3. 12 Comparison of structural force and shear plane corrections on potential energy (V_t) vs. distance (H) plots. The shear plane correction leaves a deep secondary minimum behind the barrier, while the structural force correction makes a much shallower secondary minimum.

3. 4 Conclusion

Turbidity measurement conducted with aqueous suspensions of synthetic rutile show that the stability decreases with increasing NaCl concentrations as predicted by the classical DLVO theory. At $2x10^{-2}$ M NaCl and above, however, the suspensions begin to show repulsive hydration forces not considered in the classical DLVO theory. It is believed that the hydration force is due to hydrated counter ions adsorbed on the rutile surface. Because of this additional repulsive force, the rutile suspension is peptized at i.e.p. when NaCl concentration is increased to above 1 M.

In order to account for the anomalous stability of the rutile suspensions at high electrolyte concentrations, the DLVO theory has been extended by including a structural energy term. The energy barriers calculated using the extended DLVO theory can be used in predicting the stability of the rutile suspensions over a wide range of electrolyte concentrations.

3. 5 References

1. Israelachvili, J.N., and McGuiggan P.M., *J. Mater. Res.*, **5**, 2223 (1990)

2. Israelachvili, J.N., and Adams, G.E., *J. Chem. Soc. Faraday Trans. I*, **74**, 975 (1978)

3. Pashley, R.M., *J. Colloid Interface Sci.*, **80**, 153 (1981)

4. Pashley, R.M., *Adv. Colloid Interface Sci.*, **16**, 57 (1982)

5. Pashley, R.M., and Israelachvili, J.N., *J. Colloid Interface Sci.*, **97**, 446 (1984)

6. Pashley, R.M., *J. Colloid Interface Sci.*, **102**, 23 (1984)

7. Derjaguin, B.V., and Landau, L.D., *Acta Physicochim.*, **14**, 633 (1941)

8. Verwey, E.J., and Overbeek, J.Th.G., "Theory of the stability of lyophobic colloids," 66, Elsevier, New York (1948)

9. Pashley, R.M., *J. Colloid Interface Sci.*, **83**, 531 (1981)

10. Parks, G.A., *Chem. Rev.*, **65**, 177 (1965)

11. Healy, T.W., and Fuerstenau, D.W., *J. Colloid Sci.*, **20**, 376 (1965)

12. Visser, J., *Adv. Colloid Interface Sci.*, **3**, 331 (1972)

13. Fowkes, F.M., *Ind. Chem. Eng.*, **56**, 40 (1964)

14. Pashley, R.M., and Quirk, J.P., *Colloids and Surfaces,* **9**, 1 (1984)

15. Lyklema, J., "The scientific basis of flocculation," ed. Ives, K.J., 3, Sijthof & Noordhoff, Alphen aan den Rijn (1978)

16. Sennett, P., and Oliver, J.P., *Ind. Chem. Eng.*, **57**, 32 (1965)

17. Hunter, R.J., and Wright, H.J., *J. Colloid Interface Sci.*, **37**, 564 (1971)

18. Levine, S., and Smith, A.L., *Discuss. Faraday Soc.*, **52**, 290 (1971)

19. Lyons, J.S., Furlong, D.N., Homola, A., and Healy, T.W., *Aust. J. Chem.*, **34**, 1167 (1981)

20. Webb, J.T., Bhatnagar, P.D., and Williams, D.G., *J. Colloid Interface Sci.*, **49**, 346 (1974)

Chapter 4 Secondary hydration force with stannic oxide

4. 1 Objective of research

It has been shown in the previous chapters that there are two kind of hydration forces, i.e. the primary and secondary hydration forces. The primary hydration force is observed with silica and decreases with increasing electrolyte concentration. The secondary hydration force which increases with increasing salt concentration is observed with mica and rutile. More or less, other oxides seem to have similar hydration forces, and it is interesting to know which kind of hydration force exists with other oxides. In this chapter, it will be tried to confirm the hydration force with stannic oxide, if it exists, using the same method described in the previous chapters. The mechanism of the primary and the secondary hydration forces will also be discussed. A difference in turbidities of silica and stannic oxide will be discussed at the end of this chapter.

4. 2 Experimental

4. 2. 1 Sample preparation

A regent grade synthetic stannic oxide was obtained from Wako Chemicals, Ltd. The fine fraction of it was recovered by the settling of sample in dilute aqueous suspension at pH 9. The median size of the fine fraction was 1.13 μm as measured by using a Microtrack particle size analyzer. The sample was washed repeatedly with double-distilled water until the pH of the supernatant water from the final washing step reached pH 5.8. The sample was then dried in a vacuum desiccator at ambient temperature. To facilitate the wetting process, the dried powder was re-dispersed in conductivity water at 1 % solids by weight. This suspension was used as a feed stock for preparing particle suspensions for ζ-potential and

turbidity measurements.

4. 2. 2 Contact angle measurement

The natural wood tin nodule of 20 mm x 25 mm size from San Luis Potosi, Mexico was used for contact angle measurement. The section of sample was polished using diamond paste and was cleaned by immersing in Acetone and by successive boiling in conc. HNO_3 for 2 hours followed by washing with conductivity water and drying under nitrogen. Cyclohexane, octane and decane are chosen as liquid 1 and 2 of Eq. [2. 14]. The contact angles of water droplets were measured through the hydrocarbon phase using a Ramé-hart goniometer.

4. 2. 3 ζ-potential measurement

The ζ-potential of the stannic oxide sample was measured at 20 °C using a Pen Kem Laser Zee 3000 particle electrophoresis apparatus. An aliquot of the 1 % stock suspension was diluted to 200-400 ppm in a NaCl solution of known concentration, and the pH was adjusted by adding NaOH or HCl. The suspension was agitated by means of a magnetic stirrer for 10 minutes before taking the measurement, then pH was recorded. The ζ-potentials were calculated from the mobilities of sample using Smoluchowski's equation.

4. 2. 4 Turbidity measurement

The turbidity of stannic oxide suspensions was measured at ambient temperature with the same method as used for silica suspensions in Chapter 2. The 1 % stock suspension was diluted to 200 ppm in an NaCl solution of known concentration and pH. The dilute suspension was agitated at approximately 200 rpm for 10 minutes in a 50 ml beaker by means

of a Teflon coated magnetic bar before transferring to the light scattering apparatus. The turbidity was measured after 10 minutes of settling time in the measuring cell, and pH was recorded after the turbidity measurement.

4. 2. 5 Coagulation experiment

The coagulation experiment of silica and stannic oxide suspensions was carried out with 400 ml suspension which contained the solid by 500 ppm. A glass beaker of 75 mm diameter and 150 mm height was used for agitation and settling. The suspension was agitated by Teflon-coated magnet at about 200 rpm for 30 minutes and was hold for 60 minutes for the settling of particles. After the settling, the suspension was discharged by siphoning. During each siphoning process, 29 ml suspension was remained at the bottom of the beaker and was recovered with settled coagula. The settled coagula and suspended particles in discharged suspension were recovered by filtration, and the weight of recovered solids was measured after drying at 105 °C.

4. 3 Analysis on the stability of stannic oxide suspensions

4. 3. 1 Analysis using the classical DLVO theory

Table 4. 1 shows the contact angle data, which were used for calculating the dispersion component of surface tension of wood tin (γ_s^d) using Eq. [2. 14]. The surface and interfacial tension data used for the calculation were taken from literature[1]. The γ_s^d values were then used for calculating the Hamaker constant of the wood tin (A_{131}) using Eq. [2. 13]. An average of 2.3×10^{-20} J was obtained as the value of A_{131}, which is a little smaller than literature values of Hamaker constant of stannic oxide ($2.5-5.5\times10^{-20}$ J)[1-2]. The value 2.3×10^{-20} J was used as the Hamaker constant of stannic oxide for further calculations.

Table 4. 1 Contact angles of water droplet on polished wood tin immersed in various hydrocarbons.

	Cyclohexane – Octane	Octane – Decane	Decane – Cyclohexane	Average
θ_1 (°)	46	42	45	–
θ_2 (°)	42	45	46	–
γ_s^d (mN/m)	83	75	69	76
A_{131} (10^{-21} J)	2.8	2.2	1.9	2.3

The ζ–potentials of stannic oxide measured in different NaCl concentrations of NaCl solutions are shown in Fig. 4. 1. The isoelectric point (i.e.p.) was observed in the neighborhood of pH 4.0, which is close to literature values (pH 3.9–5.5)[3-4]. Although the ζ–potentials are generally smaller in magnitude at higher NaCl concentrations, those at $2x10^{-3}$ and $2x10^{-2}$ M NaCl are almost the same at pH 3–5.

The turbidity measurements of stannic oxide suspensions conducted at different NaCl concentrations are shown in Fig. 4. 2. The decrease in turbidity (τ) is attributed to the decrease of electrostatic repulsive energy (V_e) as suggested by the classical DLVO theory. Near the i.e.p., the turbidity is at a minimum where the energy barriers (E_1) preventing coagulation are supposed to be ≤0.

Fig. 4. 3 shows the turbidity of stannic oxide suspensions at various pH and NaCl concentrations. The stannic oxide is re–dispersed at NaCl concentrations above 1 M even at its i.e.p. (pH 4.0), where there is no electrostatic repulsion. This is similar to what has been observed with rutile suspensions. At above 1 M NaCl, the turbidities at pH 3–10 are almost the same, while at pH 2 and 1 the turbidities are higher than those at pH 3–10, which is also similar to the case of rutile suspensions. It seems that there is a significant secondary hydration force in stannic oxide suspensions.

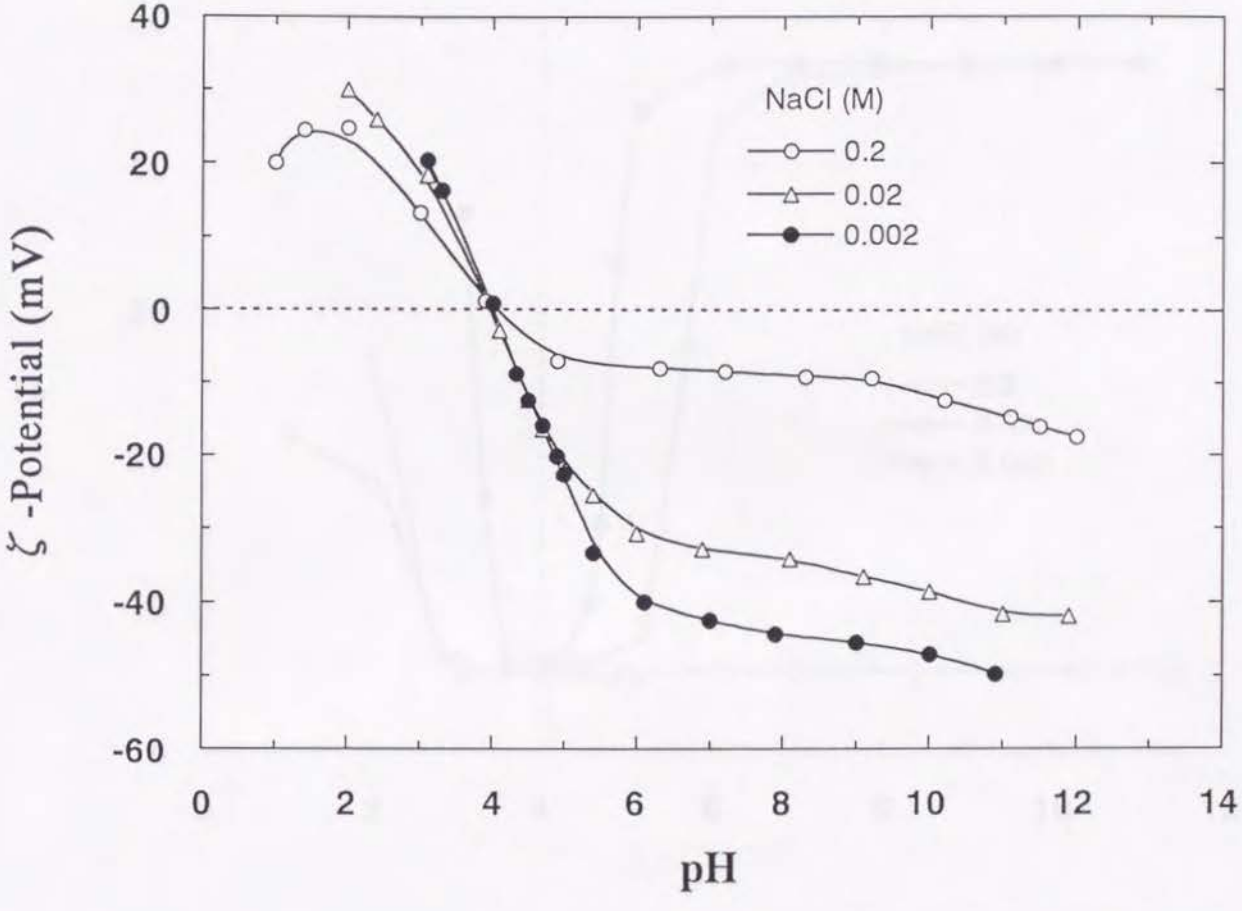

Fig. 4. 1 ζ–potentials of synthesized stannic oxide as a function of pH at different NaCl concentrations.

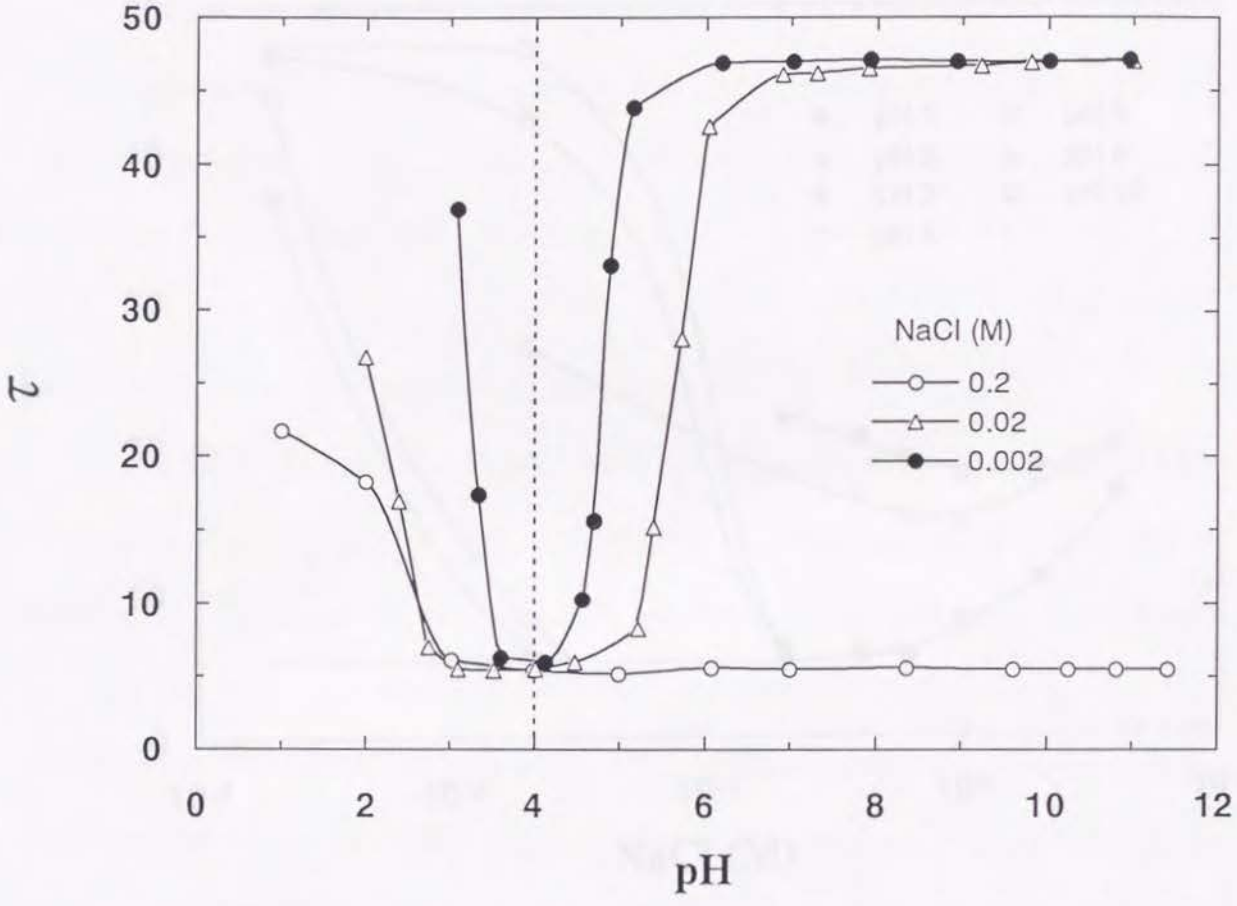

Fig. 4. 2 Turbidity (τ) measurements conducted with stannic oxide as a function of pH at different NaCl concentrations.

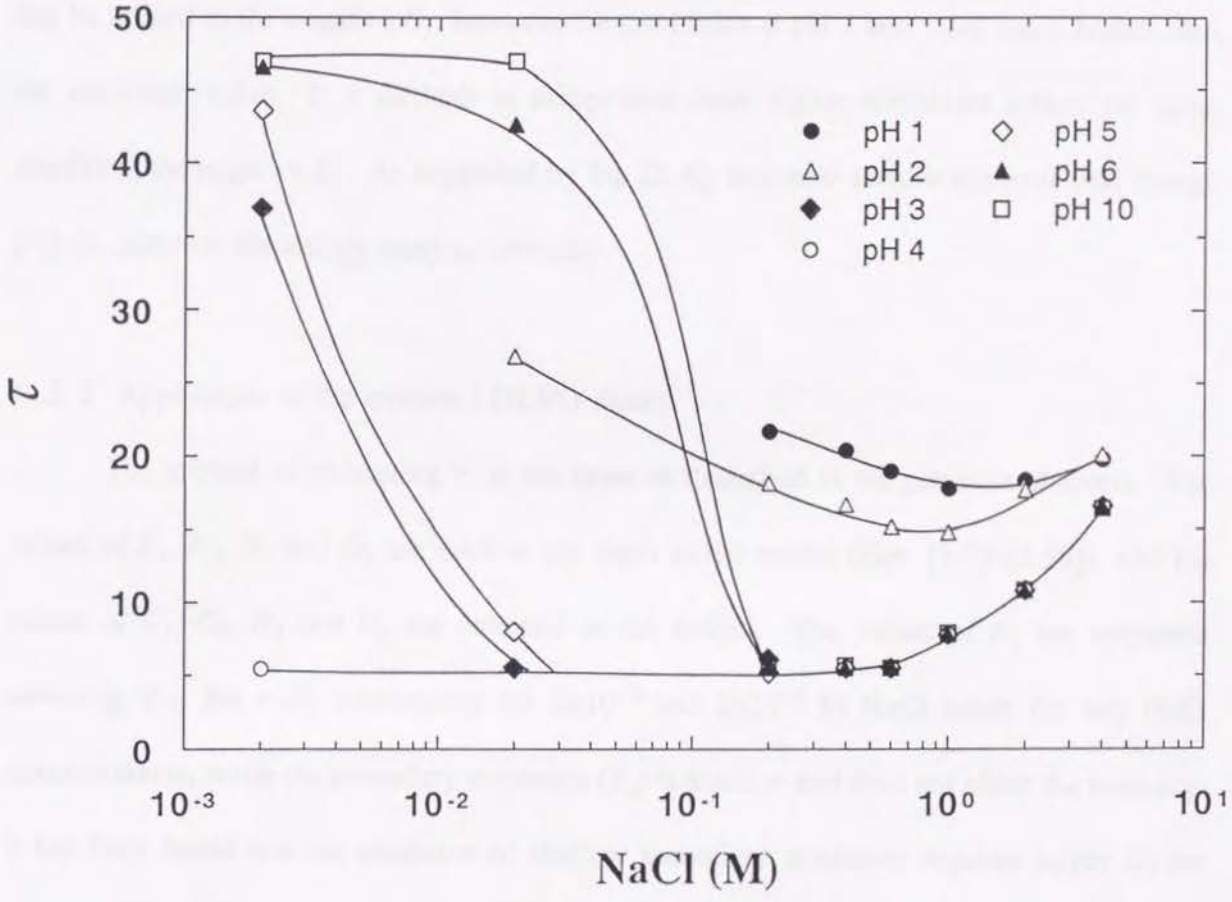

Fig. 4. 3 Turbidities (τ) of stannic oxide suspensions at different pH shown as a function of NaCl concentration.

Using the Eqs. [2. 1] and [2. 2], the total interaction energy (V_t) and, hence, the energy barrier (E_1) for each turbidity measurement in Fig. 4. 2 has been calculated. In Fig. 4. 4, τ is plotted vs. E_1 obtained above. It is shown that the τ–E_1 plots for $2x10^{-2}$ M and $2x10^{-3}$ M can be fit by a single correlation curve, suggesting that τ is uniquely defined by E_1. The result obtained at $2x10^{-1}$ M NaCl are not shown because the E_1's are negative according to the classical DLVO theory. The turbidities at $2x10^{-1}$ M NaCl are minimum at pH >2 which can be related to the negative E_1, however the turbidities at pH 2 and 1 are much higher than the minimum value. It is difficult to accept that these higher turbidities reflect the same condition, the negative E_1. As suggested by Eq. [2. 6], one must include the structural energy (V_s) to calculate the energy barriers correctly.

4. 3. 2 Application of the extended DLVO theory

The method of estimating V_s is the same as described in the previous chapters. The values of E_1, E_2, D_1 and D_2 are used as the input to the model (Eqs. [2.7]–[2.10]), and the values of C_1, C_2, H_1 and H_2 are obtained as the output. The values of E_1 are estimated assuming that the τ–E_1 relationship for $2x10^{-2}$ and $2x10^{-3}$ M NaCl holds for any NaCl concentrations, while the secondary minimum (E_2) is shallow and does not affect the turbidity. It has been found that the condition of shallow secondary minimum requires larger D_2 for stannic oxide than those of silica and rutile due to the larger Hamaker constant (A_{131}) of stannic oxide. When E_2 is assumed to be −3 kT, D_2 should be larger than or equal to 4.3 nm with stannic oxide, while 3nm of D_2 is enough for silica and rutile to make the same shallow E_2.

Fig. 4. 5 shows the effect of D_2 on E_1 for the turbidity at $2x10^{-1}$ M NaCl and pH 2.0. The value of E_1 is calculated to be 28.1 kT from the τ–E_1 curve in Fig. 4. 4. While the V_s

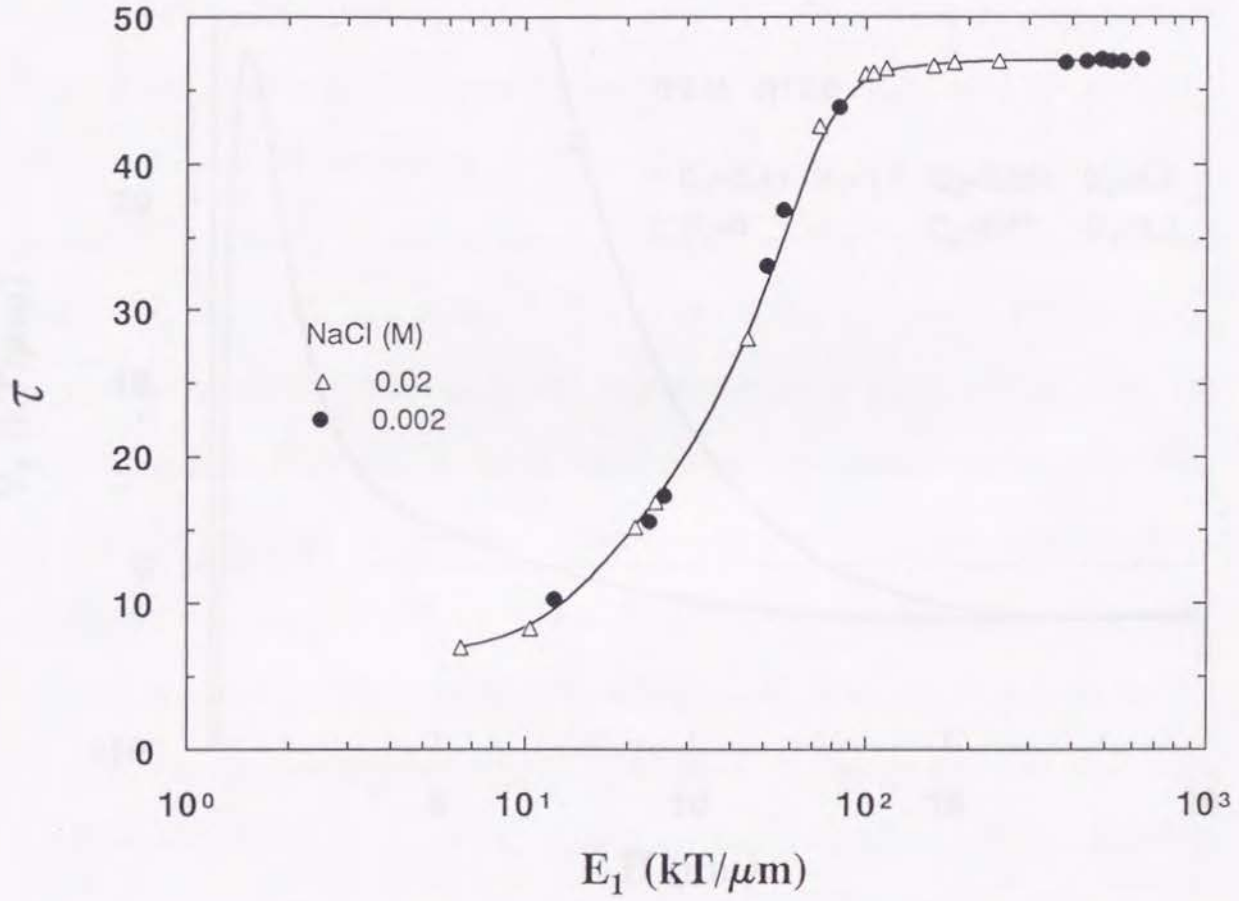

Fig. 4. 4 Turbidities (τ) of stannic oxide suspensions plotted vs. energy barriers (E_1) calculated using the classical DLVO theory. The turbidity data at 0.2 M NaCl are not shown because the total energies (V_t) are negative.

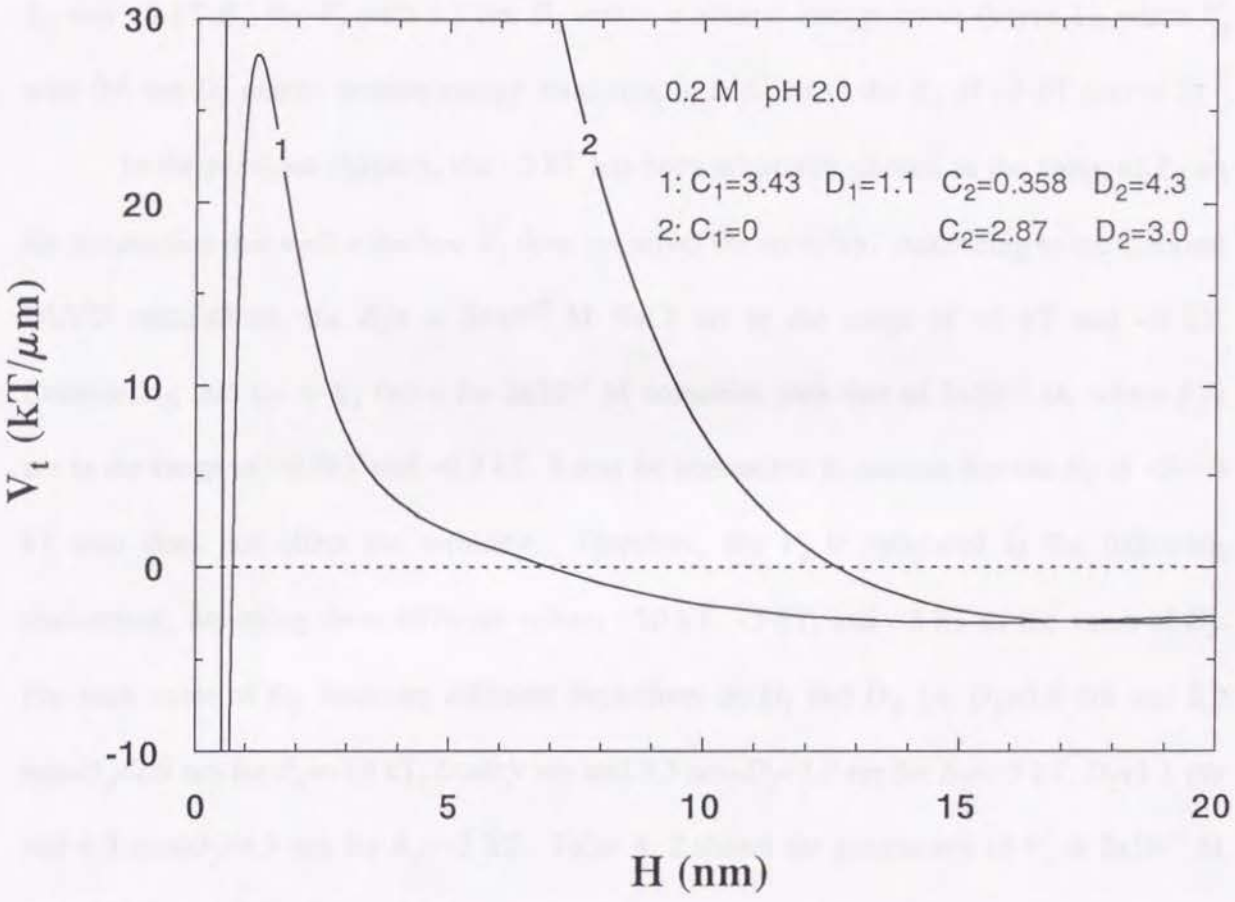

Fig. 4. 5 Total interaction energies (V_t) plotted vs. separation distance (H). The second decay lengths of structural force (D_2) are assumed to be 4.3 nm (curve 1) and 3.0 nm (curve 2), respectively. The shorter D_2 makes a very large energy barrier (E_1) with the condition of −3 kT E_2.

with 4.3 nm D_2 can satisfy both the condition of E_1=28.1 kT and E_2=−3 kT (curve 1), the V_s with 3 nm D_2 makes E_1 of 232 kT even if C_1 is assumed to be zero (curve 2), which is attributed to the fact that the shorter D_2 requires larger C_2 to satisfy the condition of −3 kT E_2 and, hence, the V_s becomes larger at small separations. In the same manner, the value of D_1 is also limited to a certain range. Fig. 4. 6 shows an example of such cases. At 1 M NaCl and pH 4.0, the value of E_1 is calculated to be 8.2 kT. With the condition of 8.2 kT E_1 and −3 kT E_2, the V_s with 1.1 nm D_1 makes a normal energy curve (curve 1), while V_s with 0.6 nm D_1 makes another energy minimum in addition to the E_2 of −3 kT (curve 2).

In the previous chapters, the −3 kT has been arbitrarily chosen as the value of E_2 on the assumption that such a shallow E_2 does not affect the turbidity. According to the classical DLVO calculations, the E_2's at 2×10^{-2} M NaCl are in the range of −5 kT and −8 kT. Considering that the τ–E_1 curve for 2×10^{-2} M coincides with that of 2×10^{-3} M, where E_2's are in the range of −0.3kT and −0.7 kT, it may be reasonable to assume that the E_2 of −5~−8 kT also does not affect the turbidity. Therefore, the V_s is estimated in the following discussions, assuming three different values, −10 kT, −5 kT, and −3 kT as the value of E_2. For each value of E_2, there are different limitations on D_1 and D_2, i.e. $D_1 \geq 0.6$ nm and 2.2 nm$\leq D_2 <$2.9 nm for E_2=−10 kT, $D_1 \geq 0.9$ nm and 3.3 nm$\leq D_2 <$3.9 nm for E_2=−5 kT, $D_1 \geq 1.1$ nm and 4.3 nm$\leq D_2 <$4.9 nm for E_2=−3 kT. Table 4. 2 shows the parameters of V_s at 2×10^{-1} M and pH 1.0 and 2.0 calculated using the lower limit values of D_1 and D_2 for each case. One can see that the V_s is larger at pH 1 than at pH 2.

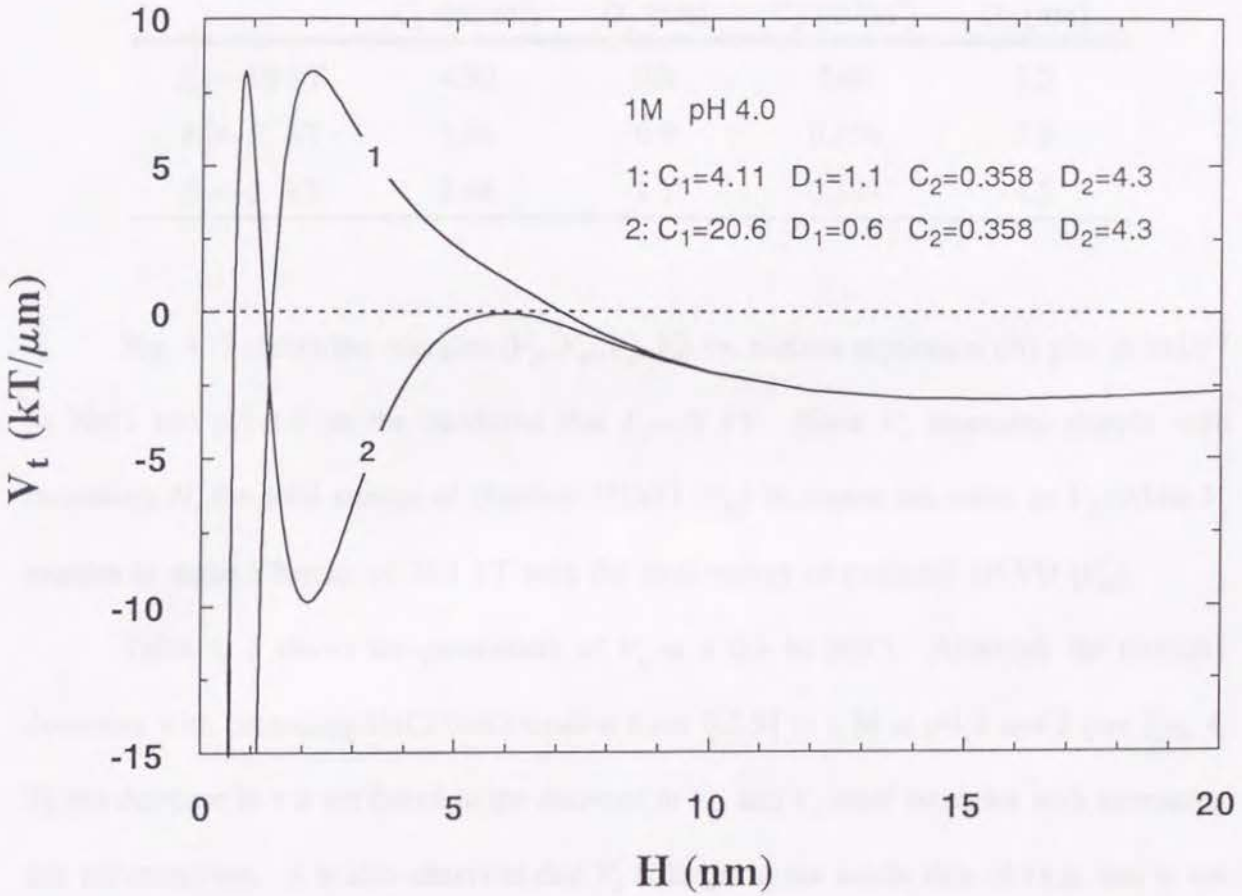

Fig. 4. 6 Total interaction energies (V_t) plotted vs. separation distance (H). The first decay lengths of structural force (D_1) are assumed to be 1.1 nm (curve 1) and 0.6 nm (curve 2), respectively. The shorter D_1 makes another minimum before the secondary energy minimum (E_2=−3 kT).

Table 4. 2 Structural energy parameters (C_1, D_1, C_2, D_2) of stannic oxide in 0.2 M NaCl solution.

pH 1

	C_1 (mJ/m^2)	D_1 (nm)	C_2 (mJ/m^2)	D_2 (nm)
E_2=−10 kT	9.43	0.6	1.60	2.2
E_2=−5 kT	5.62	0.9	0.656	3.3
E_2=−3 kT	4.52	1.1	0.358	4.3

pH 2

	C_1 (mJ/m^2)	D_1 (nm)	C_2 (mJ/m^2)	D_2 (nm)
E_2=−10 kT	4.90	0.6	1.60	2.2
E_2=−5 kT	3.94	0.9	0.656	3.3
E_2=−3 kT	3.44	1.1	0.358	4.3

Fig. 4. 7 shows the energies (V_e, V_d, V_s, V_t) vs. surface separation (H) plot at $2\text{x}10^{-1}$ M NaCl and pH 1.0 on the condition that E_2=−5 kT. Since V_e decreases sharply with increasing H, the total energy of classical DLVO (V_{t1}) is almost the same as V_d, while V_s enables to make a barrier of 34.1 kT with the total energy of extended DLVO (V_{t2}).

Table 4. 3 shows the parameters of V_s at ≥ 0.4 M NaCl. Although the turbidity decreases with increasing NaCl concentration from 0.2 M to 1 M at pH 1 and 2 (see Fig. 4. 3), the decrease in τ is attributed to the decrease in V_e, and V_s itself increases with increasing salt concentration. It is also observed that V_s is larger at the acidic side of i.e.p. and is not affected by pH at the alkaline side of i.e.p. This is quite similar to what has been observed with rutile.

In order to compare the secondary hydration forces observed with stannic oxide and rutile, the coagulation data of rutile at ≥1 M NaCl were re-processed and the parameters of V_s were obtained assuming the same E_2 and D_1 as stannic oxide. The results are shown in Table 4. 4. Although the values of D_2 used in the calculation were different from what has

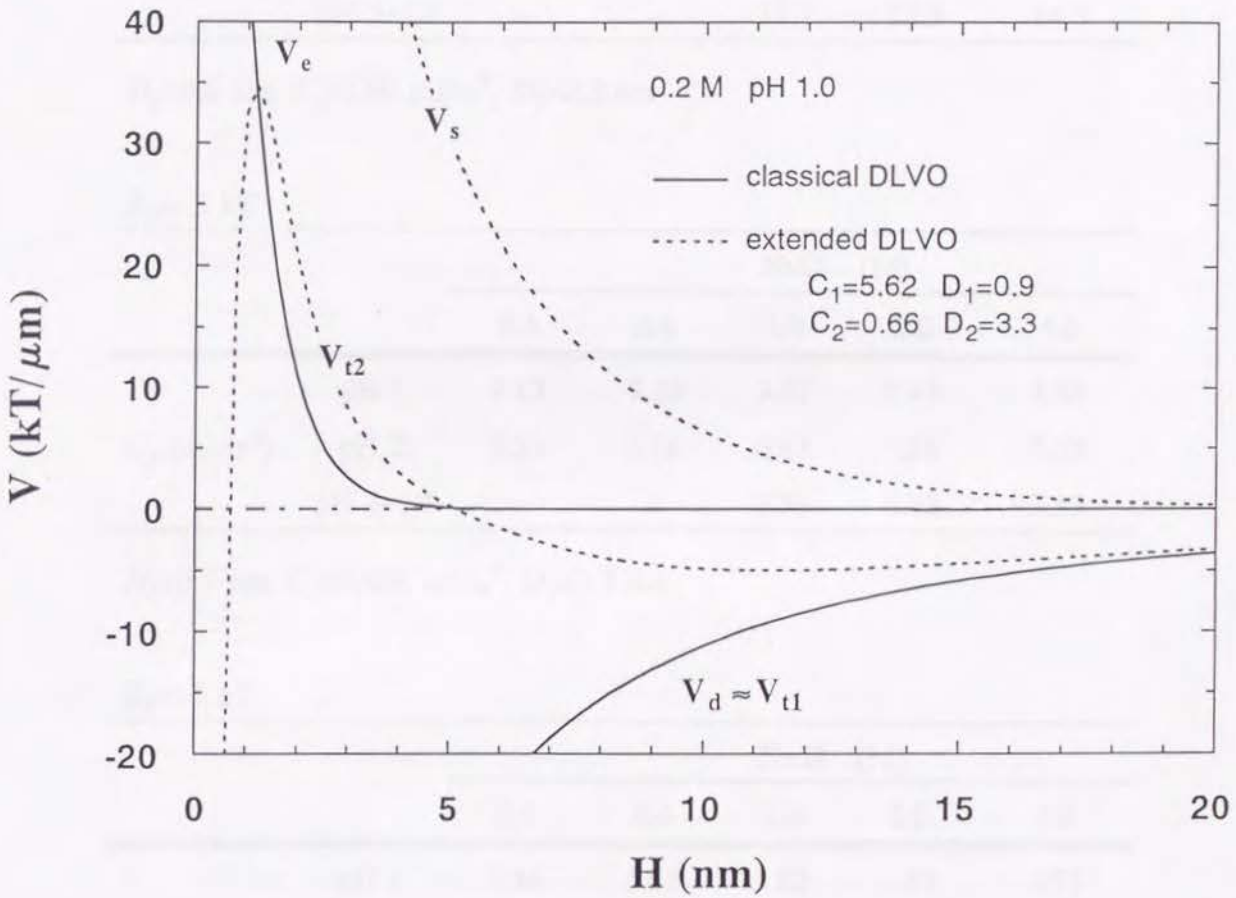

Fig. 4. 7 Interaction energies (V) plotted vs. separation distance (H). The solid lines represent the classical DLVO theory, while dashed lines the extended DLVO theory with the condition of −5 kT E_2. The structural energy (V_s) makes the 34.7 kT energy barrier (E_1) which corresponds to the turbidity of 21.7.

Table 4. 3 Structural energy constants (C_1) of stannic oxide suspension at various NaCl concentrations and pH.

E_2=−10 kT

		NaCl (M)				
		0.4	0.6	1.0	2.0	4.0
C_1 (mJ/m^2)	pH 1	13.3	14.3	14.7	14.9	15.3
	pH 2	11.4	12.8	13.7	14.7	15.4
	pH 3–10	–	–	11.1	12.3	14.3

D_1=0.6 nm, C_2=1.60 mJ/m^2, D_2=2.2 nm

E_2=−5 kT

		NaCl (M)				
		0.4	0.6	1.0	2.0	4.0
C_1 (mJ/m^2)	pH 1	7.13	7.33	7.37	7.47	7.68
	pH 2	6.33	6.66	6.83	7.36	7.73
	pH 3–10	–	–	5.36	6.02	7.17

D_1=0.9 nm, C_2=0.656 mJ/m^2, D_2=3.3 nm

E_2=−3 kT

		NaCl (M)				
		0.4	0.6	1.0	2.0	4.0
C_1 (mJ/m^2)	pH 1	5.46	5.52	5.52	5.59	5.75
	pH 2	4.93	5.07	5.13	5.51	5.78
	pH 3–10	–	–	4.11	4.56	5.37

D_1=1.1 nm, C_2=0.358 mJ/m^2, D_2=4.3 nm

Table 4. 4 Structural energy constants (C_1) of rutile at above 1 M NaCl. The calculation was conducted using the same D_1 and E_2 as used in the calculation with stannic oxide.

E_2=−10 kT

		NaCl (M)		
		1.4	2.0	4.0
C_1 (mJ/m^2)	pH 3	12.6	12.6	12.3
	pH 4	11.5	11.5	11.8
	pH 5–10	5.96	7.69	8.99

D_1=0.6 nm, C_2=1.91 mJ/m^2, D_2=1.4 nm

E_2=−5 kT

		NaCl (M)		
		1.4	2.0	4.0
C_1 (mJ/m^2)	pH 3	7.20	7.20	7.01
	pH 4	6.54	6.54	6.73
	pH 5–10	3.31	4.31	5.06

D_1=0.9 nm, C_2=0.718 mJ/m^2, D_2=2.2 nm

E_2=−3 kT

		NaCl (M)		
		1.4	2.0	4.0
C_1 (mJ/m^2)	pH 3	5.58	5.58	5.43
	pH 4	5.07	5.07	5.21
	pH 5–10	2.60	3.36	3.93

D_1=1.1 nm, C_2=0.364 mJ/m^2, D_2=3.3 nm

been used with stannic oxide, the comparison of V_s between stannic oxide and rutile at close separation (H<5 nm) is possible where the magnitude of V_s is mainly determined by the value of C_1. At the alkaline side of respective i.e.p.'s, stannic oxide exhibits stronger hydration force than rutile at the same NaCl concentrations. Since there is a difference in i.e.p.'s of stannic oxide and rutile by 2.2 pH, pH 1 for stannic oxide may be comparable to pH 3 for rutile from the standpoint that the both pH's are at the acidic sides apart from respective i.e.p's by about 3 pH. If the secondary hydration forces at the acidic side of i.e.p. are compared in this manner, the force is stronger with stannic oxide than with rutile. As will be discussed later, the secondary hydration force is supposed to be related directly to the adsorption of hydrated ions, the observation above may suggest that the ion adsorption by stannic oxide is larger than that of rutile. The confirmation of this is left for future research.

4. 4 Primary and secondary hydration forces.

The primary and secondary hydration forces show the opposite behavior with the change of electrolyte concentration. The primary hydration force decreases with increasing NaCl concentration, while the secondary hydration force increases with increasing salt concentration. This observation suggests that the forces are developed from different origins.

As has been discussed in Chapter 2, the primary hydration force of silica is probably attributed to the hydration of surface silanol groups (Si–OH), which may be represented schematically as shown in Fig. 4. 8. The thickness of water layer has been reported as one molecule deep[6], several molecules deep[7] or up to 90 nm[8]. This water layer (or structure) is supposed to develop a steric repulsion when two surfaces approach each other. The decrease of the steric repulsion with the introduction of NaCl can be explained by the

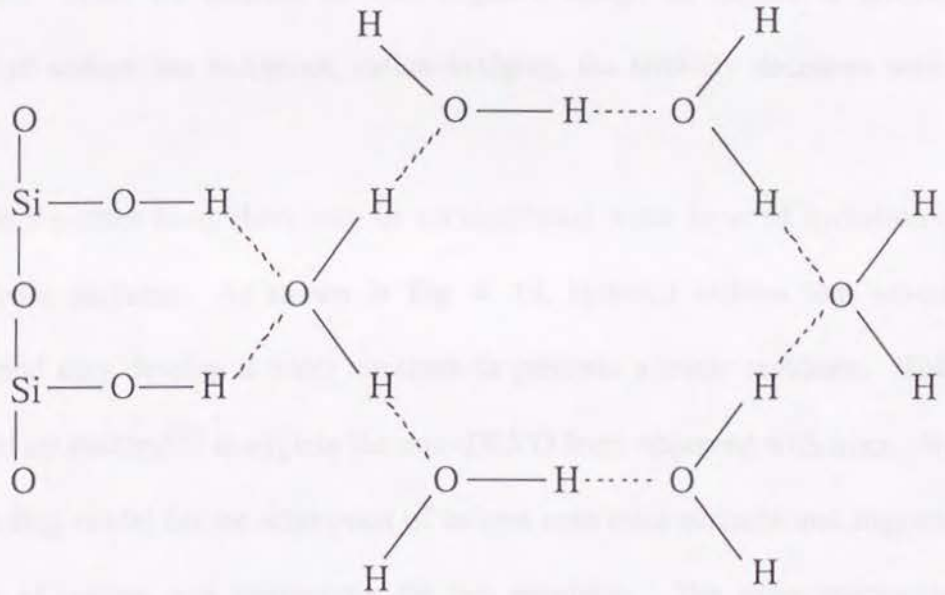

Fig. 4. 8 Schematic diagram of the structure of water molecules adsorbed on silanol groups.

"bridging mechanism" of sodium ion proposed by Iler[9]. A sodium ion in solution is surrounded by the oxygen atoms of six water molecules of hydration. As shown in Fig. 4. 9, it is suggested that when the sodium ion is adsorbed on the surface of silica particle, one or more of the oxygen atoms of the water of hydration can be displaced by the oxygens of the surface silanol group, which thus become linked directly to the sodium. In a similar manner, the rest of water molecules linked to the outwardly disposed side of the sodium ion can be displaced by the silanol groups on the surface of a second colliding particle. The sodium ion may thus act as a bridge between two silica particles. In this case, the increased concentration of NaCl may increase the cation-bridging and decrease the turbidity of suspension. Since the increase of total negative charge on surface is favorable for the approach of sodium ion and,hence, cation-bridging, the turbidity decreases with increasing pH.

On the other hand, there may be no significant water layer of hydration on rutile or stannic oxide surfaces. As shown in Fig. 4. 10, hydrated sodium ions adsorb onto the surfaces and may develop a water structure to generate a steric repulsion. This idea was introduced by Pashley[10] to explain the non-DLVO force observed with mica. He proposed a site-binding model for the adsorption of cations onto mica surfaces and suggested that the hydration of cations was responsible for this repulsion. The same mechanism may be applicable to the case of rutile and stannic oxide. Since the increased NaCl concentration increases the adsorption of sodium ions, it may increase the steric repulsion and hence increase the turbidity.

The discussion above is based on the assumption that there is an inherent hydration layer on silica surface and not on stannic oxide and rutile surfaces. There seems to be some observations to support this assumption. According to Tien [11] and Abendroth[12], the cation

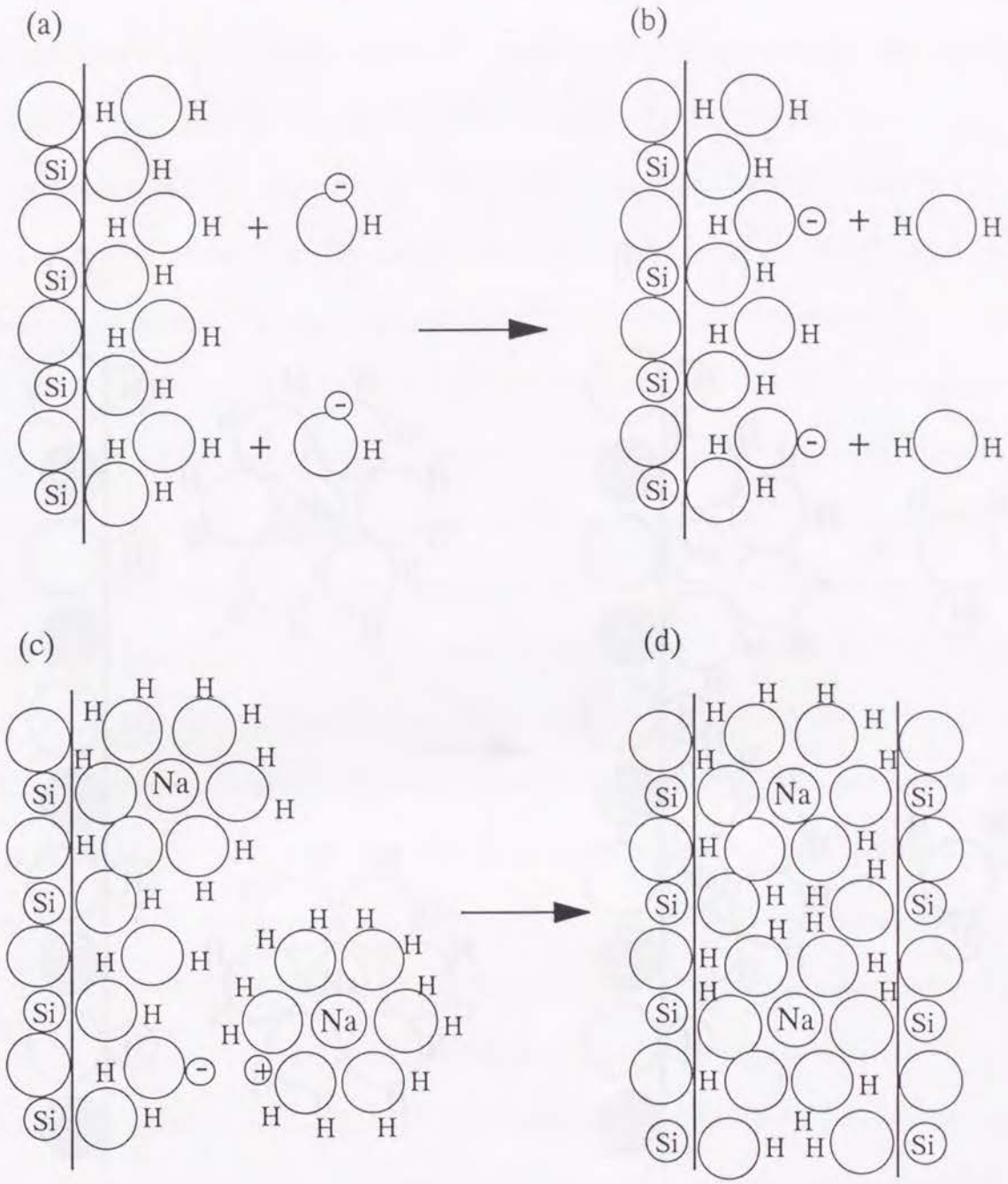

Fig. 4. 9 Cation–bridging mechanism proposed by Iler[9]. The sodium ion adsorb on silica surface by exchanging the water of hydration with the adsorbed water molecules (or silanol groups) on the silica surface.

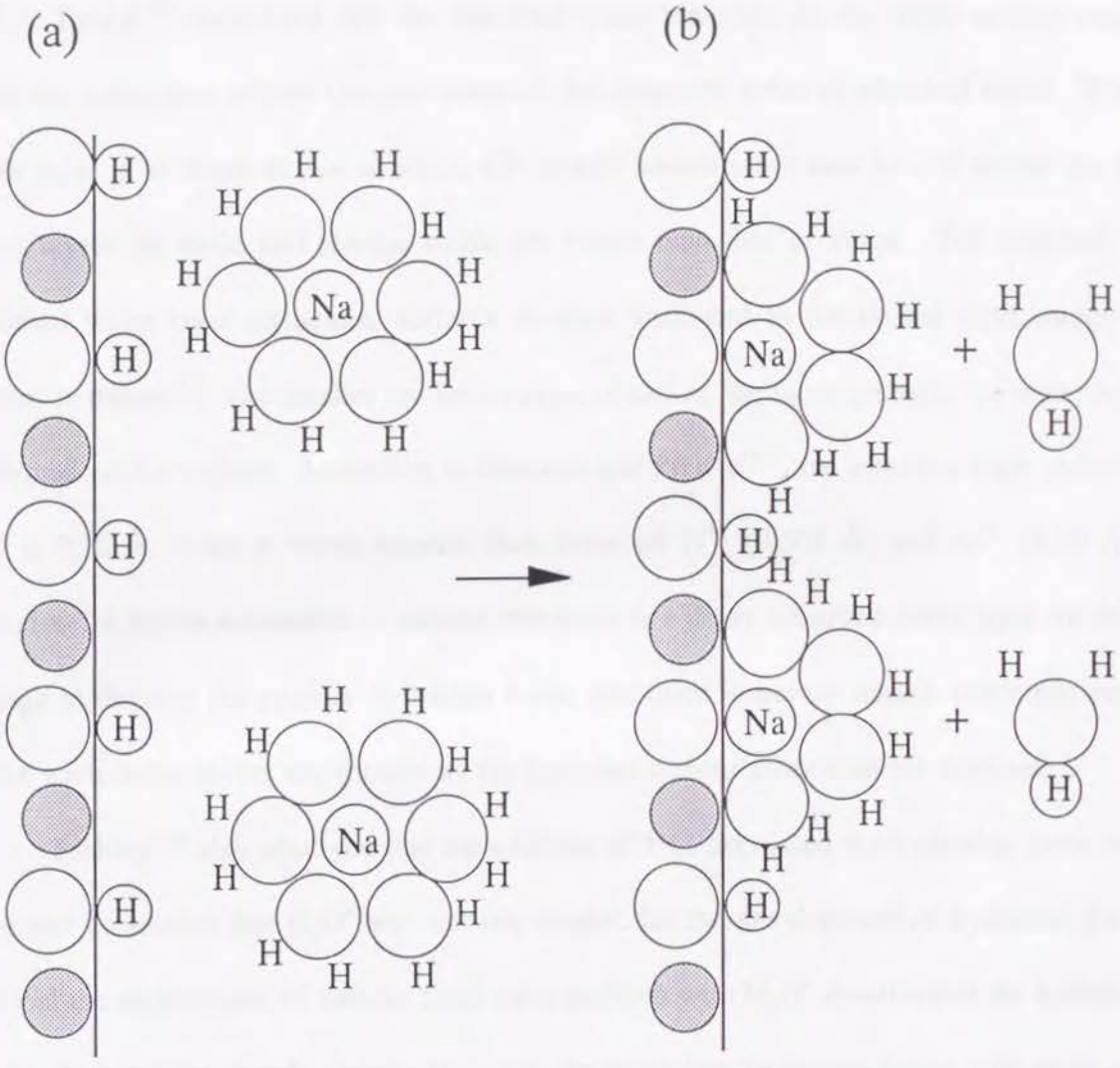

Fig. 4. 10 Assumed mechanism of the secondary hydration force. The structure of water molecules is formed as hydrated cations adsorb on the surface.

uptake by silica decreases following the order, $Cs^+ > K^+ > Na^+ > Li^+$. This sequence may be attributed to the fact that the structure breaking cation (Cs^+) is better able to penetrate the hydration layer on silica than the structure promoting cation (Li^+). On the contrary, the reverse sequence $Li^+ > Na^+ > K^+ > Cs^+$ is observed in stannic oxide[13] and rutile[14]. Bérubé and de Bruyn[14] considered that the adsorbed water molecule on the oxide surface would favor the adsorption of ions that can maintain the structural order of adsorbed water. If this water layer is as dense as that of silica, Cs^+ should adsorb more than Li^+. It seems that the water layers on rutile and stannic oxide are looser than that of silica. The existence of adsorbed water layer on oxides' surfaces is often attributed to the crystal field energy of cations in oxides[3]. The smaller the ionic radius of cation, the more probable the water layer is formed on the surface. According to Shannon and Prewitt[15], the effective ionic radius of Si^{4+} is 0.26 Å which is much smaller than those of Ti^{4+} (0.605 Å) and Sn^{4+} (0.69 Å). Therefore, it seems reasonable to assume that there is a dense adsorbed water layer on silica enough to develop the primary hydration force, and there is not on stannic oxide and rutile where such dense layers are formed as the hydrated cations adsorb on the surfaces.

Pashley[10] also observed that the addition of HCl decreased the hydration force with mica and concluded that H_3O^+ was not responsible for the development of hydration force, and that the replacement of cations from mica surfaces with H_3O^+ deteriorated the hydration force. As has been already shown, however, the secondary hydration forces with rutile and stannic oxide are stronger at each acidic side of i.e.p. than at each alkaline side. This is observed with rutile at above 1 M NaCl and with stannic oxide at above 0.2 M NaCl. While the hydration force increases with decreasing pH at the acidic side, the force is not affected by pH near i.e.p. and at the alkaline side. A possible explanation of this is the effect of the hydration of adsorbed *anions*. The enthalpy of hydration of Cl^- is −376 kJ/mol[16], which is

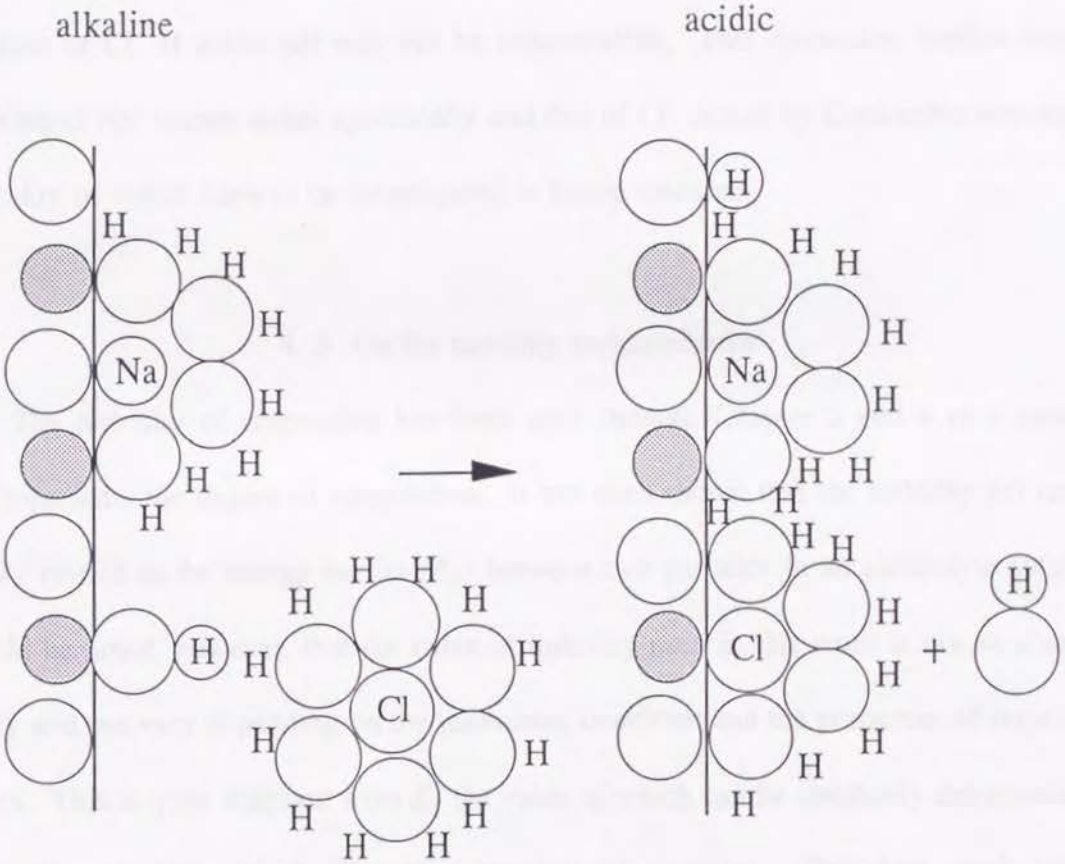

Fig. 4. 11 Assumed anion adsorption on the surface. Hydrated anions adsorb on oxide surface at acidic pH and reinforce the water structure.

smaller than that of Na^+ (−407 kJ/mol) but is larger than that of K^+ (−324 kJ/mol). According to Pashley[17], the hydration force with mica is observed with not only K^+ but also Cs^+ whose enthalpy of hydration is −274 kJ/mol. Judging from these enthalpy data, it may be reasonable to assume that the adsorption of Cl^- also develops the secondary hydration force. In an acidic solution, the Cl^- may replace OH^- adsorbed on Ti or Sn in an alkaline solution, and may reinforce the hydration layer on the surface (see Fig. 4. 11). Since the specific adsorption of ClO_4^- on rutile is reported to occur in an acidic solution[18], the adsorption of Cl^- at acidic pH may not be unreasonable. This discussion implies that the adsorption of Na^+ occurs rather specifically and that of Cl^- occurs by Coulombic interaction, the validity of which have to be investigated in future research.

4. 5 On the turbidity measurements

The turbidity of suspension has been used through Chapter 2 and 4 as a measure which represents the degree of coagulation. It has been shown that the turbidity (τ) can be uniquely related to the energy barrier (E_1) between two particles in an electrolyte solution. It should be noted, however, that the value of turbidity used in this work is not an absolute quantity and can vary depending on the measuring condition and the properties of respective particles. This is quite different from E_1 the value of which can be absolutely determined by the electric potential and the Hamaker constant of particles. Therefore, each unique correlation between τ and E_1 is peculiar to each oxide and measuring condition.

One can see an example of this by comparing τ–E_1 curves for silica and stannic oxide. In both cases, the turbidities were measured by the same method using the same light scattering apparatus. However, the τ–E_1 curves are quite different as shown in Fig. 4. 12, where curves are extracted from Fig. 2. 9 (silica; E_1^{25}=100 kT) and Fig. 4. 4 (stannic oxide).

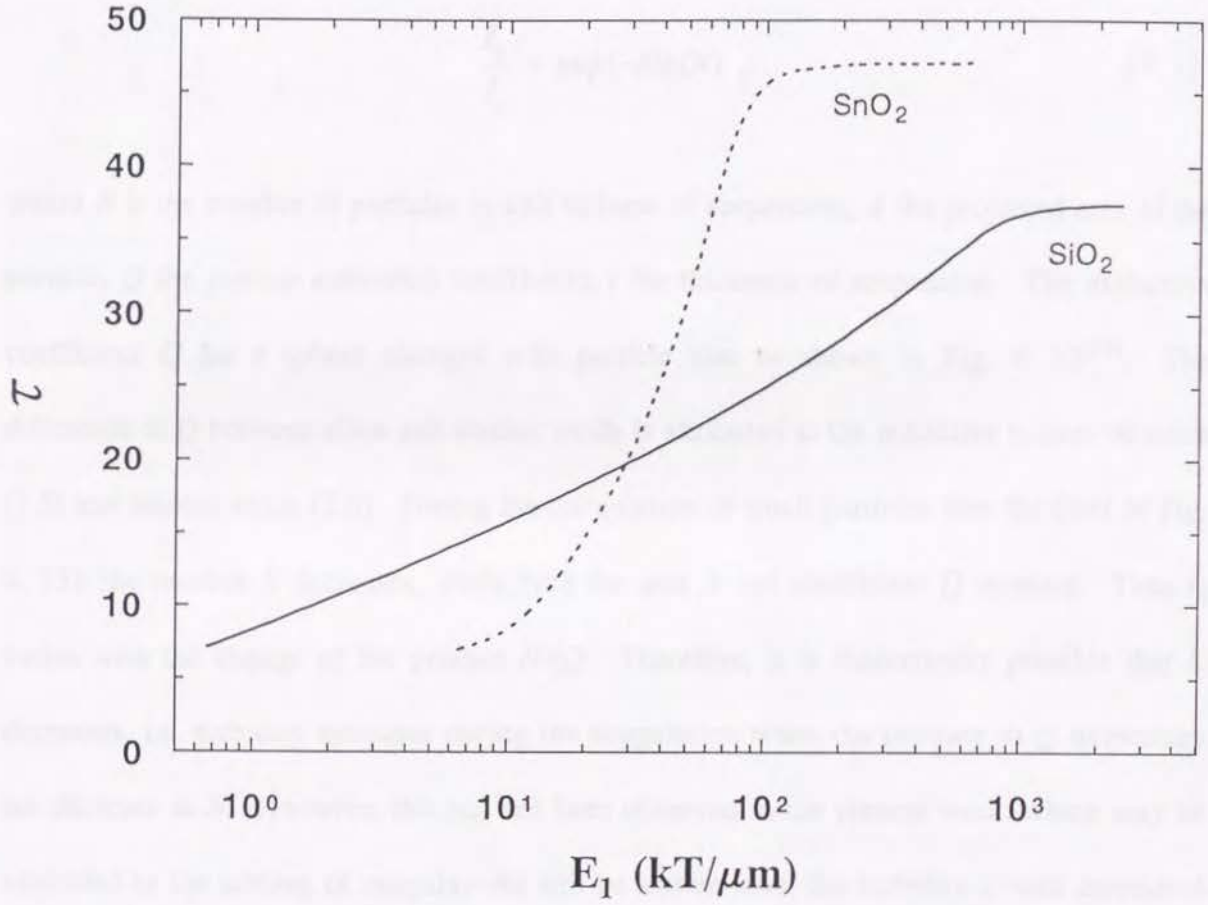

Fig. 4. 12 Turbidity (τ) vs. energy barrier (E_1) relationship of silica (E_1^{25}=100 kT) and stannic oxide.

The turbidity of silica starts to decrease at E_1=600 kT/μm, while that of stannic oxide does at E_1=100 kT/μm. It seems as if silica coagulated easier than stannic oxide in spite of much larger energy barrier. However, this is not the case and can be explained in the following by considering the complex behavior of turbidity.

When the intensity of transmitted and incident light are given as I_0 and I_i respectively, the following relation can be written:

$$\frac{I_0}{I_i} = \exp(-NAQt) \ , \qquad [4.\ 1]$$

where N is the number of particles in unit volume of suspension, A the projected area of the particle, Q the particle extinction coefficient, t the thickness of suspension. The extinction coefficient Q for a sphere changes with particle size as shown in Fig. 4. 13[19]. The difference in Q between silica and stannic oxide is attributed to the refractive indices of silica (1.5) and stannic oxide (2.0). During the coagulation of small particles (see the inset of Fig. 4. 13), the number N decreases, while both the area A and coefficient Q increase. Then I_0 varies with the change of the product NAQ. Therefore, it is theoretically possible that I_0 decreases, i.e. turbidity increases during the coagulation when the increase in Q overcomes the decrease in N. However, this has not been observed in the present work, which may be attributed to the settling of coagula. As will be shown later, the turbidity is well correlated to the settled amount of solid which may be another indicator for coagulation.

Since the slope of Q vs. particle size is larger with stannic oxide than silica for small particles, the decrease in N may be well compensated by the increases in Q with stannic oxide, while it may not with silica. Then the increase in I_0 during the coagulation may be larger with silica than with stannic oxide. This increase in I_0 brings the decrease in τ, because τ is defined as I_{90} / I_0. Although I_{90} also increases with coagula size, the increment

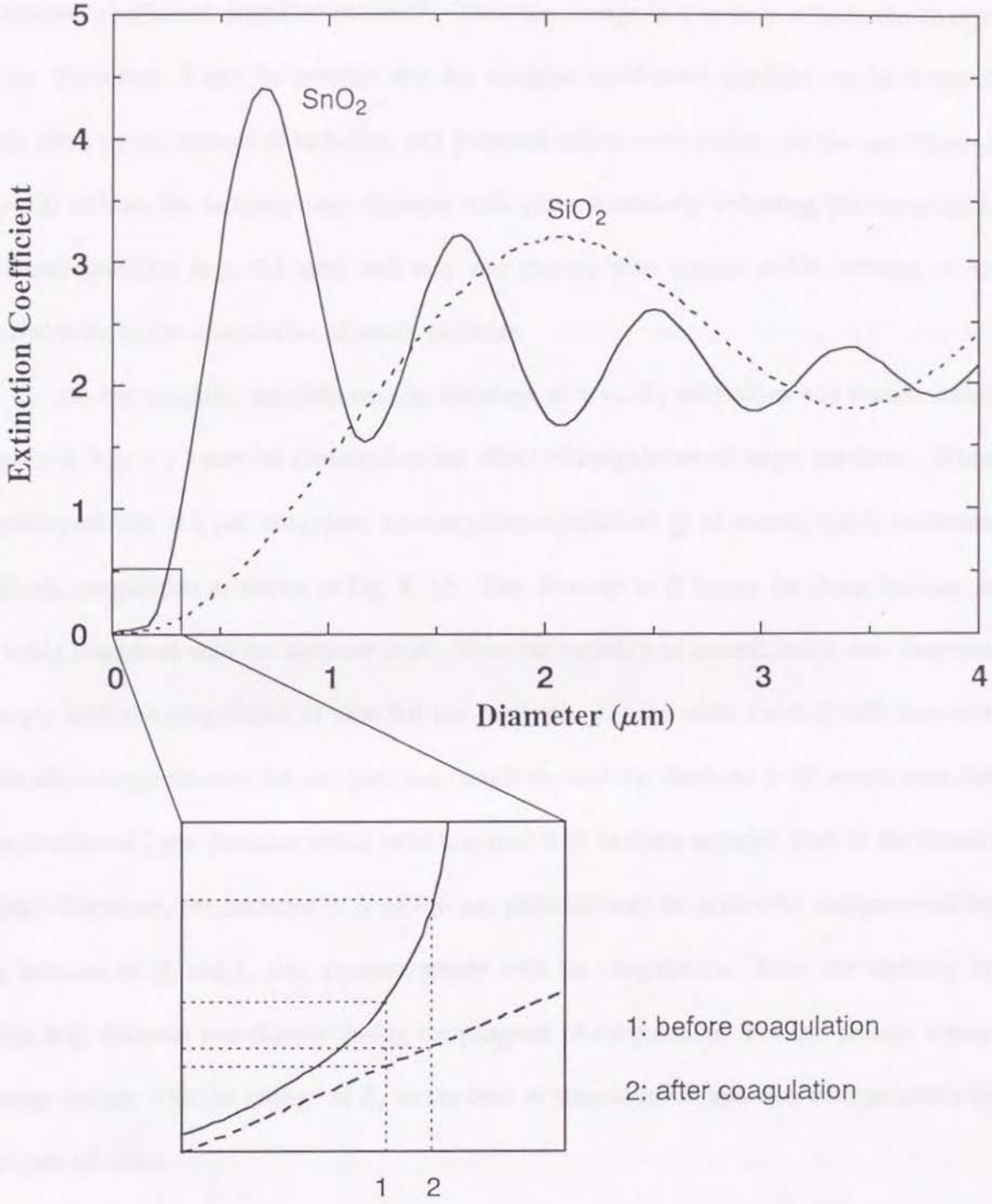

Fig. 4. 13 Particle extinction coefficient of silica and stannic oxide shown as a function of particle diameter.

of I_{90} vs. particle size does not differ as distinctly with the refractive index as in the case of extinction coefficient described above[20]. Thus the change in τ mainly reflects the change in I_0. Therefore, it may be possible that the coagulation of small particles can be detected with silica by the change of turbidity, and it cannot with stannic oxide. At the condition of E_1=600 kT/μm, the turbidity may decrease with silica sensitively reflecting the coagulation of small particles (e.g. 0.1 μm) and may not change with stannic oxide because of its insensitivity to the coagulation of small particles.

On the contrary, the difference in the slope of τ vs. E_1 with silica and stannic oxide shown in Fig. 4. 12 may be explained as the effect of coagulation of larger particles. When particles of near 0.6 μm coagulate, the extinction coefficient Q of stannic oxide decreases with the coagulation as shown in Fig. 4. 13. This decrease in Q brings the sharp increase in I_0 being combined with the decrease in N. Thus the turbidity of stannic oxide may decrease sharply with the coagulation of near 0.6 μm particles. On the other hand, Q still increases with silica when its near 0.6 μm particles coagulate, and the decrease in Q occurs with the coagulation of 2 μm particles which exist less than 6 % in silica samples used in the present work. Therefore, the decrease in N of 0.6 μm particles may be somewhat compensated by the increase of Q, and I_0 may decrease gently with the coagulation. Thus, the turbidity of silica may decrease less sharply during the progress of coagulation. For this reason, τ may change steeply with the change of E_1 in the case of stannic oxide and may change gently in the case of silica.

The discussion above implies that the turbidity of silica is sensitive to the coagulation of small particles and that of stannic oxide is sensitive to the coagulation of larger particles. Thus the τ–E_1 relationship seems to be peculiar to each oxide. The same value of τ for different oxides does not mean the same coagulation condition with each oxide. The value

of τ itself varies depending of the definition of τ (e.g. $\tau=I_{90} / I_0$ or $\tau=I_0$) and its measuring conditions (e.g. settling time). It seems, therefore, important to check whether the obtained result in the extended DLVO calculations, e.g. C_1, D_1, etc. should change if another parameter is used as an indicator of coagulation. In order to answer this question, the settled amount of solid in the coagulation experiment has been chosen as the indicator, and the correlation between the settled amount and turbidity has been investigated. The result is shown in Fig. 4. 14. Since the 29/400 of total solid (14.5 mg) in the 29 ml siphoning residue is not brought about by the settling, it was subtracted from the siphoning residue and was added to the solid recovered with the supernatant. As shown in Fig. 4. 14, the settled amount vs. turbidity can be regressed by 2nd order polynomials, which suggests that there is 1 to 1 relationship between the settled amount of solid and turbidity.

Using these regression curves, all the turbidity data in Chapter 2 & 4 can be replaced by settled amount of solid. Then it is possible to assume hypothetical experiments where the degree of coagulation is expressed by the settled amount. Thus the τ–E_1 of silica obtained by the classical DLVO theory (Fig. 2. 5) and that of stannic oxide (Fig. 4. 4) have been replaced with settled amount vs. E_1 relationships as shown in Fig. 4. 15. One can see the similarity between τ–E_1 and settled amount vs. E_1. As has been already shown, the magnitude of primary hydration force with silica has been determined so as to obtain a unique relationship between τ and E_1, and the magnitude of secondary hydration force with stannic oxide has been calculated by assuming that the τ–E_1 relationship obtained at ≤0.02 M NaCl holds for ≥0.2 M NaCl. The same procedures have been applied to the settled amount vs. E_1. The result of this with silica is shown in Table 4. 5.

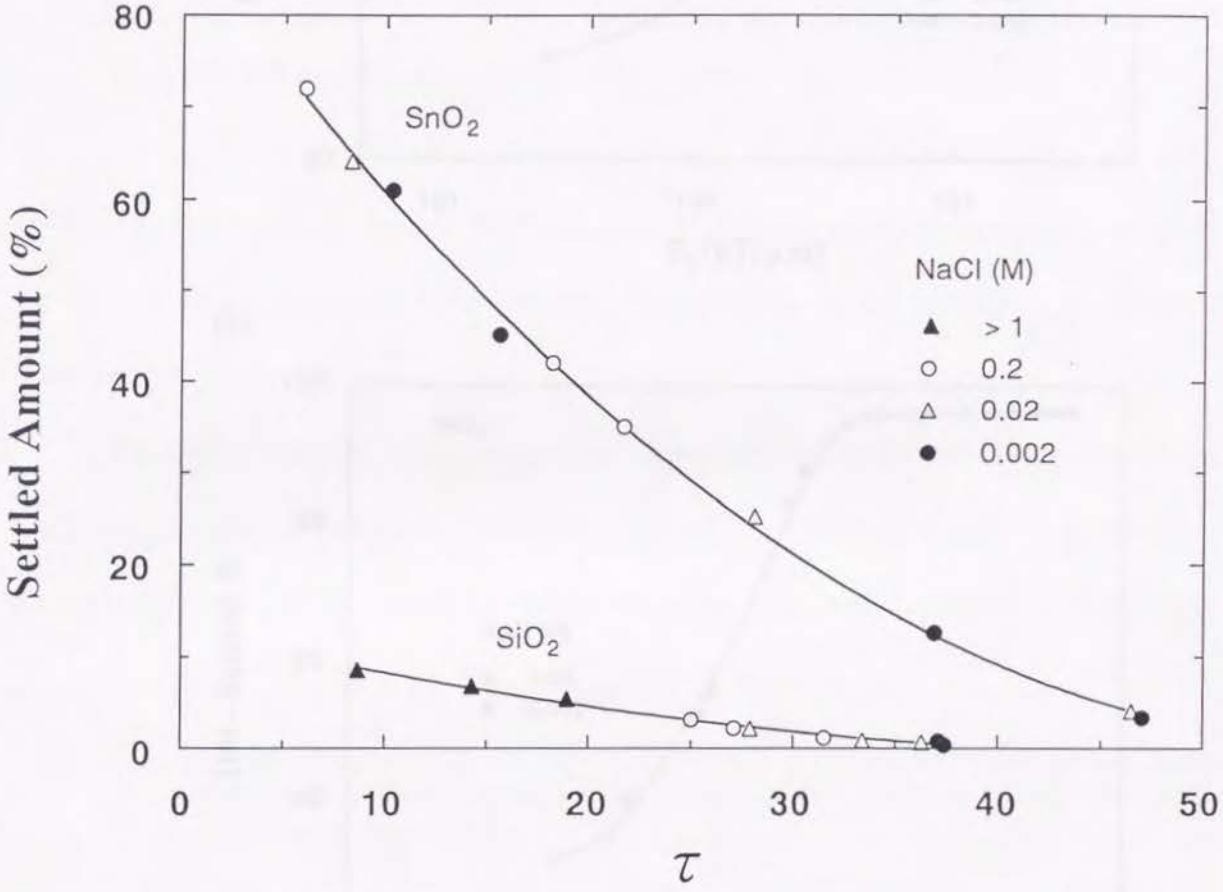

Fig. 4. 14 Correlation between the settled amount of solid and turbidity (τ). The settled amount is obtained with the coagulation experiment of 400 ml suspensions which contain 500 ppm solid by weight. The turbidity is obtained by the same method described earlier.

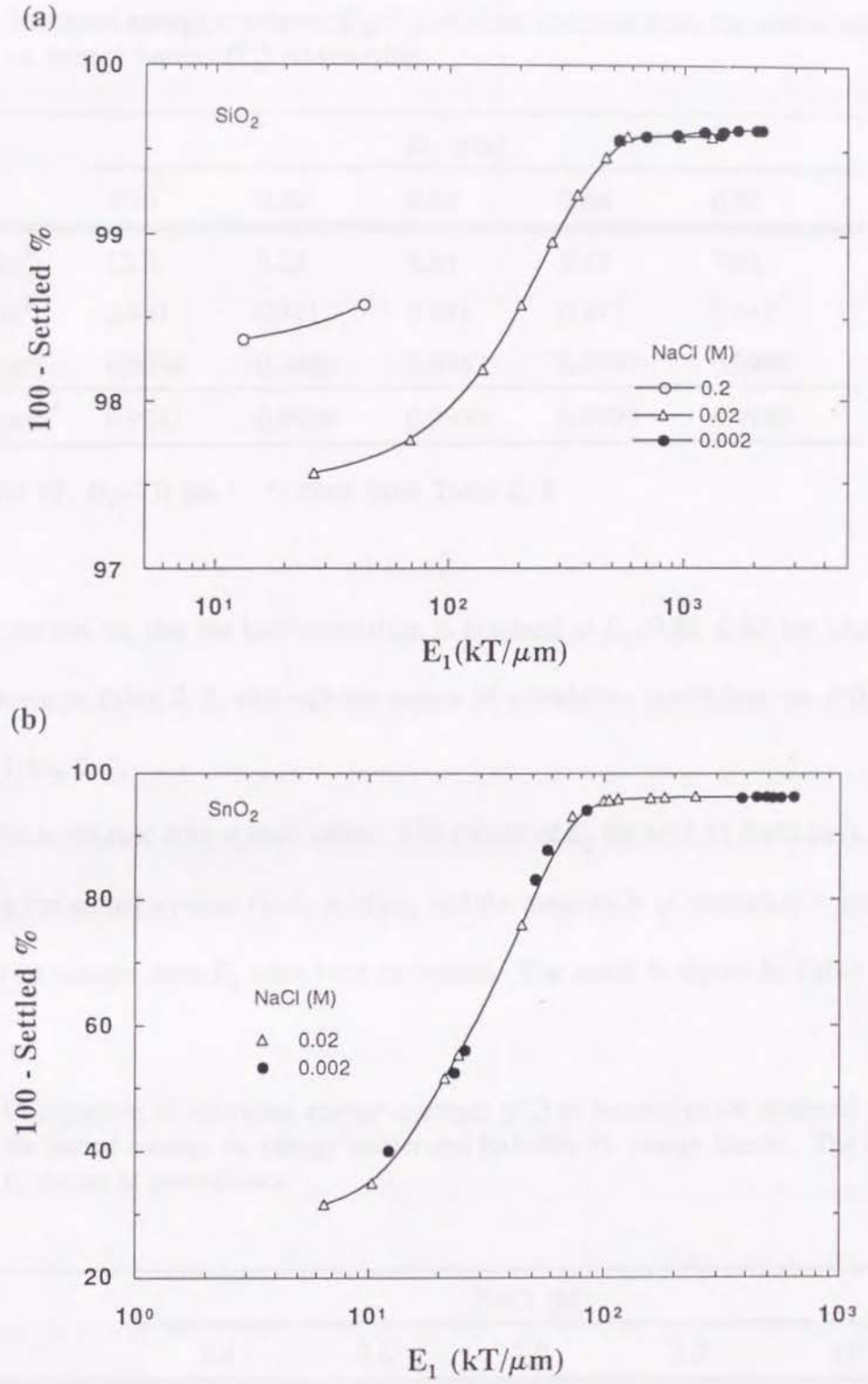

Fig. 4. 15 Settled amount of silica (a) and stannic oxide (b) plotted vs. energy barriers (E_1) calculated using the classical DLVO theory.

Table 4. 5 Structural energy constants (C_1, C_2) of silica obtained from the settled amount vs. energy barrier (E_1) relationship.

	D_1 (nm)				
	0.70	0.82	0.84	0.86	0.92
C_1 (mJ/m^2)	12.3	9.23	8.84	8.47	7.51
C_2 (mJ/m^2)	0.441	0.441	0.441	0.441	0.441
Corr. Coeff.	0.9984	0.9986	0.9987	0.9987	0.9986
Corr. Coeff.*	0.9981	0.9989	0.9990	0.9990	0.9989

E_{125}=100 kT, D_2=3.0 nm *: cited from Table 2. 2

In Table 4. 5, one can see that the best correlation is obtained at D_1=0.84–0.86 nm which is the same as shown in Table 2. 2, although the values of correlation coefficient are different from those in Table 2. 2.

The same is the case with stannic oxide. The values of E_1 for >0.2 M NaCl have been calculated using the settled amount vs. E_1 relation, and the magnitude of secondary hydration force necessary to achieve each E_1 have been estimated. The result is shown in Table 4. 6.

Table 4. 6 Comparison of structural energy constant (C_1) of stannic oxide obtained from the settled amount vs. energy barrier and turbidity vs. energy barrier. The latter is shown in parentheses.

E_2=–10 kT

		NaCl (M)				
		0.4	0.6	1.0	2.0	4.0
	pH 1	13.4(13.3)	14.4(14.3)	14.7(14.7)	14.8(14.9)	15.3(15.3)
C_1 (mJ/m^2)	pH 1	11.4(11.4)	12.8(12.8)	13.7(13.7)	14.6(14.7)	15.3(15.4)
	pH 3–10	–	–	11.1(11.1)	12.1(12.3)	14.3(14.3)

D_1=0.6 nm, C_2=1.60 mJ/m^2, D_2=2.2 nm ( ): cited from Table 4. 3

By comparing the figures in Table 4. 6, one can see that the result is almost the same in both calculations based on the settled amount and the turbidity. The small difference is attributed to the calculation error.

As has been discussed above, the turbidity of suspensions correctly represents the degree of coagulation. Any parameters, as long as they have 1 to 1 relationship with the turbidity, can replace the turbidity and give the same result in the extended DLVO calculations.

4. 6 Conclusion

The analysis of coagulation data on stannic oxide suspensions suggests that there exists the secondary hydration force at NaCl concentrations ≥0.2 M. The force increases with increasing NaCl concentration. It also increases with decreasing pH at the acidic side of i.e.p., while the force is not affected by pH at the alkaline side of i.e.p. The magnitudes of the secondary hydration force is larger with stannic oxide than with rutile at the same NaCl concentrations, the difference of which may be attributed to the amount of ions adsorbed on respective oxides.

The differences between the primary and the secondary hydration forces can be explained by assuming that an inherent hydration layer exists on silica surface and does not exist on other oxides. The validity of this assumption seems to be supported by the opposite sequences of cation affinity with silica and other oxides. In order to explain the increase of the secondary hydration force at acidic pH, the concept of anion adsorption and its hydration are introduced.

Although τ–E_1 curves obtained with silica and stannic oxide are different each other, it can be explained by considering the complex behavior of light extinction, which is affected

by both refractive index and particle size. Therefore, the variation in τ–E_1 curve does not seem to spoil the reliability of turbidity as a measure of coagulation. A series of calculations of extended DLVO theory has been conducted using the settled amount of solid as an indicator of coagulation. The result of it has been confirmed as the same as that obtained earlier using the turbidity.

4. 7 References

1. Fowkes, F.M., *Ind. Chem. Eng.*, **56**, 40 (1964)

2. Visser, J., *Adv. Colloid Interface Sci.*, **3**, 331 (1972)

3. Parks, G.A., *Chem. Rev.*, **65**, 177 (1965)

4. Healy, T.W., and Fuerstenau, D.W., *J. Colloid Sci.*, **20**, 376 (1965)

5. Pashley, R.M., and Quirk, J.P., *Colloids and Surfaces*, **9**, 1 (1984)

6. Dalton R.L., and Iler, R.K., *J. Phys. Chem.*, **60**, 955 (1956)

7. Drost-Hansen, W., *J. Colloid. Interface Sci.*, **58**, 251 (1977)

8. Derjaguin, B.V., *Disc. Faraday Soc.*, **42**, 109 (1966)

9. Iler, R.K., "The Chemistry of Silica," 375, John Wiley and Sons (New York), 1979

10. Pashley, R.M., *J. Colloid Interface Sci.*, **80**, 153 (1981)

11. Tien, H.T., *J. Phys. Chem.*, **69**, 350 (1965)

12. Abendroth, R.P., *J. Colloid Interface Sci.*, **34**, 591 (1970)

13. Inoue, Y., and Yamazaki, H., *Bull. Chem. Soc. Jpn.*, **57**, 3437 (1984)

14. Bérubé, Y.G., and de Bruyn, P.L., *J. Colloid. Interface Sci.*, **28**, 92 (1968)

15. Shannon, R.D., and Prewitt, C.T., *Acta Cryst.*, **B25**, 925 (1969)

16. Marcus, Y., "Ion Solvation," 107, John Wiley and Sons (Chichester), 1985

17. Pashley, R.M., *J. Colloid Interface Sci.*, **83**, 531 (1981)

18. Marabini, A.M., and Barbaro, M., *Int. J. Miner. Process.*, **7**, 159 (1980)

19. Van de Hulst, H.C., "Light Scattering by Small Particles," 151, John Wiley & Sons (New York), 1962

20. Hodkinson, J.R., "Aerosol Science," Davies, C.N. ed., 337, Academic Press (London), 1966

Chapter 5 Effects of alcohol and surfactant on the stability of suspensions

5. 1 Objective of research

It has been shown in the previous chapters that there exist two different hydration forces and that both of them are affected by the pH of suspensions. Since the hydration forces are supposed to depend on the surface hydration of oxides, a slight change of hydration state on the surfaces may greatly affect the hydration forces. It is well known that alcohols dehydrates the surface of hydrophilic colloids and promotes their coagulation[1]. Many surface active agents adsorb on hydrophilic surfaces and change them into hydrophobic. It can be easily imagined that the hydration forces may decrease in both cases.

It is the objective of this chapter to investigate the effect of alcohol and surfactant on the coagulation of silica and rutile. The results will be analyzed using the extended DLVO theory developed in the previous chapters.

5. 2 Experimental

The same precipitated silica and synthetic rutile as prepared in the previous chapters were used for ζ-potential and turbidity measurements. Reagent grade ethanol and dodecylamine-hydrochloride (DAH) were used without further purification to investigate the effect of each reagent on hydration force with silica and rutile. The turbidities of silica suspensions were measured using Brice-Phoenix DM2000 with the same treatment explained in Chapter 2, while the turbidities of rutile suspensions were measured using Monitek Model 21 with the same procedures shown in Chapter 3. The ζ-potentials of rutile suspensions were measured by Pen Kem Laser Zee 500 at $2x10^{-3}$ M NaCl, changing the concentration of DAH in the suspensions. The procedures of ζ-potential measurement were the same as explained

in Chapter 3.

5. 3 Effect of ethanol on hydration forces

The turbidities (τ) of 300 ppm silica suspensions at pH 2.0 containing various amount of ethanol are shown in Fig. 5. 1. As has been expected, the turbidity decreases with increasing amount of ethanol in suspensions. Since the ζ–potential of silica is negligibly small at this pH, the decrease in turbidity is solely attributed to the decrease of primary hydration force. The magnitude of hydration force has been estimated based on the τ–E_1 relationship (E_1^{25}=100 kT) shown in Fig. 2. 8. Assuming that D_1=0.84 nm, C_2=0.441 mJ/m^2 and D_2=3.0 nm, which are the same as derived in Chapter 2, the magnitudes of C_1 have been estimated, the results of which are shown in Fig. 5. 2. It is shown that C_1 decreases with increasing amount of ethanol. This decreases in hydration force can be explained that ethanol promotes the surface dehydration of silica and breaks the structure of water layer which is supposed to be responsible for the primary hydration force.

A completely opposite result has been obtained with rutile suspensions. Fig. 5. 3 shows the turbidity of 200 ppm rutile suspensions at the i.e.p. of rutile (pH 6.2). The turbidity increases with increasing amount of ethanol in the suspensions. An electrostatic interaction does not exist at i.e.p. Even if the i.e.p. shifts due to the ethanol addition, the electrostatic interaction is still negligible at NaCl concentrations above 1 M owing to a double layer compression. Therefore, the increase in turbidity of rutile suspension is solely attributed to the increase of hydration force. The hydration force constant C_1 has been estimated based on the τ–E_1 relationship shown in Fig. 3. 6 assuming that D_1=0.6 nm, C_2=0.364 mJ/m^2 and D_2=3.0 nm which is the same condition as has been used in Chapter 3. The results are shown in Fig. 5. 4. The increase in C_1 is the opposite of the case of silica. Therefore, the surface

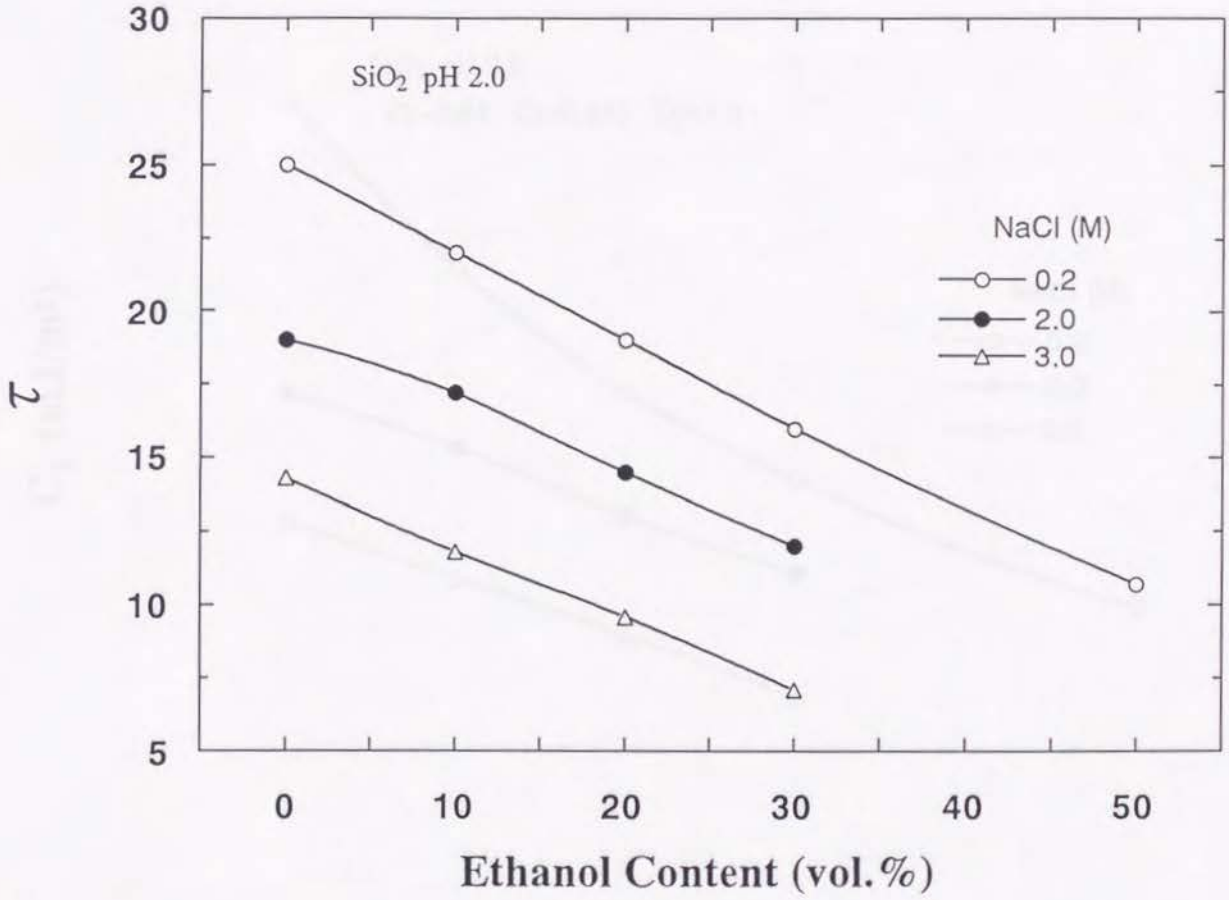

Fig. 5. 1 Turbidity (τ) measurements conducted with silica as a function of ethanol amount in suspensions.

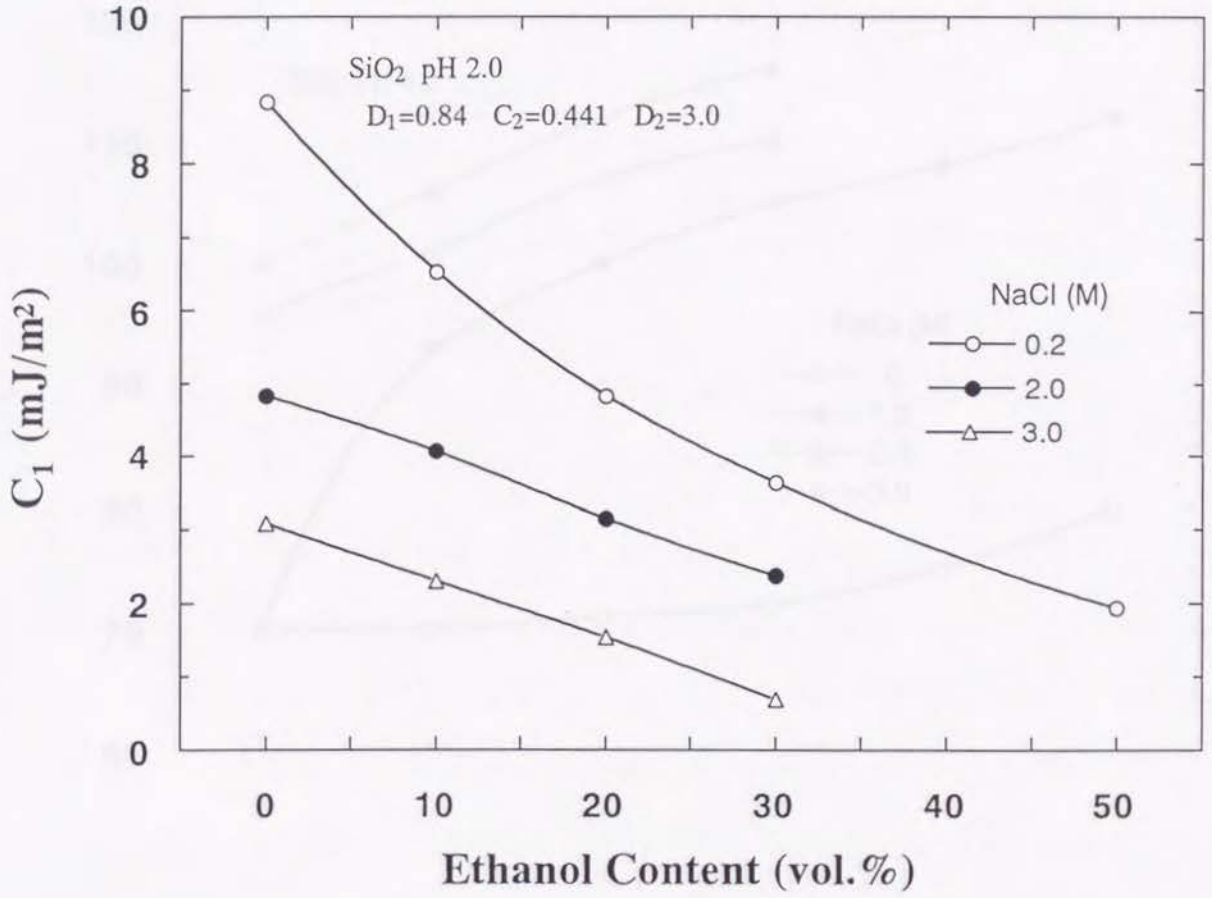

Fig. 5. 2 The change in structural energy parameter (C_1) of silica with increasing amount of ethanol in suspensions.

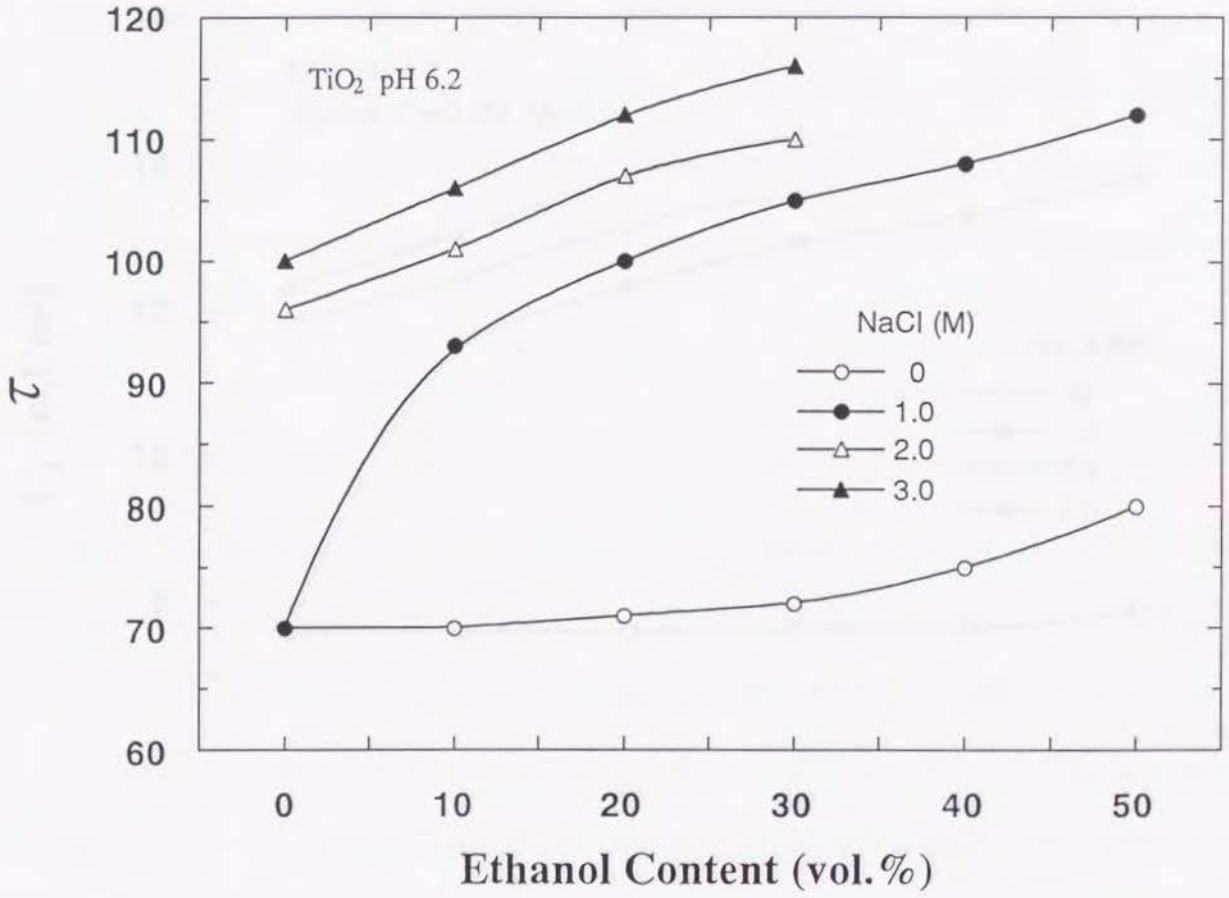

Fig. 5. 3 Turbidity (τ) measurements conducted with rutile as a function of ethanol amount in suspensions.

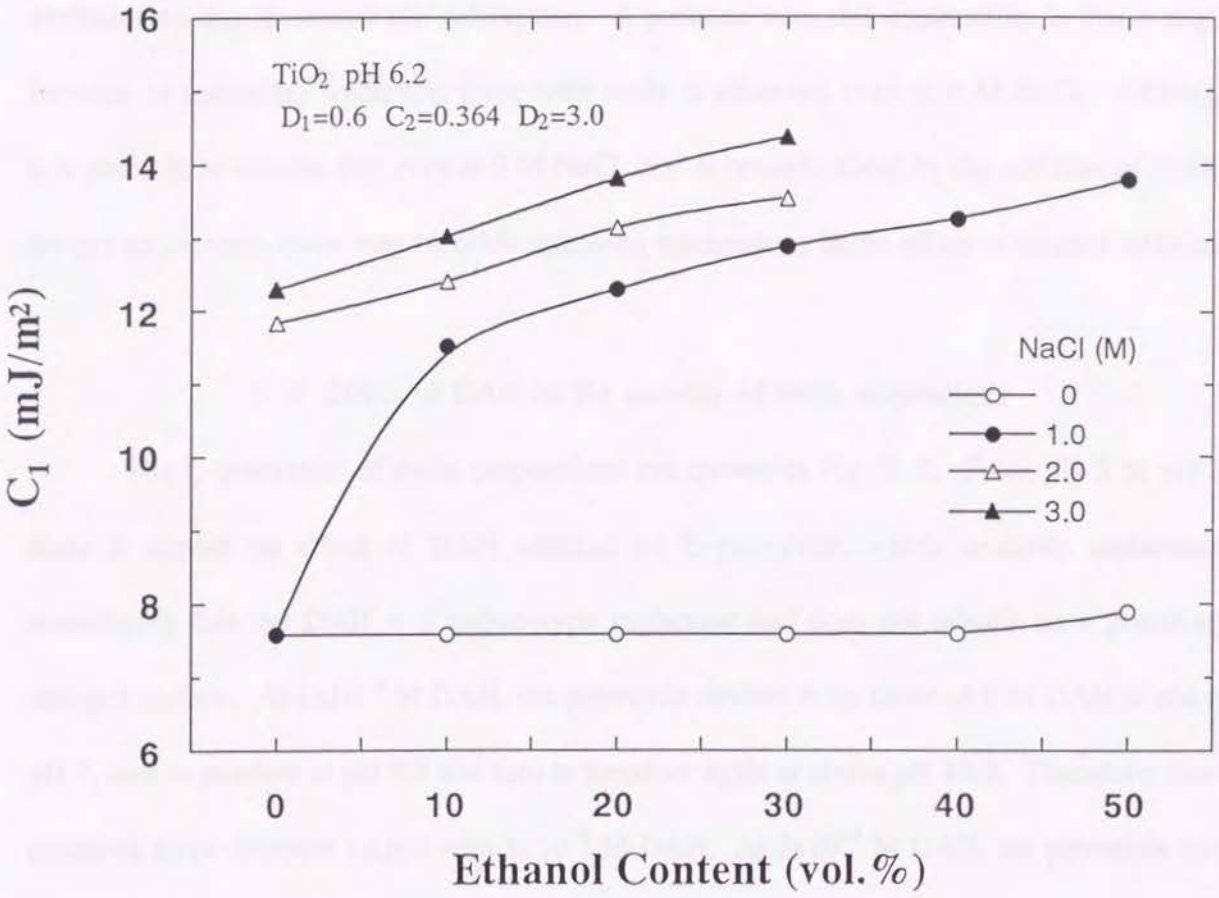

Fig. 5. 4 The change in structural energy parameter (C_1) of rutile with increasing amount of ethanol in suspensions.

dehydration by ethanol seems to be irrelevant to rutile. It has been reported that the addition of alcohols increase the adsorption of alkali metal and other cations from aqueous solutions on various oxide surfaces[2-6]. It is, therefore, possible that the increased adsorption of Na^+ on rutile surface increases the secondary hydration force. Since the increased adsorption of Na^+ on the hydrated layer on silica surface is supposed to increase the opportunity of cation-bridging, the decrease in primary hydration force with silica by ethanol addition may also be attributed to this increased Na^+ adsorption. A problem with this explanation is that a slight increase in secondary hydration force with rutile is observed even at 0 M NaCl. Although it is possible to assume that even at 0 M NaCl, Na^+ is brought about by the addition of NaOH for pH adjustment, there may be other unknown mechanisms in the effect of ethanol addition.

5. 4 Effect of DAH on the stability of rutile suspensions

The ζ-potentials of rutile suspensions are shown in Fig. 5. 5. From pH 3 to pH 7, there is almost no effect of DAH addition on ζ-potentials, which is easily understood considering that the DAH is a cation-type surfactant and does not adsorb on a positively charged surface. At $1x10^{-4}$ M DAH, the potentials deviate from those of 0 M DAH at above pH 7, turn to positive at pH 9.7 and turn to negative again at above pH 10.3. Therefore, there observed three different i.e.p.'s with $1x10^{-4}$ M DAH. At $5x10^{-4}$ M DAH, the potentials turn to positive at pH 7.7, being at the maximum near pH 9, and turn to negative again at pH 11. There are also three i.e.p.'s. These complex behavior of ζ-potential is attributed to the adsorption of positively charged DAH ions.

The change of ζ-potentials shown above also affects the turbidities of suspensions. Fig. 5. 6 shows the effect of DAH on the turbidities of 200 ppm rutile suspensions. At $1x10^{-4}$ M DAH, the turbidities deviate from those of 0 M DAH above pH 8.7, and take the

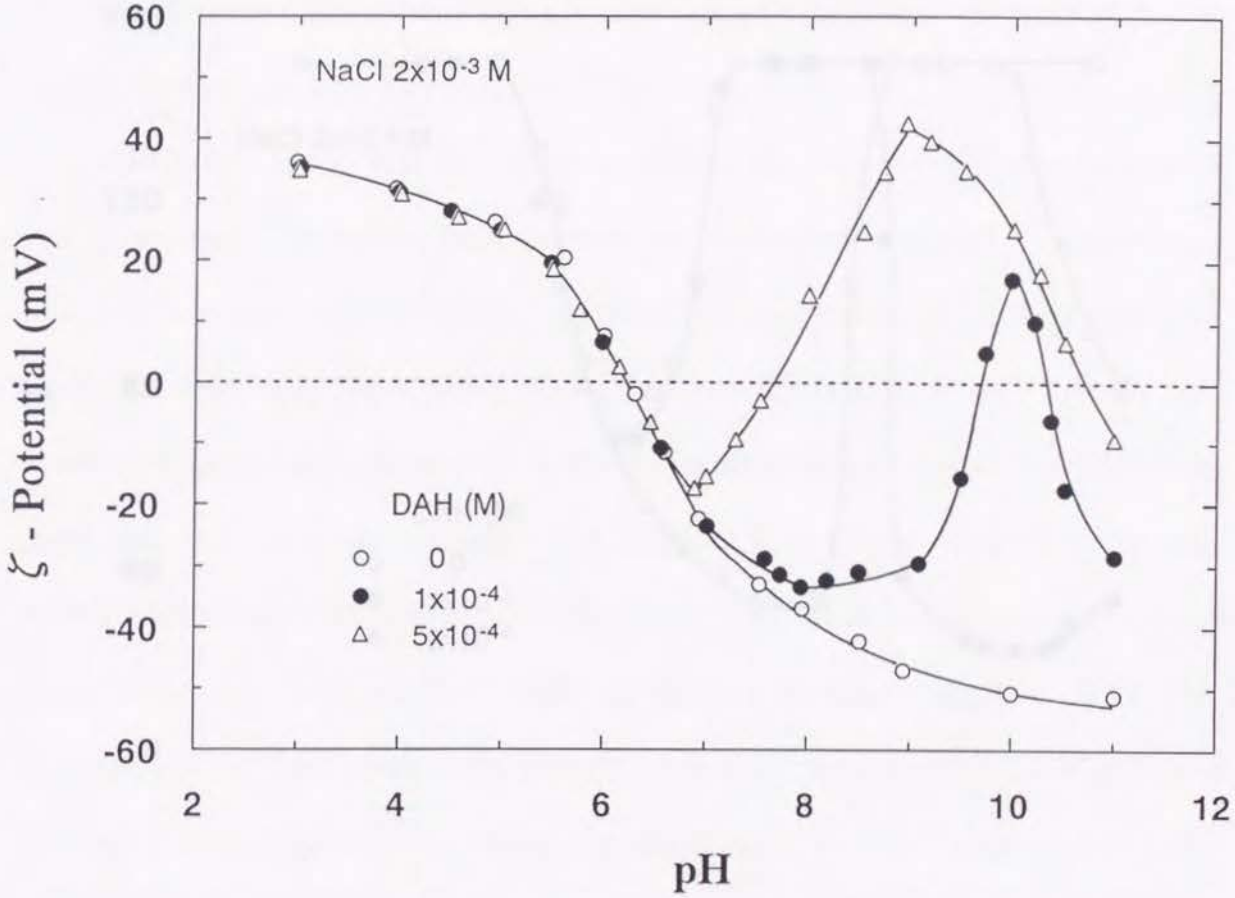

Fig. 5. 5 ζ–potentials of synthesized rutile as a function of pH at $2x10^{-3}$ M NaCl and different DAH concentrations.

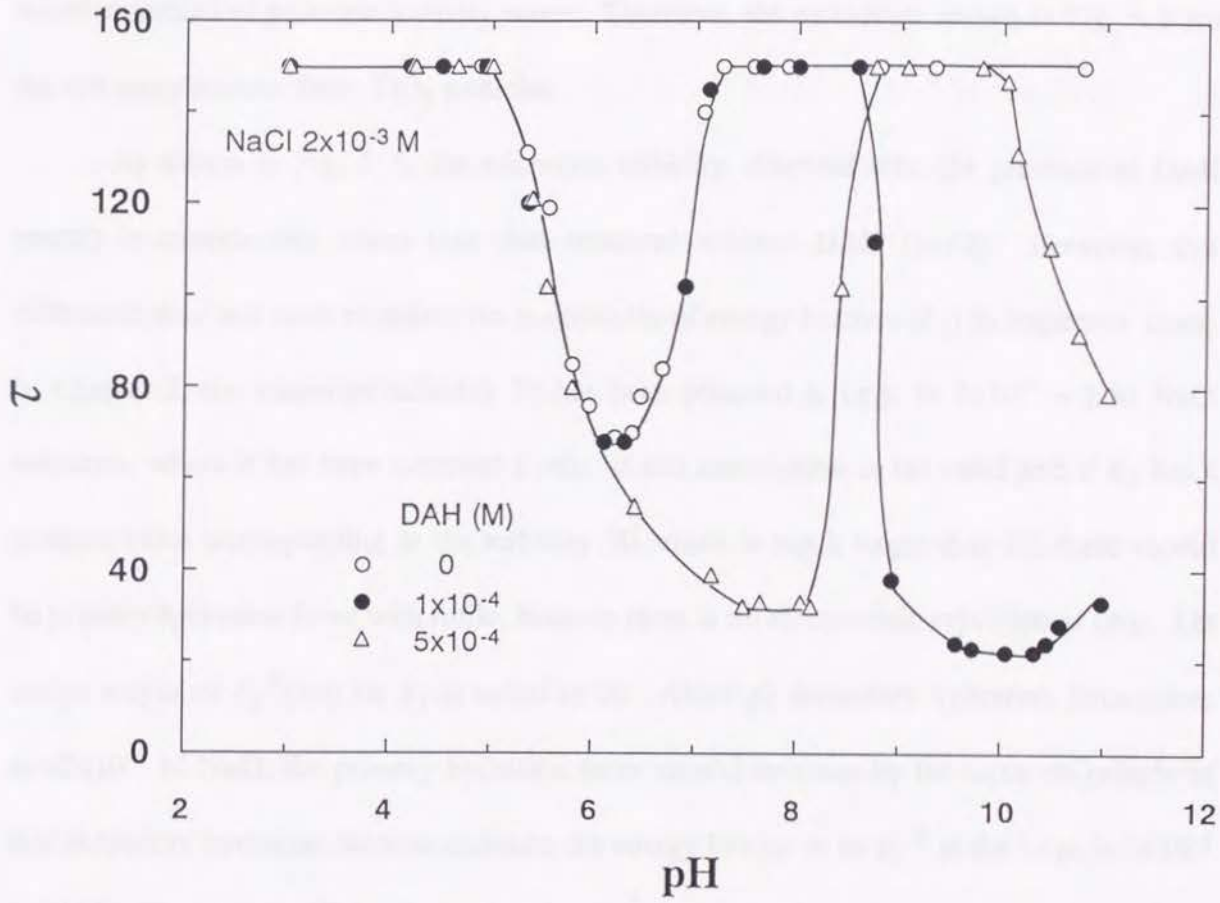

Fig. 5. 6 Results of turbidity (τ) measurements conducted with rutile as a function of pH at $2x10^{-3}$ M NaCl and different DAH concentrations.

minimum value of 22 around pH 10 and slightly increase to 33 at pH 11. At $5x10^{-4}$ M DAH, the turbidities deviate from that of 0 M DAH above pH 6.2 (i.e.p.), being at a minimum (32) around pH 8, then increase again and are at a maximum (150) between pH 9 and 10, and decrease again at above pH 10. It should be noted that since DAH precipitates in the solutions at above pH 10 and raises blank turbidities up to 10 ($5x10^{-4}$ M at pH 11), the turbidity measurement at above pH 10 have been conducted adjusting base–zero to each DAH solution instead of pure conductivity water. Therefore, the turbidities shown in Fig. 5. 6 are the net contributions from TiO_2 particles.

As shown in Fig. 5. 6, the minimum turbidity observed with the presence of DAH (τ=22) is considerably lower than that observed without DAH (τ=70). However, this difference does not seem to reflect the magnitudes of energy barriers (E_1) in respective cases. In Chapter 3, the minimum turbidity 70 has been obtained at i.e.p. in $2x10^{-4}$ – 1 M NaCl solutions, where it has been assumed $E_1 \leq 0$. If this assumption is not valid and if E_1 has a positive value corresponding to the turbidity 70 which is much larger than 22, there should be *primary hydration force* with rutile, because there is no electrostatic repulsion at i.e.p. Let assign a symbol $E_1^{70}(>0)$ for E_1 at turbidity 70. Although secondary hydration force arises at $>2x10^{-2}$ M NaCl, the primary hydration force should decrease by the same magnitude of that secondary hydration force to maintain the energy barrier to be E_1^{70} at the i.e.p. in $2x10^{-4}$ – 1 M NaCl solutions. This assumption, however, seems to be quite unnatural. As has been discussed in the previous chapter, the primary and secondary hydration forces are mutually exclusive, judging from their development mechanisms. If the decrease in the primary hydration force due to cation–bridging is compensated by the increase in the secondary hydration force caused by cation adsorption in the case of rutile, it is difficult to understand why the same process does not occur with silica.

A completely different explanation may be possible for the turbidity difference between 70 and 22. The difference may reflect how large the coagula grow and how stable it is under a given shearing force by agitation, which is affected by the magnitude of a binding force between particles. Since this binding force can be regarded as the resistance against re-dispersion, it may reflects the depth of primary energy minimum (see Fig. 1. 1), although it cannot be evaluated by the extended DLVO theory. At the same condition of $E_1 \leq 0$, if DAH is assumed to supply extra binding force, it can explain the difference in turbidity. A similar phenomenon is observed when polymer is added to a suspension. As will be shown in Chapter 6, polyacrylamide reduce the turbidity of stannic oxide suspension down to 0.4 while the minimum turbidity without the polymer is 5.5 at the i.e.p. of stannic oxide. The difference in turbidity may also be explained by the extra binding force of the polymer and a resultant difference in size distribution of coagula.

For the reason above, the turbidity difference with rutile (70 and 22) has not been attributed to a difference in E_1, and E_1 has been assumed to be ≤ 0 for turbidity 70 in the following discussion.

By using the ζ-potential data in Fig. 5. 5, the classical DLVO calculation was conducted and the E_1 values for each turbidity point were estimated. The relationship between turbidity (τ) and E_1 thus obtained is shown in Fig. 5. 7. All the points of 0 M DAH and some points of 1×10^{-4} M and 5×10^{-4} M DAH fit on one correlation curve. It suggests that the classical DLVO theory works well in calculating E_1 for each turbidity point. However, some points of DAH solutions are placed below the curve, which suggest that there is an additional attraction not considered in the classical DLVO theory. As have been introduced in Chapter 1, there exists a *hydrophobic attraction* between surfactant-coated mica surfaces[7-12]. The force is 10-100 times larger than the London-van der Waals attraction.

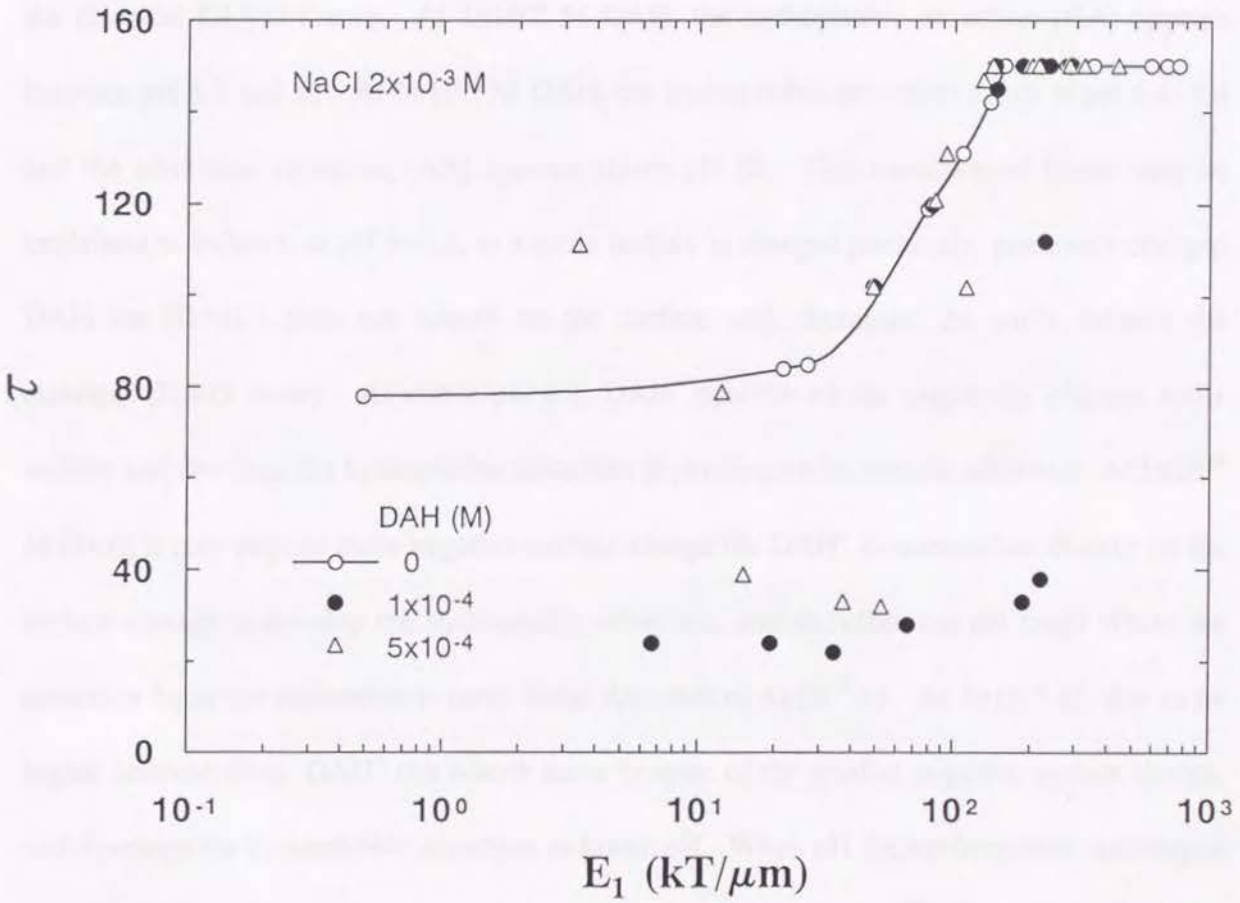

Fig. 5. 7 Turbidities (τ) of rutile suspensions plotted vs. energy barriers (E_1) calculated using the classical DLVO theory. Points below the τ–E_1 correlation curve suggests that the magnitudes of E_1 for the points are overestimated by the classical DLVO theory.

However, the origin of hydrophobic attraction is not yet clear at this moment[13-14]. On the contrary, some points of $5x10^{-4}$ M are placed above the correlation curve, which suggests that there is an additional repulsion similar to the hydration forces discussed in the previous chapters.

Fig. 5. 8 exhibits the relation of additional forces and the range of pH. As has been shown, at 0 M DAH there is no additional force at pH 3–11 and the E_1 can be described by the classical DLVO theory. At $1x10^{-4}$ M DAH, the hydrophobic attraction (HA) appears between pH 8.7 and 11. At $5x10^{-4}$ M DAH, the hydrophobic attraction arises at pH 6.4–8.4 and the additional repulsion (AR) appears above pH 10. This transition of forces may be explained as follows: at pH 3–6.2, as a rutile surface is charged positively, positively charged DAH ion (DAH^+) does not adsorb on the surface and, therefore, the rutile follows the classical DLVO theory. At above pH 6.2, DAH^+ adsorbs on the negatively charged rutile surface and develops the hydrophobic attraction depending on its amount adsorbed. At $1x10^{-4}$ M DAH, it may require more negative surface charge for DAH^+ to accumulate closely on the surface enough to develop the hydrophobic attraction, and therefore the pH range where the attraction becomes noticeable is more basic than that of $5x10^{-4}$ M. At $5x10^{-4}$ M, due to its higher concentration, DAH^+ can adsorb more in spite of the smaller negative surface charge, and develops the hydrophobic attraction at lower pH. When pH further increases, uncharged dodecylamine molecule adsorbs on the surface together with DAH^+ [15-16] and may shield the positive charge of adsorbed DAH^+. Thus the positive ζ–potential starts to decrease at certain pH which differs depending on the initial DAH concentration. The neutral amine molecules are supposed to adsorb on the hydrophobic group of DAH^+ as in the case of micelle formation[17] and, therefore, turn their polar (hydrophilic) groups outwardly to the solution. This orientation of neutral amine reduce the hydrophobicity of the surface. For this reason,

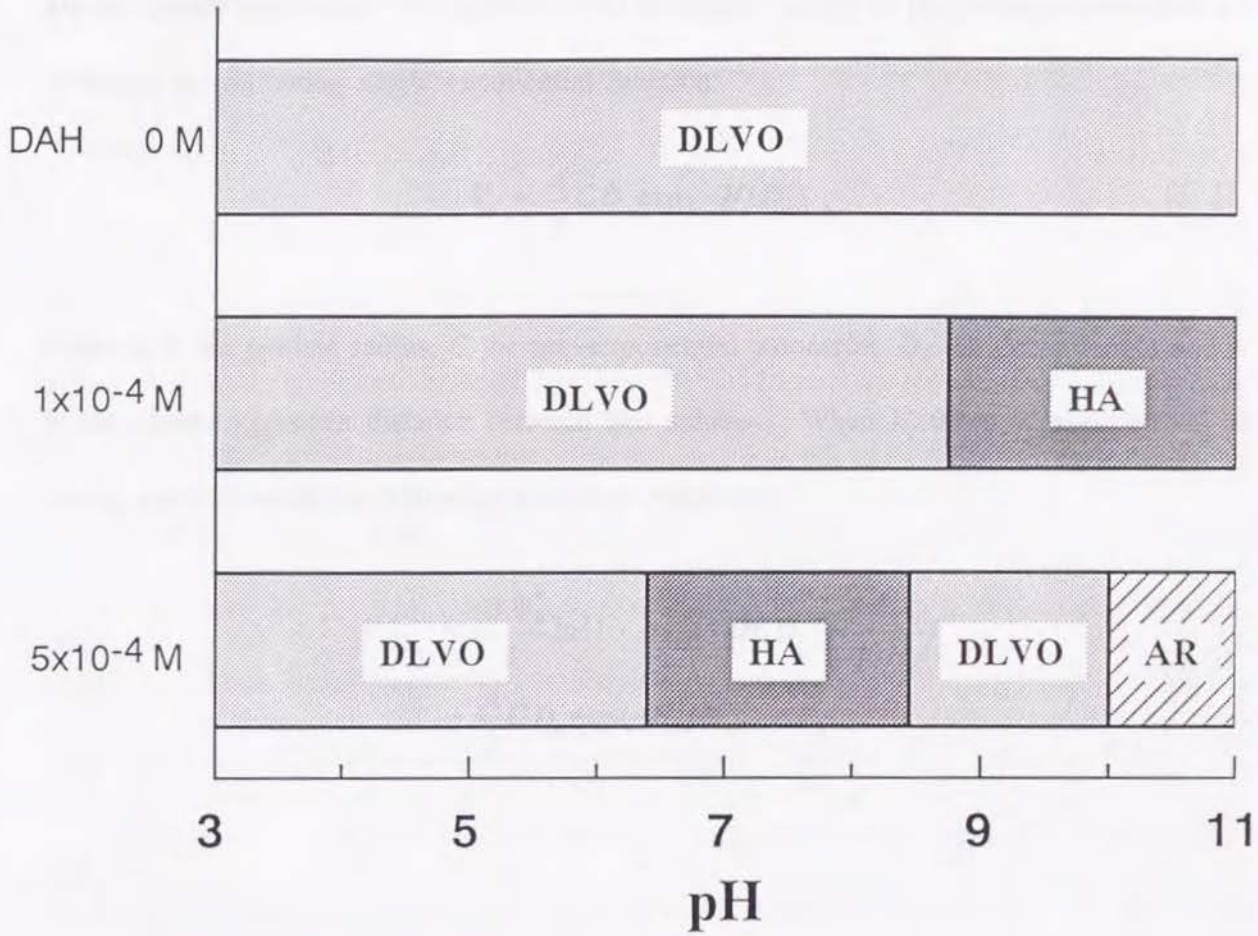

Fig. 5. 8 The pH region where additional forces are observed with rutile suspensions. DLVO: suspension follows the classical DLVO theory, HA: hydrophobic attraction is observed, AR: additional repulsion is observed.

the rutile with $5x10^{-4}$ M DAH follows the classical DLVO theory at above pH 8.4. When the amount of adsorbed neutral amine molecules further increases, the surface may be coveredwith hydrophilic group of the neutral amine, and may induce the structure forming of water molecules which develop a hydration force (or repulsion). A steric repulsion due to the adsorbed surfactant layer[18] may contribute to the repulsion to some extent.

The magnitudes of hydrophobic attraction have been estimated using the extended DLVO theory introduced in Chapter 2. The structural energy of hydrophobic attraction are given by the following single exponential function:

$$V_s = \frac{a}{2} C D_o \exp(-H/D_o) \ , \qquad [5.\ 1]$$

where a is the particle radius, C the pre-exponential parameter, D_o the decay length and H is the closest approach distance between two spheres. When V_t takes a maximum E_1 at $H=H_1$, one can write the following boundary conditions:

$$V_t|_{H_1} = \frac{a\varepsilon\psi_\delta^2}{2} \ln\{1 + \exp(-\kappa H_1)\} - \frac{aA_{131}}{12H_1} f + \frac{a}{2} C D_o \exp(-H_1/D_o) = E_1 \ , \qquad [5.\ 2]$$

and

$$\left.\frac{dV_t}{dH}\right|_{H_1} = -\frac{a\varepsilon\psi_\delta^2 \kappa \exp(-\kappa H_1)}{2[1 + \exp(-\kappa H_1)]} + \frac{aA_{131}}{12}\left\{\frac{f}{H_1^2} - \frac{1}{H_1}\left(\frac{df}{dH}\right)_{H_1}\right\} - \frac{a}{2} C \exp(-H_1/D_o) = 0 \ . \qquad [5.\ 3]$$

Eqs.[5. 2]-[5. 3] have four unknowns, i.e., C, D_o, E_1 and H_1. If two of these parameters are given, the equations can be solved simultaneously to determine the rest of parameters.

The E_1 values for turbidity 112 (at $1x10^{-4}$ M DAH and pH 8.7) and 102 (at $5x10^{-4}$ M DAH and pH 8.4) are calculated using τ–E_1 relationship of rutile shown in Fig. 3. 6. The E_1's for the points which give turbidities less than 70, i.e. pH 8.9–11.0 at $1x10^{-4}$ M DAH and pH 6.4–8.2 at $5x10^{-4}$ M DAH, are assumed to be zero. When the total energy (V_t) is negative throughout all the surface separation (H), there is no method to estimate how negative it is from the coagulation phenomenon. Therefore, only *the minimum possible values* of hydrophobic attraction can be obtained for each turbidities less than 70. Among these points, the larger the ζ–potential of the points, the larger the calculated hydration attraction to compensate the electrostatic repulsion. In this regard, the hydrophobic attraction is calculated to be the largest at pH 8.9 (ζ=–-29.9 mV, τ=38) in $1x10^{-4}$ M DAH solution and at pH 8.2 (ζ=17.4 mV, τ=32) in $5x10^{-4}$ M DAH solution. Although at other pH's in respective DAH solutions, the minimum possible hydrophobic attractions are smaller than those shown above due to the smaller ζ–potentials, it is not clear whether the hydrophobic attractions are actually smaller. For turbidity points at pH 8.7 and 8.9 in $1x10^{-4}$ M DAH, and at pH 8.2 and 8.4 in $5x10^{-4}$ M DAH, the hydrophobic attraction have been calculated assuming various decay lengths (D_o), the results of which are shown in Table 5. 1. One can see that the hydrophobic attraction changes drastically with the small changes of pH.

According to surface force measurements reported by researchers, the D_o values with alkyl–mono–amine layer adsorbed on mica from the solutions are 1–3 nm[7–12]. The decay length is longer with layers formed by the Langmuir–Brodget deposition[11–13, 19–20]. For this reason D_o has been chosen as 1–3 nm. By comparing the C values in Table 5. 1 with the C_1 values of hydration repulsion in Table 3. 2, one can see that the hydrophobic attraction is much stronger than the hydration force. In Fig. 5. 9, the hydration repulsion observed with

Table 5. 1 Structural energy parameter (C) of rutile in DAH solution.

$1x10^{-4}$ M DAH				
		D_o (nm)		
		1.0	2.0	3.0
C (mJ/m^2)	pH 8.7	$-1.23x10^4$	−29.3	−4.10
	pH 8.9	$-1.18x10^{12}$	$-6.05x10^4$	−244
$5x10^{-4}$ M DAH				
		D_o (nm)		
		1.0	2.0	3.0
C (mJ/m^2)	pH 8.2	$-8.45x10^7$	−570	−11.6
	pH 8.4	−710	−5.81	−1.20

rutile at 0.02–4.0 M NaCl and the hydrophobic attraction with D_o of 3 nm listed in Table 5. 1 are plotted versus surface separation H. As has already been expected from Table 5. 1, the hydrophobic attractions are much larger in magnitude than hydration repulsions.

The magnitudes of additional repulsions observed in $5x10^{-4}$ M DAH solution at above pH 10 have been estimated applying the same procedures described above. The results are shown in Table 5. 2. At pH 10 and 10.5, secondary minima (E_2) are already as shallow as −2 kT without adding the longer decay length (D_2), which is attributed to the electrostatic repulsion decaying with κ^{-1}=6.8 nm in $2x10^{-3}$ M NaCl solution. Therefore, the additional repulsions for these two points have been expressed by a single exponential function with decay length 0.6 nm, which has been chosen to compare the repulsion with hydration repulsion. At pH 10.8, however, E_2 is −35 kT without the second decay length D_2 (C_1=16.2, C_2=0) due to an almost zero ζ-potential. For this point, D_2 of 3 nm is added to the function of the repulsion. Although the C_1 at pH 10.8 is smaller than that of pH 10.5, the repulsion is stronger at pH 10.8 due to the contribution from the second decay length. The magnitude

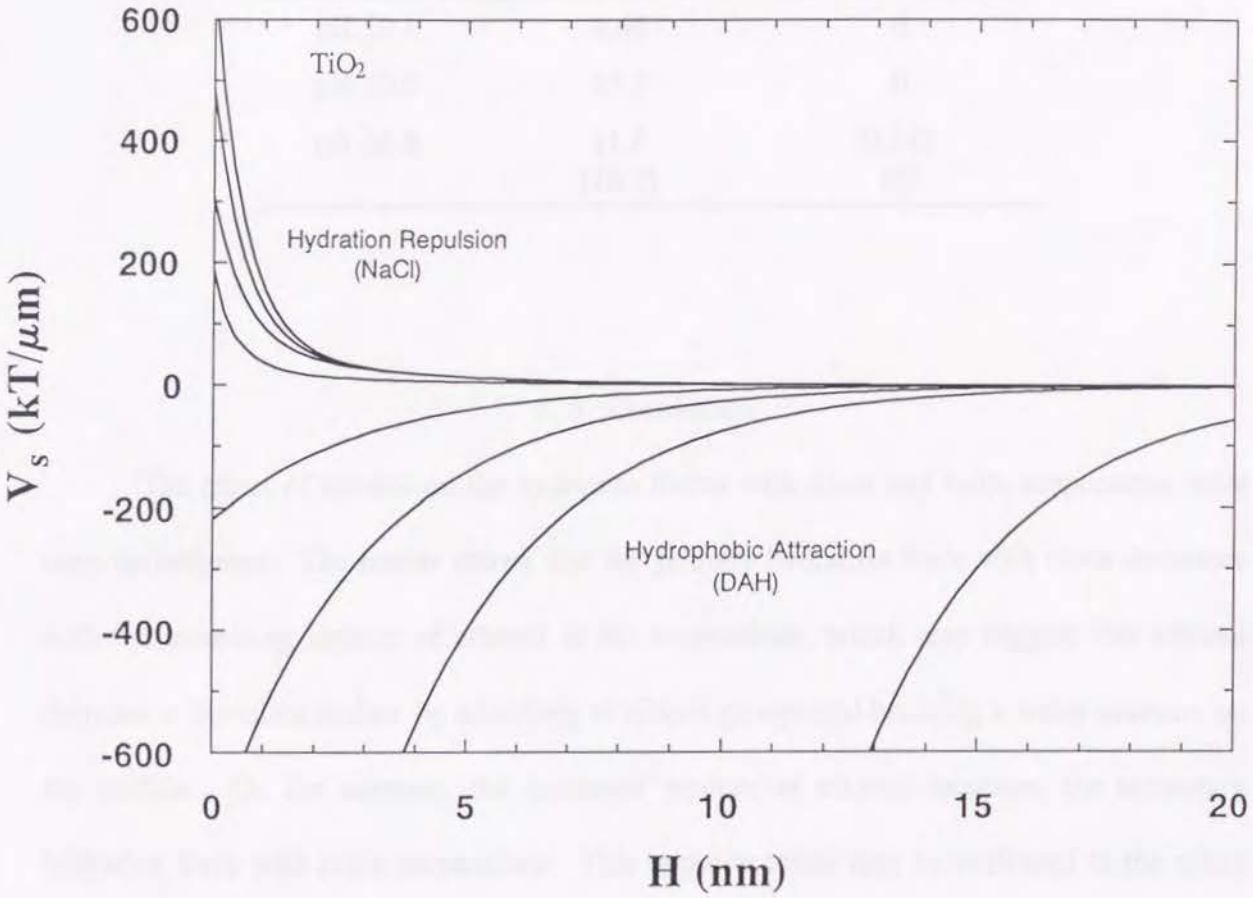

Fig. 5. 9 Comparison of hydration repulsion and hydrophobic attraction. Both forces are expressed as the form of structural energies (V_s) and are plotted vs. separation distance (H). Hydration repulsions are the ones observed with rutile in $2x10^{-2}$ – 4.0 M NaCl solutions, and hydrophobic attractions are the ones listed in Table 5. 1 with 3.0 nm D_o.

of the additional repulsion is comparable to the hydration forces observed with rutile in NaCl solution shown in Table 3. 2.

Table 5. 2 Parameters (C_1, C_2) of additional repulsion observed with rutile in $5x10^{-4}$M DAH at alkaline pH. The forces is expressed using the same decay lengths (D_1=0.6 nm, D_2=3.0 nm) as used in the hydration force.

	C_1 (mJ/m$^{2)}$	C_2(mJ/m^2)
pH 10.1	9.66	0
pH 10.5	15.7	0
pH 10.8	11.6 (16.2)	0.342 (0)

5. 5 Conclusion

The effect of alcohol on the hydration forces with silica and rutile suspensions have been investigated. The results shows that the primary hydration force with silica decreases with the increasing amount of ethanol in the suspensions, which may suggest that ethanol dehydrates the silica surface by adsorbing to silanol groups and breaking a water structure on the surface. On the contrary, the increased amount of ethanol increases the secondary hydration force with rutile suspensions. This opposite result may be attributed to the effect of ethanol enhancing cation adsorption at the solid–liquid interface.

The effect of surfactant on the coagulation of rutile has also been studied. By adding DAH in the suspension, there has been observed a hydrophobic attraction between rutile particles. The magnitude of this attraction has been estimated using the extended DLVO theory and has been found that it is much larger than that of secondary hydration force observed with rutile at high NaCl concentrations. It has been also observed that an additional

repulsion arises at $5x10^{-4}$ M DAH at above pH 10, the magnitude of which is comparable to that of secondary hydration force observed with rutile.

5. 6 References

1. Nakagaki, M., "Hyomen-jotai to Koroido-jotai," 23, Tokyo Kagaku Dojin, Tokyo, (1981)
2. Egorov, Yu.V., Pushkarev, V.V., and Tkachenko, E.V., *Radiokhimiya*, **4**, 371 (1962)
3. Bessonov, V.A., and Krylova, N.N., *Kolloid. Zh.*, **36**, 832 (1974)
4. Misak, N.Z., and Ghoneimy, H.F., *J. Chem. Technol. Biotechnol.*, **32**, 709 and 893 (1982)
5. Misak, N.Z., and Ghoneimy, H.F., *Colloids and Surfaces*, **7**, 89 (1983)
6. Ghoneimy, H.F., Mikhail, E.M., Shabana, E.S.I., and Misak, N.Z., *J. Colloid Interface Sci.*, **153**, 199 (1992)
7. Pashley, R.M., and Israelachvili, J.N.. *Colloids and Surfaces*, **2**, 169 (1981)
8. Kekicheff, P., Christenson, H.K., and Ninham, B.W., *Colloids and Surfaces*, **40**, 31 (1989)
9. Herder, P.C., *J. Colloid Interface Sci.*, **134**, 346 (1990)
10. Pashley, R.M., McGuiggan, P.M., Ninham, B.W., and Evans, D.F., *Science*, **229**, 1088 (1985)
11. Claesson, P.M., and Christenson, H.K., *J. Phys. Chem.*, **92**, 1650 (1988)
12. Christenson, H.K., Claesson, P.M., Berg, J., and Herder, P.C., *J. Phys. Chem.*, **93**, 1472 (1989)
13. Christenson, H.K., and Claesson, P.M., *Science*, **239**, 390 (1988)
14. Tsao, Y.H., Yang, S.X., Evans, D.F., and Wennerstrom, H., *Langmuir*, **7**, 3154 (1991)
15. Mukai, S., Wakamatsu, T., Ichidate, M., and Park, C.H., *Nihon Kogyo Kaishi*, **91**, 1045 (1975)
16. Somasundaran, P., *Int. J. Mineral Processing*, **3**, 35 (1976)
17. Israelachvili, J.N., "Intermolecular and Surface Forces," 366, Academic Press, London (1985)
18. Napper, D.H., *J. Colloid Interface Sci.*, **58**, 390 (1977)

19. Claesson, P.M., Blom, C.E., Herder, P.C., and Ninham, B.W., *J. Colloid Interface Sci.*, **114**, 234 (1986)

20. Herder, P.C., *J. Colloid Interface Sci.*, **134**, 336 (1990)

Chapter 6 Selective coagulation of stannic oxide in mixed suspensions with silica

6. 1 Objective of research

The stabilities of oxides suspensions have been investigated in the previous chapters, and it has been shown that one must consider structural forces in order to predict the stabilities precisely. The knowledge of structural forces seems to be useful for many practical processes dealing fine particles. Selective coagulation is one of the examples, where it is important to prevent the hetero-coagulation between different component particles. It may be interesting to analyze the hetero-coagulation and to investigate the role of structural forces in the heterogeneous system. In this chapter, the stabilities of mixed suspension of silica and stannic oxide will be studied and the hydration force between silica and stannic oxide will be evaluated.

Polymeric flocculants are often used to promote the aggregation of particles. In this case, the aggregation is generally referred to as flocculation. In the selective coagulation of stannic oxide, the use of polymeric flocculants may be effective to enhance the flocculation of stannic oxide. Therefore, the modification of polyacrylamide was conducted and the effect of the modified polymer on the selective flocculation of stannic oxide in a mixed suspensions with silica was investigated. The results will be shown in the following sections.

6. 2 Experimental

6. 2 .1 Samples and chemicals

Synthesized stannic oxide and silica samples prepared in the previous chapters were used for the experiment. Polyacrylamide (PAM) the commercial name of which was "Acco Floc N100S" was obtained from Mitsui Cyanamid Ltd. The nominal average molecular

weight of it was $1.3x10^7$, and the content of carboxylate groups was less than 1 %. A reagent grade stilbazo was obtained from Tokyo Kasei Ltd. and was used for the modifier of the PAM. Partially hydrolyzed polyacrylamide were also obtained from Mitsui Cyanamid Ltd. The hydrolyzed percent of them were 2.5, 5, 10, 15, 20, and 30 %, respectively, and the average molecular weights were $1.6–1.9x10^7$. The chemical structures of PAM and stilbazo are shown in Fig. 6. 1. All the chemicals were used without further purification.

6. 2. 2 Modification of polyacrylamide

PAM reacts with formaldehyde under alkaline conditions to produce methylolated polyacrylamide[(1)]. Phenol and formaldehyde normally condense to form polymers consisting of aromatic rings linked together mainly by methylene bridges[(2)]. The reactions are usually carried out in the presence of catalysts which can be either bases or acids. Attia attempted the condensation of glyoxal–bis–(2–hydroxyanil) (GBHA) and polyacrylamide using the reaction above and reported that 8 % of the amide groups were substituted by GBHA[(3-4)]. Since stilbazo also has phenol groups, it may react with polyacrylamide in the same manner.

The modification of PAM was conducted with the conditions shown in Table 6. 1. Polymer P1 was obtained by heating 100 ml of 0.2 % aqueous PAM solution at pH 10.7 and 75 °C for 30 minutes under reflux in a water bath. Polymer P2 was obtained by adding 0.1 ml formalin (F; 37 % formaldehyde solution) to 100 ml of 0.2 % PAM solution and heating the solution at pH 10.7 and 75 °C for 30 minutes under reflux. Polymer P3 was obtained by conducting the following 2–stage processes: 0.1 ml formalin was added to 50 ml of 0.4 % aqueous stilbazo (SB) solution and the pH was adjusted to 10.5. Then the solution was heated under reflux at 75 °C for 30 minutes in a water bath. After cooling, the solution was mixed with 50 ml of 0.4 % aqueous PAM solution, and the pH was adjusted to 10.7. The

Polyacrylamide

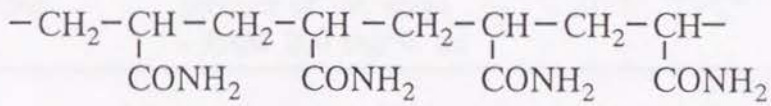

Stilbazo

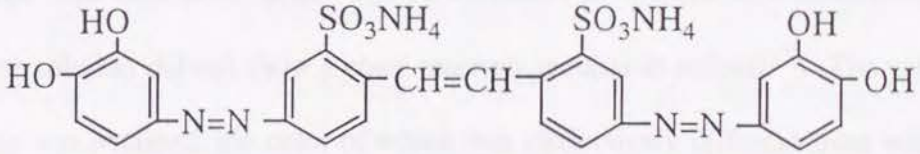

Fig. 6. 1 Chemical structures of polyacrylamide (PAM) and stilbazo (SB).

mixture was heated again at 75 °C for 30 minutes under reflux. All the products (P1–P3) were obtained as 0.2 % polymer solutions and were used for coagulation experiments without further purification.

Table 6. 1 Conditions of polymer modification.

		Conditions			
		Chemicals	pH	temp.	time
P1		PAM 200 mg/100 ml	10.7	75 C°	30 min
P2		PAM 200 mg/100 ml + F 100 μl	10.7	75 C°	30 min
P3	1st.	SB 200 mg/50 ml + F 100 μl	10.5	75 C°	30 min
	2nd.	product of 1st. stage + PAM 200 mg/50 ml	10.7	75 C°	30 min

A part of the polymer P3 was taken for an ultrafiltration to separate the polymer with un-reacted low molecular components. A polysulfon membrane the molecular weight of which was $2x10^5$ was used as the filter. The P3 solution was washed with conductivity water until the filtrate solution did not show a color reaction peculiar to stilbazo[5]. The yellowish-brown polymer was obtained, the color of which was distinctively different from white color of original PAM. The aqueous solution of the polymer changed its color into deep red at pH 10 and developed orange precipitates when mixed with stannic chloride solution at pH 5. Since this color reaction is inherent to stilbazo, it is supposed that the stilbazo was incorporated in the polymer structure without loosing the reactivity with Sn^{2+} ions.

6. 2. 3 Coagulation experiment

The turbidities of 300 ppm silica suspension and 200 ppm stannic oxide suspension

were measured with various amount of polymer addition using Brice-Phoenix DM2000 light scattering apparatus. The measuring procedures were the same as described in the previous chapters.

The coagulation experiment of mixed suspensions of silica and stannic oxide was carried out with 400 ml suspension which contains silica and stannic oxide of 0.2 g (500 ppm) each. A glass beaker of 75 mm diameter and 150 mm height was used for agitation and settling. The suspension was agitated by Teflon-coated magnet at about 200 rpm for 10 minutes and was hold for 10 minutes for the settling of particles. The coagulation without using polymers was also studied, where the agitation time was extended to 30 minutes and the settling time was extended to 60 minutes. After the settling, the suspension was discharged by siphoning. The settled coagula and suspended particles in discharged suspension were recovered by filtration and successive drying at 105 °C. During each siphoning process, 29 ml suspension was remained at the bottom of the beaker and was recovered with settled coagula. The silica content in each recovered solid was obtained by a chemical analysis using the hydrofluoric acid and sulfuric acid. Since 99.5 % silica was volatilized during the heating in the mixed acid and none of stannic oxide was not volatilized, the weight loss of each recovered solid during the acid treatment was regarded as the silica content of the solid.

6. 3 Analysis on the selective coagulation of stannic oxide

6. 3. 1 Hydration force in hetero-coagulation system

Fig. 6. 2 shows the turbidities of 300 ppm silica suspension and 200 ppm stannic oxide suspension at $2x10^{-3}$ M NaCl, which are taken from Figs. 2. 3 and 4. 2. It is shown that stannic oxide coagulates around pH 4.0, while silica does not coagulate at pH 3-11. At pH

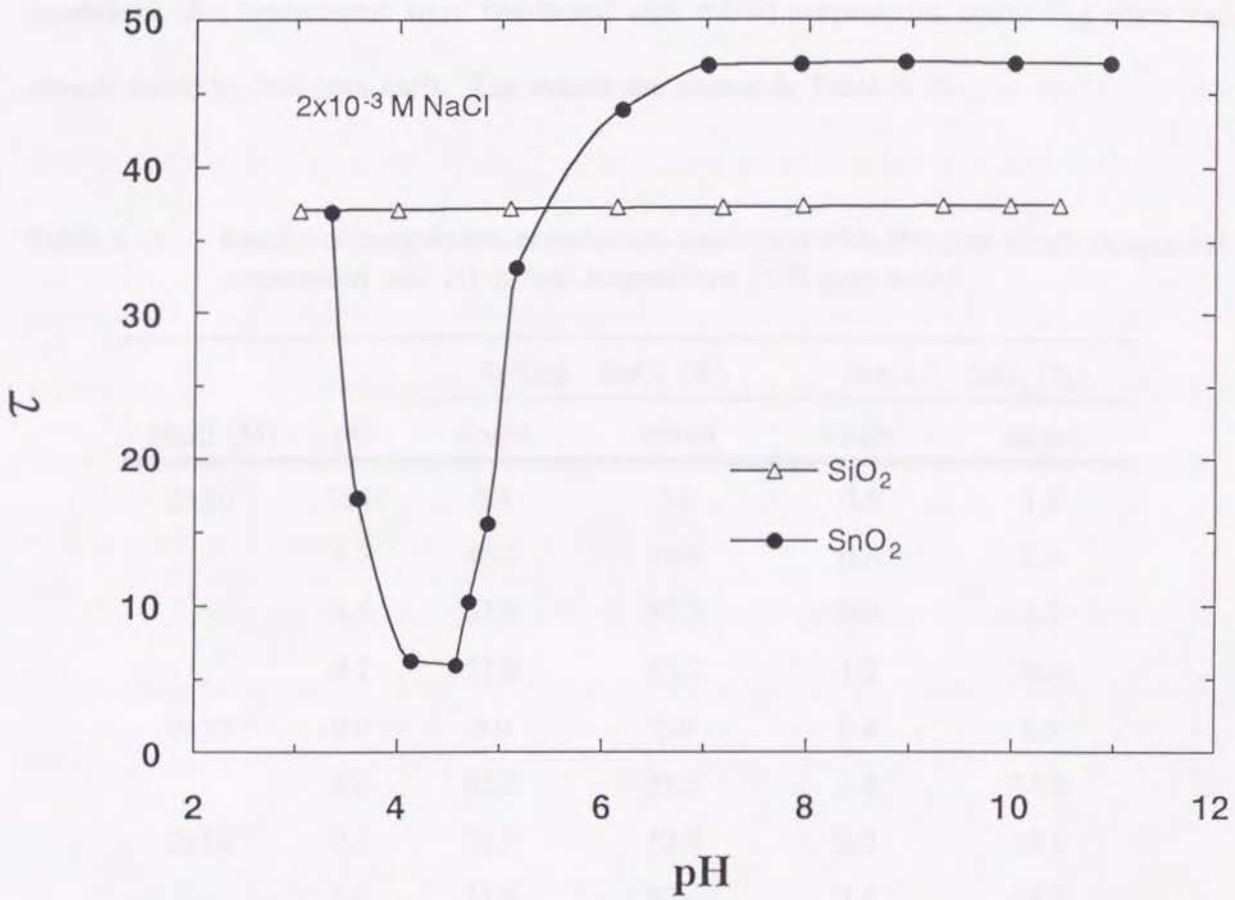

Fig. 6. 2 Turbidities (τ) of 300 ppm silica suspensions and 200 ppm stannic oxide suspensions at $2x10^{-3}$ M NaCl shown as a function of pH.

less than 4, the hetero-coagulation between silica and stannic oxide will occur in a mixed suspension, because the former has a negative charge and the latter has a positive charge. At above pH 4, however, there may be a pH range where the selective coagulation of stannic oxide is achieved. This has been confirmed by the following coagulation experiments.

The coagulation experiments were conducted with 500 ppm single component suspension of silica and of stannic oxide at various NaCl concentrations and pH. At the same conditions, the experiments were conducted with mixed suspensions containing silica and stannic oxide by 500 ppm each. The results are shown in Table 6. 2.

Table 6. 2 Results of coagulation experiments conducted with 500 ppm single component suspensions and 1:1 mixed suspensions (500 ppm each).

		Settled SnO_2 (%)		Settled SiO_2 (%)	
NaCl (M)	pH	single	mixed	single	mixed
$2x10^{-3}$	10.0	3.4	3.6	0.4	1.9
	4.7	45.1	36.4	0.8	2.4
	4.5	61.0	50.7	0.9	4.2
	4.1	72.0	53.2	1.2	30.6
$2x10^{-2}$	9.0	5.0	5.0	0.4	1.9
	5.0	62.2	51.5	1.8	11.9
$2x10^{-1}$	9.0	72.0	52.8	2.2	10.8
	5.0	71.8	52.4	3.6	14.2

The 29/400 of total solid (15 mg each for silica and stannic oxide) are initially contained in the 29 ml residual suspension and recovered with coagula. In an ideal separation process, this part of solid could be recovered with the supernatant suspension. The figures in Table 6. 2 are corrected by subtracting this amount of solid from the siphoning residue and

adding it to the siphoned suspension. As shown in the table, stannic oxide selectively coagulates at $2x10^{-3}$ M NaCl in the pH range 4.5–4.7, where an electrostatic repulsion is small enough for the coagulation of stannic oxide and is large enough to prevent a hetero–coagulation between stannic oxide and silica. It is also shown that the hetero–coagulation occurs at pH 4.1 in $2x10^{-3}$ M NaCl solution, at pH 5.0 in $2x10^{-2}$ M, and at pH 5.0 and 9.0 in $2x10^{-1}$ M, where silica settles considerably more in mixed suspensions than in single suspensions.

In the previous chapters, it has been shown that there is a considerable hydration force with silica at $2x10^{-3}$ to $2x10^{-1}$ M NaCl. The hydration force is not noticeable with stannic oxide at NaCl concentrations less than $2x10^{-1}$ M. At $2x10^{-1}$ M NaCl, the hydration force exists at pH 1 and 2, however it is not certain whether the hydration force exists at above pH 3. There may be a hydration force which is not large enough to raise the energy barriers above zero. It is interesting to check whether a hydration force exist between silica and stannic oxide at the conditions shown in Table 6. 2.

The interaction energies between silica and stannic oxide can be calculated using the hetero–coagulation model of DLVO theory proposed by Hogg et al[6]. According to the model, the electrostatic energy (V_e) between two spheres is expressed as:

$$V_e = \frac{\varepsilon a_1 a_2 (\psi_{\delta 1}^2 + \psi_{\delta 2}^2)}{4(a_1 + a_2)} \times \left[\frac{2\psi_{\delta 1}\psi_{\delta 2}}{(\psi_{\delta 1}^2 + \psi_{\delta 2}^2)} \ln \left\{ \frac{1 + \exp(-\kappa H)}{1 - \exp(-\kappa H)} \right\} + \ln \{1 - \exp(-2\kappa H)\} \right], \quad [6.\ 1]$$

where ε is the dielectric constant of medium, a_1 and a_2 are the radii of particle 1 and 2, $\psi_{\delta 1}$ and $\psi_{\delta 2}$ are their Stern potentials, κ is Debye parameter, and H is the closest separation distance between the particles. The London–van der Waals energy (V_d) is given as:

$$V_d = -\frac{A_{132} a_1 a_2}{6(a_1 + a_2)H} \quad , \qquad [6.\ 2]$$

where A_{132} is the Hamaker constant between solid 1 and 2 surrounded in the medium 3, and is given approximately by the following equation:

$$A_{132} \fallingdotseq (\sqrt{A_{11}} - \sqrt{A_{33}})(\sqrt{A_{22}} - \sqrt{A_{33}}) \quad , \qquad [6.\ 3]$$

where A_{ii} (i=1, 2, 3) is the Hamaker constant of each substance in vacuum.

Using the classical DLVO theory ($V_t = V_e + V_d$), the energy barrier (E_1) between silica and stannic oxide particles have been calculated for each condition listed in Table 6. 2. The results are shown in Fig. 6. 3. The % settled SiO_2 in the vertical axis of Fig. 6. 3 represents the settled percent in mixed suspension minus that in single component suspension, which may reflect the net amount of SiO_2 settled by hetero-coagulation with stannic oxide. One can find the similarity between Fig. 6. 3 and τ-E_1 relations discussed in the previous chapters. The data at $2x10^{-1}$ M are not shown in Fig. 6. 3, because the E_1 values are negative according to the classical DLVO theory. However, the percent settled at pH 5.0 and $2x10^{-1}$ M is 10.6 % (14.2 %-3.6 %) and is considerably lower than that of 29.4 % (30.6 %-1.2 %) at pH 4.1 and $2x10^{-3}$ M where E_1 is 0.4 kT. Considering that there is a unique correlation between τ and E_1 with homo-coagulation of silica and stannic oxide, and that τ is related to the settled amount of solid, there may be an unique correlation between the settled amount of SiO_2 and the E_1 of hetero-coagulation of silica with stannic oxide. Therefore, at pH 5.0 and $2x10^{-1}$ M where the settled amount is 10.6 %, the magnitude of energy barrier may be comparable to 51 kT which is calculated for the data point at pH 5.0 and $2x10^{-2}$ M, where 10.1 % of silica is supposed to settle by the hetero-coagulation with stannic oxide. Although the reliability of the correlation curve in Fig. 6. 3 is not certain due

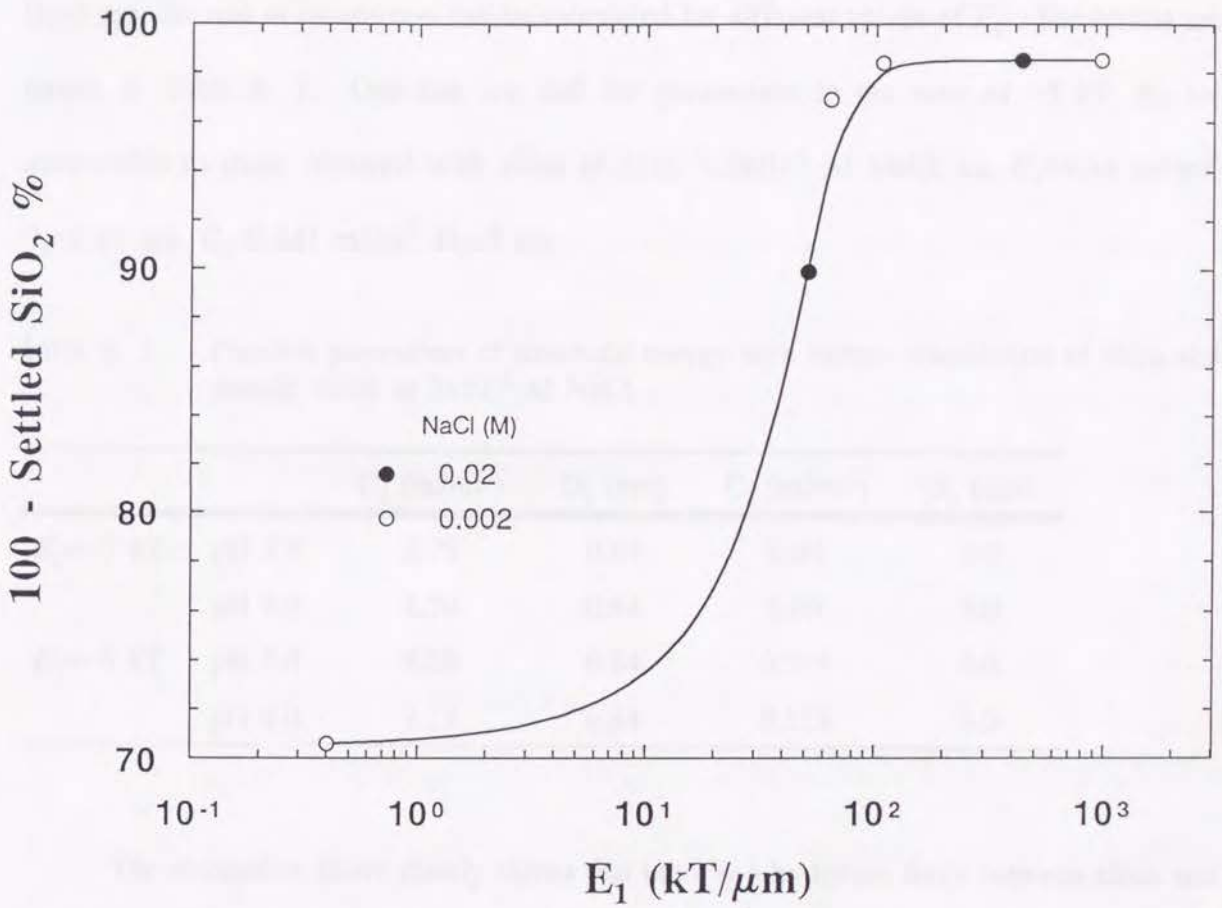

Fig. 6. 3 Relationship between the settled amount of silica and the energy barrier (E_1) of hetero–coagulation calculated using the classical DLVO theory. The percent settled SiO_2 is obtained by subtracting the percent settled in single component suspension from that in mixed suspension the both of which are shown in Table 6. 2. The data at $2x10^{-1}$ M NaCl are not shown because of negative E_1.

to the small number of data points, it is possible to estimate the value of E_1 corresponding to each settled SiO_2 percent.

The values of E_1 at $2x10^{-1}$ M NaCl are thus calculated to be 50 kT at pH 9.0 (8.6 % net settled) and 54 kT at pH 5.0 (10.6 % net settled). In order to raise the energy barrier to these values, V_s should be added to the V_t, where V_s is expressed by substituting the radius parameter a / 2 in Eq. [2. 5] with $a_1 a_2 / (a_1 + a_2)$. If it is assumed that D_1=0.84 nm and D_2=3 nm, the rest of parameters can be calculated for different values of E_2. The results are shown in Table 6. 3. One can see that the parameters in the case of −5 kT, E_2 are comparable to those obtained with silica at $2x10^{-3}$–$2x10^{-1}$ M NaCl, i.e. C_1=8.84 mJ/m^2, D_1=0.84 nm, C_2=0.441 mJ/m^2, D_2=3 nm.

Table 6. 3 Possible parameters of structural energy with hetero–coagulation of silica and stannic oxide at $2x10^{-1}$ M NaCl.

		C_1 (mJ/m^2)	D_1 (nm)	C_2 (mJ/m^2)	D_2 (nm)
E_2=−3 kT	pH 5.0	2.78	0.84	1.09	3.0
	pH 9.0	1.79	0.84	1.09	3.0
E_2=−5 kT	pH 5.0	8.28	0.84	0.519	3.0
	pH 9.0	7.12	0.84	0.519	3.0

The discussion above clearly shows that there is a hydration force between silica and stannic oxide at $2x10^{-1}$ M NaCl. At NaCl concentrations less than $2x10^{-1}$ M, the hetero–coagulation of silica and stannic oxide seems to be well correlated with the energy barriers (E_1) calculated using the classical DLVO theory. If it is assumed that there also exists the hydration force at less than $2x10^{-1}$ M NaCl, the E_1's for the data at $2x10^{-2}$ M are raised considerably due to the contributions from the hydration force, while the E_1 at $2x10^{-3}$ M does not change largely. As the results, the E_1 at $2x10^{-2}$ M and pH 5, where 10.1 % silica is

supposed to settle by hetero-coagulation, becomes larger than that at $2x10^{-3}$ M and pH 4.7, where only 1.6 % silica is supposed to settle by hetero-coagulation. Since the distance at the energy barrier located (H_1) is smaller at $2x10^{-2}$ M due to the double layer compression, the barrier is sensitive to the additional hydration force with short decay length. On the other hand, the barrier at $2x10^{-3}$ M is located further and is not affected largely by the short range repulsion. A example of this situation is shown in Fig. 6. 4. It seems, therefore, to be reasonable to conclude that the hydration force does not exist with the hetero-coagulation system at NaCl concentrations less than $2x10^{-1}$ M.

In dilute NaCl solutions, silica is supposed to develop the structure of water, while stannic oxide does not. In this condition, the hydration force may not be large enough to affect the energy barrier, and the magnitude of the barrier can be calculated by the classical DLVO theory. When NaCl concentration increases and stannic oxide develops the structure of water by the adsorption of ions, the hydration force becomes noticeable between silica and stannic oxide.

6. 3. 2 Effect of polymers on the selective flocculation of stannic oxide

The effect of polymers on the flocculation of stannic oxide is shown in Fig. 6. 5. The turbidity (τ) was measured at $2x10^{-3}$ M NaCl and pH 5.7. Polymer P1 and P2 show almost the same turbidities as unmodified PAM up to 0.6 ppm. Above this concentration, the turbidity increases with increasing amount of added P1 or P2, while it remains at the minimum when PAM is used. Polymer P3 shows the highest turbidity for all concentrations but 0.2 ppm, and the turbidity also increases above 0.6 ppm polymer concentration. It can be said that the flocculation of stannic oxide with the addition of polymer decreases in the order PAM > P1 > P2 > P3. Fig. 6. 6 shows the effect of polymers on the flocculation of

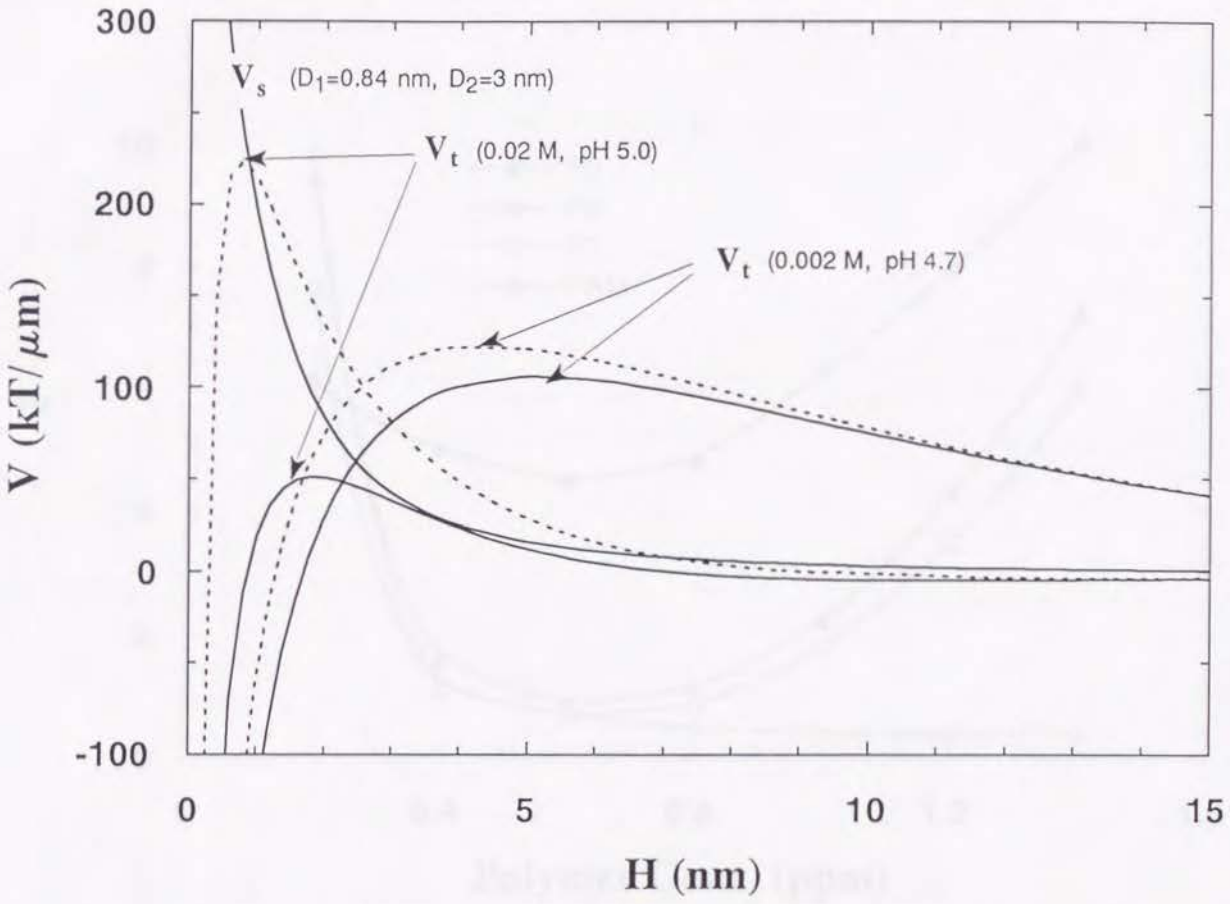

Fig. 6. 4 The change of energy barriers by the addition of hydration force. The dashed line is the total energy (V_t) after adding the structural energy (V_s). At $2x10^{-2}$ M NaCl, the barrier is largely affected by the short-range repulsion, while the barrier at $2x10^{-3}$ M NaCl is not.

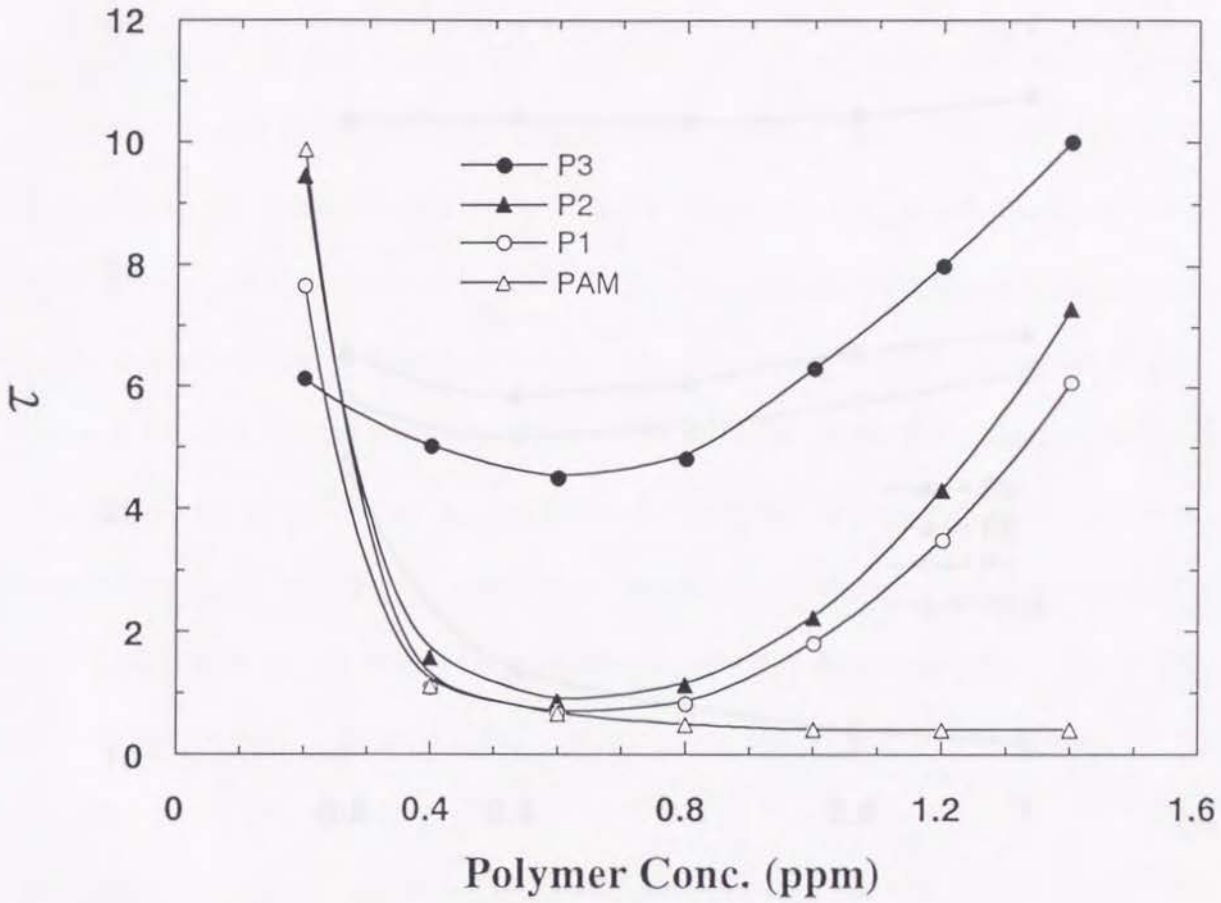

Fig. 6. 5 Effect of polymers on the turbidity (τ) of 200 ppm stannic oxide suspensions at $2x10^{-3}$ M NaCl and pH 5.7.

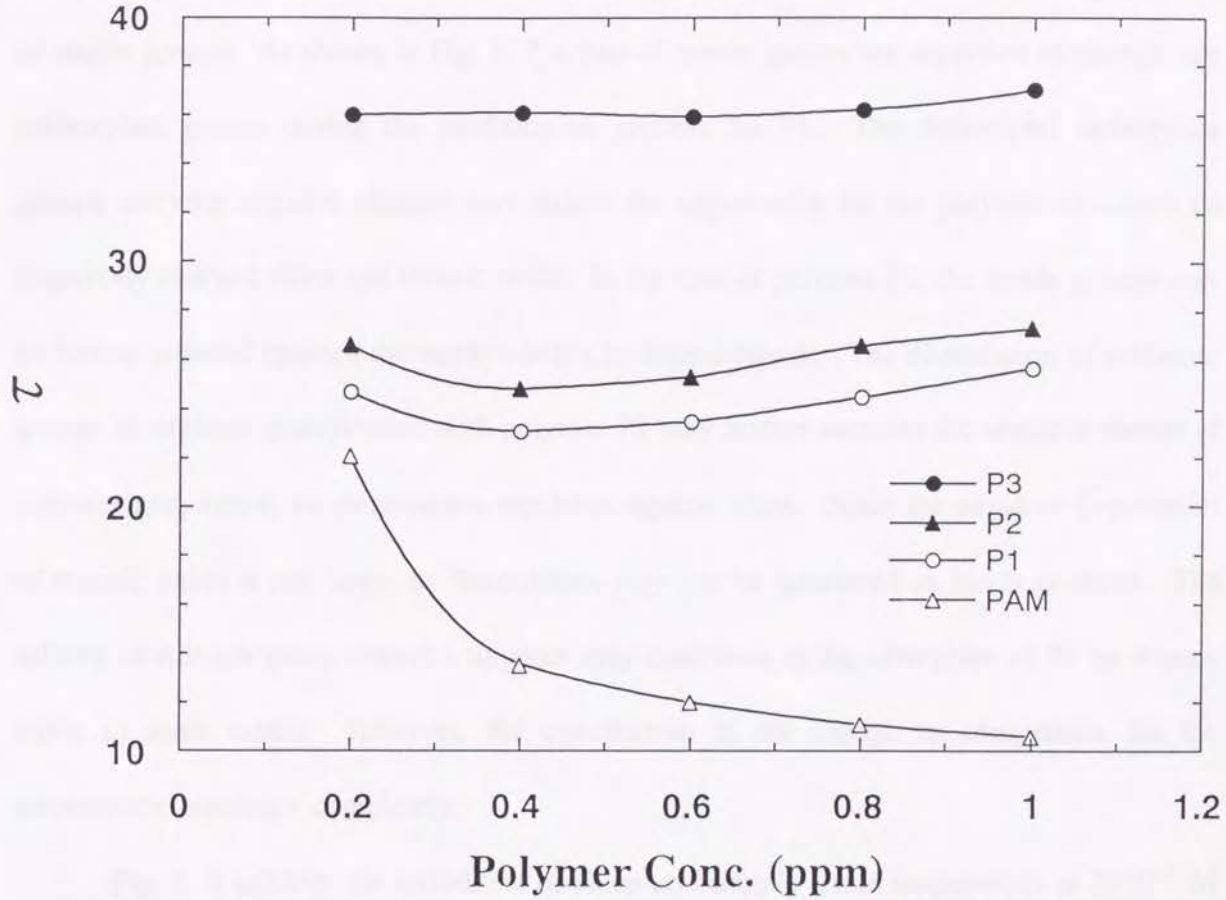

Fig. 6. 6 Effect of polymers on the turbidity (τ) of 300 ppm silica suspensions at $2x10^{-3}$ M NaCl and pH 5.4.

silica. The turbidities were measured at $2x10^{-3}$ M NaCl and pH 5.4. It is shown that PAM flocculates silica considerably, while P3 does not at all. The order of polymer effect on the flocculation is the same as in stannic oxide, i.e. PAM > P1 > P2 > P3.

Griot and Kitchener[7] suggests that the adsorption of polyacrylamide onto silica is attributed to the hydrogen bonding between amide groups in the polymer and silanol groups on silica surface. The order of polymer effect observed above may be related to the decrease of amide groups. As shown in Fig. 6. 7, a part of amide groups are supposed to change into carboxylate groups during the modification process for P1. The dissociated carboxylate groups carrying negative charges may reduce the opportunity for the polymer to adsorb on negatively charged silica and stannic oxide. In the case of polymer P2, the amide groups may be further reduced through the methylolation by formaldehyde. The dissociation of sulfonate groups in stilbazo incorporated with polymer P3 may further increase the negative charge of polymer and, hence, an electrostatic repulsion against silica. Since the negative ζ-potential of stannic oxide is not large, its flocculation may not be interfered as much as silica. The affinity of stilbazo group toward a tin atom may contribute to the adsorption of P3 on stannic oxide to some extent. However, the contribution is not enough to compensate for the electrostatic repulsion completely.

Fig. 6. 8 exhibits the turbidities of silica and stannic oxide suspensions at $2x10^{-3}$ M NaCl when polyacrylamide hydrolyzed in various degrees are added to the suspensions. The pH of silica suspension was adjusted to pH 5.4, while that of stannic oxide pH 5.7. Two different polymer concentrations, 0.1 ppm and 0.4 ppm, were studied. It is shown that the turbidity increases with increased percent of hydrolysis with both silica and stannic oxide suspensions. This result may support the discussion above that the increased negative charge in polymer reduces the polymer adsorption and reduces the flocculation of particles. It should

(a)

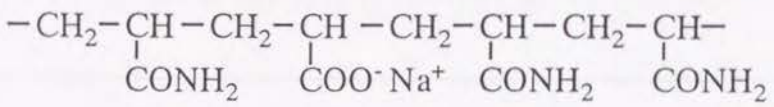

(b)

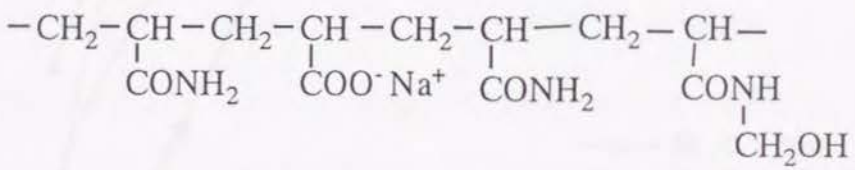

(c)

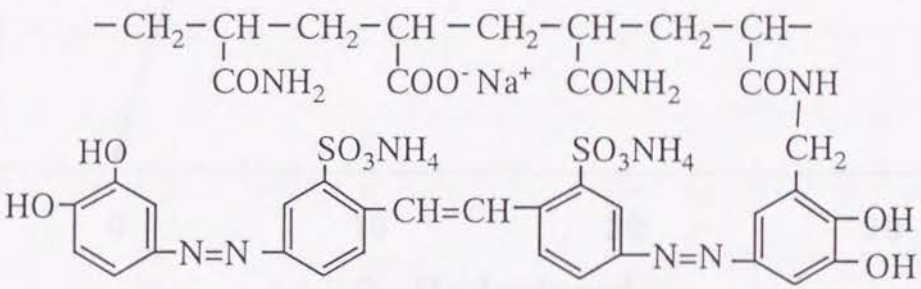

Fig. 6. 7 Assumed structures of polyacrylamide in its modification process: (a) hydrolysis of amide groups, (b) methylolation of amide groups, (c) combined with stilbazo

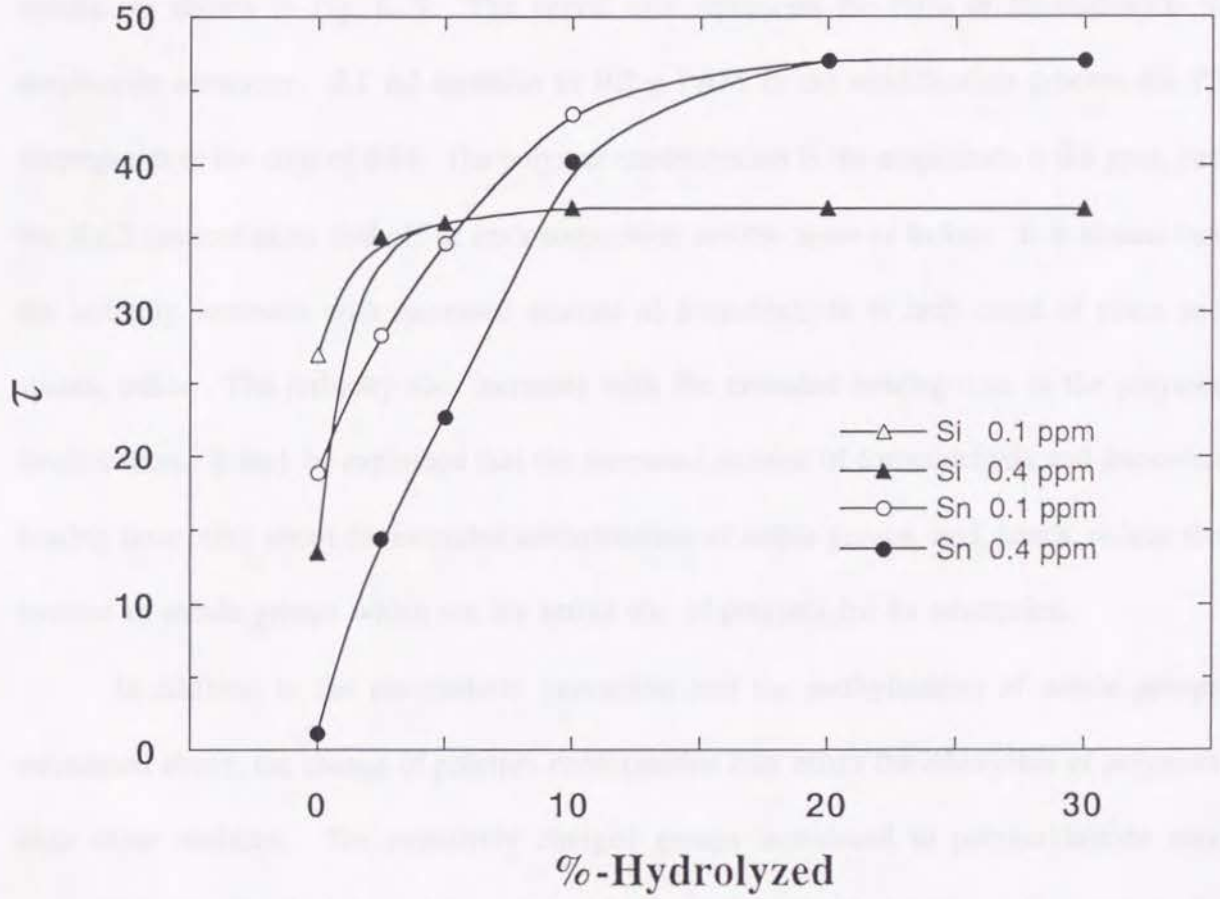

Fig. 6. 8 The effect of polyacrylamide hydrolyzed in various degrees on the turbidity (τ) of 300 ppm silica and 200 ppm stannic oxide suspensions at $2x10^{-3}$ M NaCl. The pH is adjusted to pH 5.4 with silica and pH 5.7 with stannic oxide.

be noted, however, that the partial hydrolysis of polyacrylamide is generally regarded as a favorable factor to polymer adsorption and the bridging of particles[8]. The increased flocculation by the hydrolyzed polymers may be observed with the particle of low negative charge or of positive charge.

The amount of formaldehyde and heating time in the modification process for P2 were varied in order to investigate the effect of methylolation on the flocculation of oxides. The results are shown in Fig. 6. 9. The lateral axis represents the ratio of formaldehyde to acrylamide monomer. 0.1 ml formalin to 0.2 g PAM in the modification process for P2 corresponds to the ratio of 0.44. The polymer concentration in the suspension is 0.6 ppm, and the NaCl concentration and pH of each suspension are the same as before. It is shown that the turbidity increases with increased amount of formaldehyde in both cases of silica and stannic oxide. The turbidity also increases with the extended heating time in the polymer modification. It may be explained that the increased amount of formaldehyde and increased heating time bring about the extended methylolation of amide groups, and, hence, reduce the number of amide groups which are the active site of polymer for its adsorption.

In addition to the electrostatic interaction and the methylolation of amide groups mentioned above, the change of polymer conformation may affect the adsorption of polymers onto oxide surfaces. The negatively charged groups introduced to polyacrylamide may promote the "coiling" of the polymer molecule due to the attraction with amidium groups ($-CONH_3^+$) when the number of incorporated group is not large[9]. It is also possible that the formaldehyde connect two amide groups with methylene bridge and promote the coiling of polymer. Thus the poor conformation of polymer may occur at the same time in the modification process and may contribute to the turbidity increase to some extent.

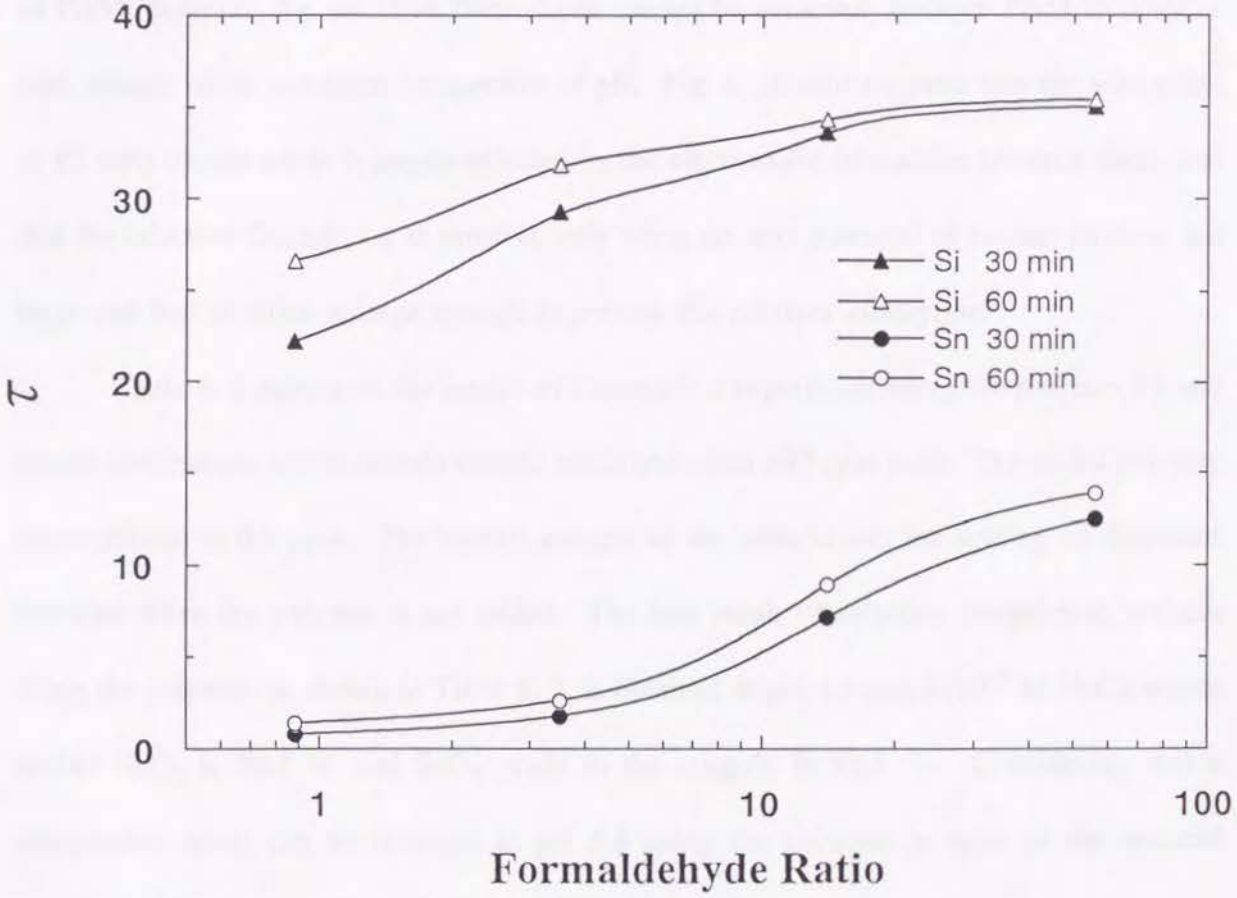

Fig. 6. 9 The effect of added formaldehyde and heating time in the modification of polyacrylamide on the turbidity (τ) of 300 ppm silica and 200 ppm stannic oxide suspensions at $2x10^{-3}$ M NaCl. The pH of silica suspension is pH 5.4, while that of stannic oxide pH 5.7. The added polymer is 0.6 ppm.

The effect of polymer on the flocculation of silica and stannic oxide has been studied with various pH, the results of which are shown in Fig. 6. 10. The concentration of PAM and P3 added to the suspension are 0.4 ppm. When P3 is used, stannic oxide flocculates between pH 5.5 and 6, while silica does not flocculate at the same pH range. It suggests that the selective flocculation of stannic oxide is possible in mixed suspensions with silica, if a hetero-flocculation is prevented by carefully controlling the pH of suspension. In the case of PAM, however, the selective flocculation cannot be achieved, because PAM flocculates both stannic oxide and silica irrespective of pH. Fig. 6. 10 also suggests that the adsorption of P3 onto stannic oxide is largely affected by the electrostatic interaction between them, and that the selective flocculation is possible only when the zeta potential of stannic oxide is not large and that of silica is large enough to prevent the polymer adsorption.

Table 6. 4 represents the results of flocculation experiment using the polymer P3 and mixed suspensions which contain stannic oxide and silica 500 ppm each. The added polymer concentration is 0.6 ppm. The bottom column of the table shows the settling of dispersed particles when the polymer is not added. The best result of selective coagulation without using the polymer, as shown in Table 6. 2, is obtained at pH 4.5 and $2x10^{-3}$ M NaCl, where settled SnO_2 is 50.7 % and SnO_2 grade in the coagula is 92.3 %. Considering that a comparable result can be obtained at pH 5.8 using the polymer in spite of the reduced agitation time (1/3) and settling time (1/6), it is clear that the polymer enhances the flocculation of stannic oxide. It is also shown in Table 6. 4 that the flocculation of both silica and stannic oxide decreases with increasing pH.

Table 6. 5 shows the influence of the mixing ratio of silica to stannic oxide on the selective flocculation of stannic oxide. The concentration of silica is varied from 500 ppm to 4500 ppm, while that of stannic oxide is maintained at 500 ppm. The figures at the left

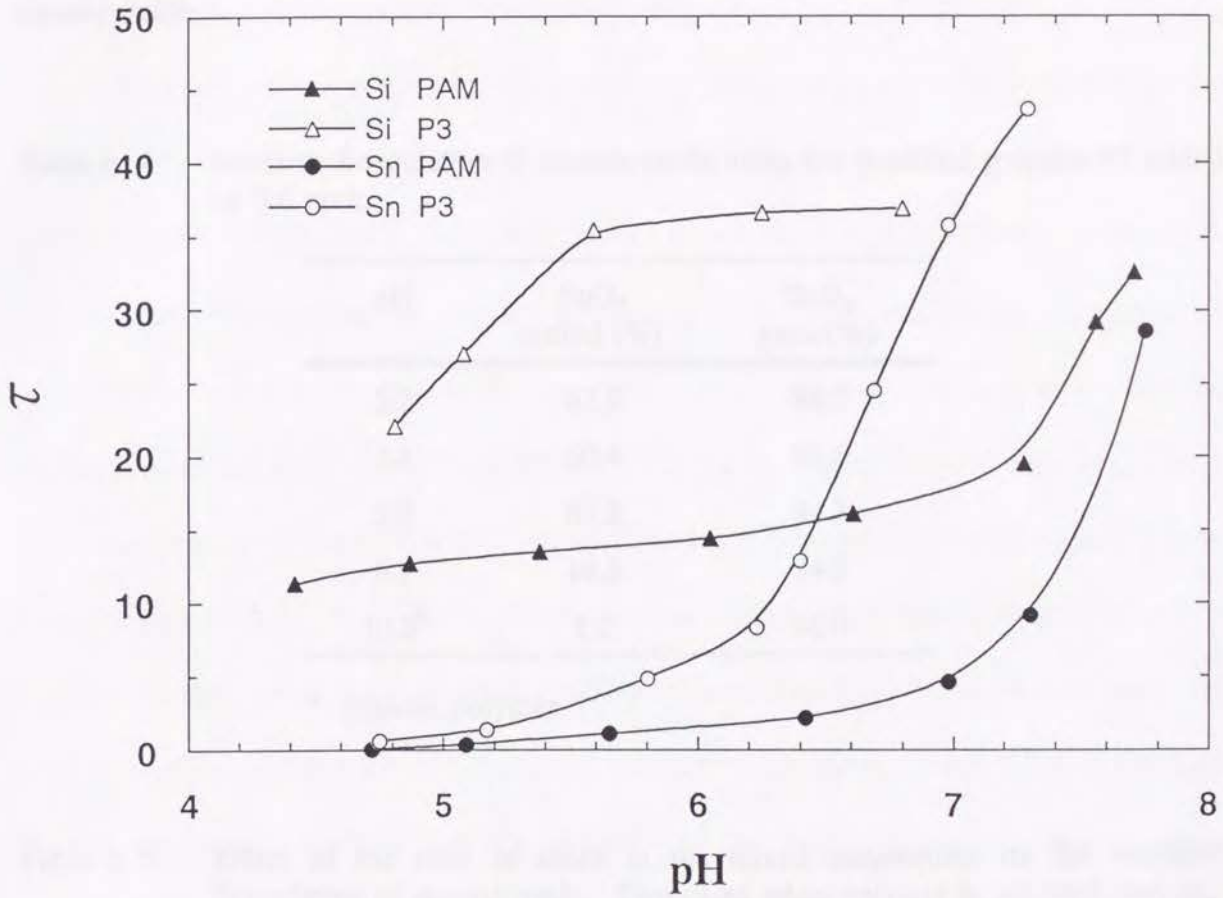

Fig. 6. 10 Effect of pH on the turbidity (τ) of 300 ppm silica and 200 ppm stannic oxide suspensions at $2x10^{-3}$ M NaCl when polymers are added by 0.4 ppm.

side in each column represent the result of experiment conducted at pH 4.5 without adding the polymer, the figures at the right side show the results of experiment conducted at pH 5.7 adding the polymer P3 by 0.6 ppm. It is shown that the increased ratio of silica in the suspensions deteriorates the selective coagulation (and flocculation) of stannic oxide. However, the decrease in the flocculation of stannic oxide is smaller when P3 is added to the mixed suspensions. It also exhibits that the polymer promotes the selective flocculation of stannic oxide.

Table 6. 4 Selective flocculation of stannic oxide using the modified polymer P3 added by 0.6 ppm.

pH	SnO_2 settled (%)	SnO_2 grade(%)
5.2	62.9	86.5
5.5	60.4	89.5
5.8	53.2	94.3
6.1	19.8	94.3
10.0*	1.2	96.0

*: without polymer

Table 6. 5 Effect of the ratio of silica in the mixed suspensions on the selective flocculation of stannic oxide. Two cases when polymer is not used (no) and polymer P3 is used are compared.

	SnO_2 settled (%)		SnO_2 grade (%)	
Sn:Si	no	P3	no	P3
1:1	50.7	53.2	92.3	94.3
1:2	12.5	42.4	82.8	89.8
1:4	10.7	30.1	59.6	82.5
1:9	8.1	22.3	36.2	67.4

6. 4 Conclusion

The coagulation in mixed suspensions of silica and stannic oxide has been investigated. The result shows that there is a hydration force between silica and stannic oxide at $2x10^{-1}$ M NaCl. Less than this NaCl concentration, the hydration force does not seem to exist between the silica and stannic oxide. However, the best selective coagulation of stannic oxide can be achieved at $2x10^{-3}$ M NaCl, where the hydration force exists only between silica particles and not between silica and stannic oxide.

In order to promote the selective coagulation, polymeric flocculants have been added to the mixed suspensions and their effect have been investigated. Among the polymers, a polyacrylamide modified with formaldehyde and stilbazo has been most effective to promote the selective flocculation of stannic oxide. In all the modification processes of polyacrylamide studied in this work, the ability of the polyacrylamide to flocculate the particles decreases for both silica and stannic oxide. The decrease may be attributed to that the amide groups of polyacrylamide decrease in the modification processes though their hydrolysis or methylolation. While polyacrylamides simply hydrolyzed or methylolated in different degrees lose the flocculating ability for stannic oxide as well as silica, the polyacrylamide modified with stilbazo can still flocculate stannic oxide. The affinity of stilbazo toward tin atom may help the adsorption of the polymer on stannic oxide to some extent.

6. 5 References

1. Schiller, A.M., and Suen, T.J., *Ind. Eng. Chem.*, **48**, 2132 (1956)
2. Imoto, M, and Uno, K., "Jugou to Fuka-shukugou," 141, Tokyo Kagaku Dojin, Tokyo (1972)
3. Attia, Y.A., and Kitchener, J.A., Proceedings 11th International Mineral Processing Congress, 1233 (1976)
4. Attia, Y.A., *Int. J. Miner. Processing*, **4**, 191 (1977)
5. Sakaguchi, T., and Ueno, K., "Kinzoku Kireto," **2**, 233, Nankodo, Tokyo (1966)
6. Hogg, R., Healy, T.W., and Fuerstenau, D.W., *Trans. Faraday Soc.*, **62**, 1638 (1966)
7. Griot, G., and Kitchener, J.A., *Trans. Faraday Soc.*, **61**, 1028 (1965)
8. Nagasawa, M., and Takizawa, A., "Kobunshi Mizushori-zai," 64, Chijin Shokan, Tokyo (1976)
9. Michaels, A.S., *Ind. Eng. Chem.*, **46**, 1485 (1954)

Chapter 7 Conclusion

In many industrial processes, it is important to predict the stability of fine particle suspensions. Since the development of the DLVO theory, which is the first theoretical approach to the prediction of the stability, it has been believed that the stability of most suspensions can be explained by the DLVO theory. However, the direct force measurement between mica sheets in aqueous solutions revealed that there was a non-DLVO force, which made it necessary to reconstruct the theory describing colloidal systems.

Due to the difficulties in sample preparation, the application of direct force measurement has been limited to mica and glass. For this reason, it has not been clear whether the non-DLVO force is peculiar to the mica and glass or it commonly exists with many solids. It is, therefore, the objective of this work to present a method of evaluating the non-DLVO force from a coagulation experiment which is basically applicable to any solids, and to confirm the existence of non-DLVO force with various oxides.

In the first chapter of this paper, the historical review of the theoretical treatment for the stability of colloidal suspensions was made and the evidences in which the classical DLVO theory failed were shown. As one of the practical approaches to the reconstruction of theory which can describe any colloidal systems, the idea of structural energy and the extended DLVO theory were introduced. The necessity of experimental determination of structural energy and the expected contributions from the present work to such determination were also explained.

In the second chapter, it was shown that the aqueous suspension of silica was stable at low pH where the electrostatic repulsion was negligible due to the very small zeta-potentials. The anomalous stability was attributed to the *primary hydration force* which might

arise from the surface hydration of silica. A method of evaluating the hydration force was presented. It is based on the assumed 1:1 relationship between the turbidity of suspension and the energy barrier controlling the coagulation of particles, and on a series of calculations to determine the parameters of structural energy. It was shown that the primary hydration force was at a maximum in suspensions with dilute NaCl concentrations and decreased with increasing NaCl concentration.

The coagulation of rutile in its aqueous suspensions was investigated in the third chapter, in which it was found that rutile did not coagulate completely even at its isoelectric point when NaCl concentration in the suspension was above 1 M. Since there was no electrostatic repulsion at the isoelectric points, the incomplete coagulation was attributed to the existence of a repulsive hydration force. A series of calculations showed that the hydration force was noticeable at $2x10^{-2}$ M NaCl and increases with increasing NaCl concentration. This was similar to the hydration force first observed with mica by surface force measurements and was the opposite of what was observed with silica as shown in the second chapter. It was considered that the adsorption of hydrated ions on rutile surface and successive structure formation of water molecules at the interface might be responsible for the hydration force. In this regard, the force was classified as the *secondary hydration force*.

The coagulation of stannic oxide in its aqueous suspensions was studied in the forth chapter. As was the case with rutile, stannic oxide showed an anomalous stability at its isoelectric point when NaCl concentration in the suspension was above 1 M. It was found that the secondary hydration force was noticeable at $2x10^{-1}$ M NaCl and increased with increasing NaCl concentration. The mechanisms of the primary and the secondary hydration forces were also discussed in this chapter. It was postulated that the silica surface was originally hydrated in water and developed the structure of water molecules at the interface,

while the surfaces of rutile and stannic oxide were not strongly hydrated as silica and formed the water structure with the help of adsorbed hydrated ions. The difference in the effective ion radii of Si^{4+}, Ti^{4+} and Sn^{4+}, and the difference in the order of specific adsorption of alkaline metal cations were referred to as the evidences which indirectly support this assumption. The fact that the same electrolyte decreases the primary hydration force with silica and increases the secondary hydration force with rutile and stannic oxide made it difficult to accept Allen and Matijević's idea of destruction of water layer by adsorbing cations. For this reason, Iler's concept of cation–bridging was introduced to explain the decrease of the primary hydration force. It was also pointed out that the secondary hydration force was stronger at acidic side of isoelectric point with both rutile and stannic oxide at high NaCl concentrations, which might suggest that hydrated anions also contribute to the secondary hydration force in addition to cations. The reliability of turbidity as a measure of coagulation was examined in this chapter. The different behavior of turbidity between silica and stannic oxide was explained by considering the complex nature of light extinction as to refractive index and particle size. It was shown that the turbidity could be replaced by the settled amount of solid, and it was confirmed that the extended DLVO calculation based on the settled amount gave the same result as that obtained earlier using the turbidity.

In the fifth chapter, the effect of ethanol on the hydration forces with silica and rutile was investigated. The results showed that the ethanol decreased the primary hydration force with silica, while it increased the secondary hydration force with rutile. It was considered that the decrease in the primary hydration force could be attributed to the dehydration of the silica surface by ethanol, while the increase of the secondary hydration force might be attributed to the increased cation adsorption enhanced by the presence of ethanol. The effect of dodecylamine–hydrochloride (DAH) on the stability of rutile suspension was also studied

in this chapter. It was found that the *hydrophobic attraction* was observed with rutile at alkaline pH where the increased amount of adsorbed DAH ions brought about the charge reversal of the zeta-potential of rutile. The magnitude of hydrophobic attraction was found to be considerably larger than that of the repulsive hydration force observed with rutile, which was the same as what had been reported in the direct force measurements conducted with hydrophobized mica.

As one of the applications of the knowledge on the stability of aqueous oxide suspensions, the selective coagulation of stannic oxide in mixed suspensions with silica was chosen and was investigated in the sixth chapter. It was found that the selective coagulation of stannic oxide could be achieved at pH 4.5–4.7 and $2x10^{-3}$ M NaCl, where silica particles were dispersed due to the large electrostatic repulsion and the contributions from primary hydration force, while stannic oxide particles coagulated because of the small electrostatic repulsion and the lack of the secondary hydration force due to the low NaCl concentration. At this condition, the hetero-coagulation are supposed to be prevented by the electrostatic repulsion between silica and stannic oxide. The hydration force between silica and stannic oxide was observed at $2x10^{-1}$ M NaCl, the magnitude of which was comparable to the primary hydration force with silica. The effect of polymer on the selective coagulation was also studied in this chapter. Polyacrylamide was modified in various manners and added to the mixed suspensions. It was found that the decrease of amide group achieved by the their hydrolysis or methylolation reduced the ability of the polymer to flocculate both silica and stannic oxide. A polyacrylamide modified with the presence of stilbazo was found to be effective for the selective flocculation of stannic oxide, which was attributed to the selective adsorption of the polymer on stannic oxide surfaces.

The present work has shown that there exist hydration forces with silica, rutile and

stannic oxide in addition to mica and glass. It is possible that hydration forces commonly exist with most oxides. The hydration forces can be evaluated by analyzing the coagulation of particles, but it means, on the other hand, that the coagulation is greatly affected by the hydration forces. It is, therefore, important to use the extended DLVO theory for predicting the stability of aqueous oxide suspensions.